Stem Cells International

Stem Cells in Cancer Progression and Therapy

Lead Guest Editor: Hua Tan
Guest Editors: Weijun Su and Xing-Ding Zhang

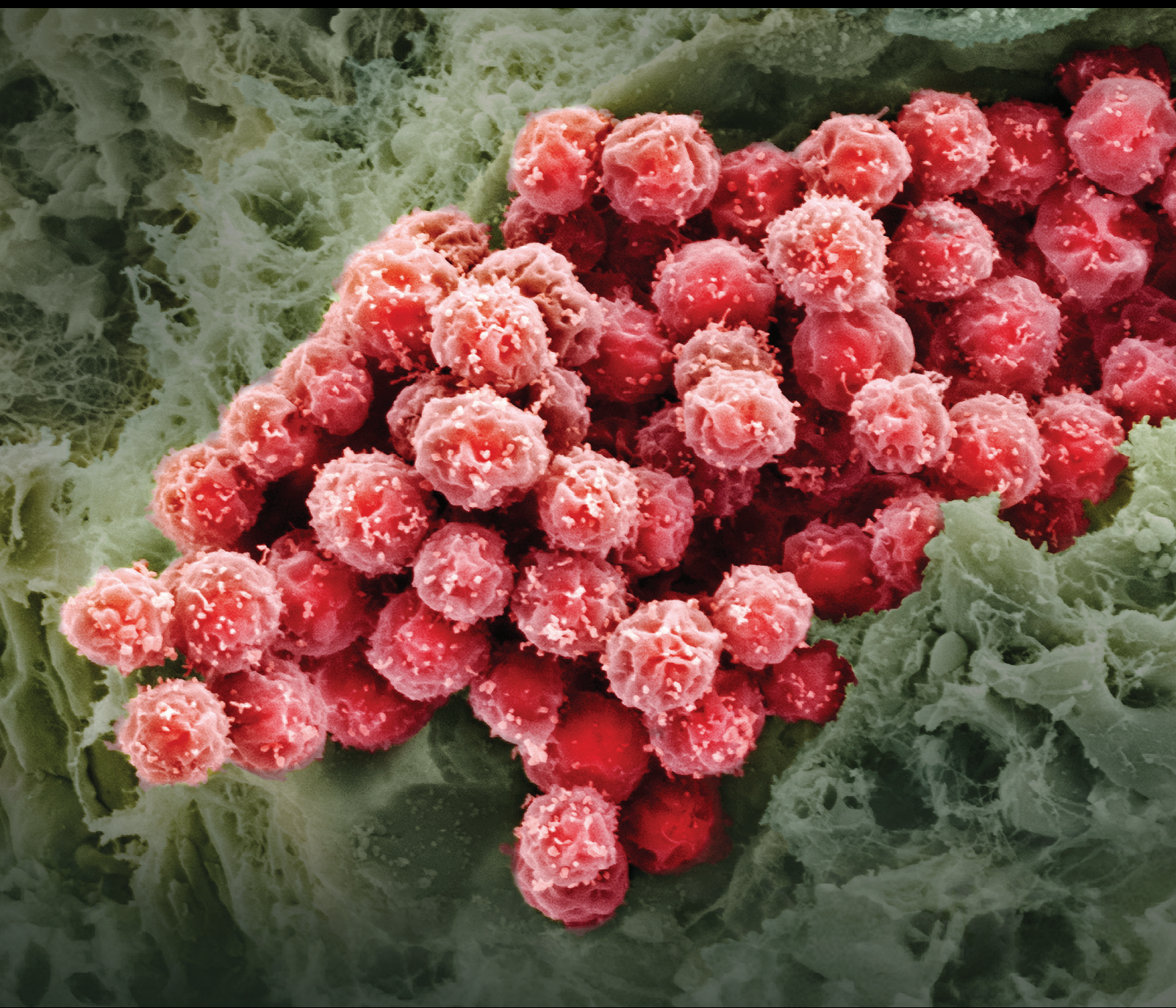

Stem Cells in Cancer Progression and Therapy

Stem Cells International

Stem Cells in Cancer Progression and Therapy

Lead Guest Editor: Hua Tan
Guest Editors: Weijun Su and Xing-Ding Zhang

Copyright © 2019 Hindawi. All rights reserved.

This is a special issue published in "Stem Cells International." All articles are open access articles distributed under the Creative Commons Attribution License, which permits unrestricted use, distribution, and reproduction in any medium, provided the original work is properly cited.

Editorial Board

James Adjaye, Germany
Cinzia Allegrucci, UK
Eckhard U. Alt, USA
Francesco Angelini, Italy
James A. Ankrum, USA
Stefan Arnhold, Germany
Marta Baiocchi, Italy
Andrea Ballini, Italy
Dominique Bonnet, UK
Philippe Bourin, France
Daniel Bouvard, France
Anna T. Brini, Italy
Annelies Bronckaers, Belgium
Silvia Brunelli, Italy
Stefania Bruno, Italy
Bruce A. Bunnell, USA
Kevin D. Bunting, USA
Benedetta Bussolati, Italy
Leonora Buzanska, Poland
A. C. Campos de Carvalho, Brazil
Stefania Cantore, Italy
Yilin Cao, China
Marco Cassano, Switzerland
Alain Chapel, France
Sumanta Chatterjee, USA
Isotta Chimenti, Italy
Mahmood S. Choudhery, Pakistan
Pier Paolo Claudio, USA
Gerald A. Colvin, USA
Mihaela Crisan, UK
Radbod Darabi, USA
Joery De Kock, Belgium
Frederic Deschaseaux, France
Marcus-André Deutsch, Germany
Varda Deutsch, Israel
Valdo Jose Dias Da Silva, Brazil
Massimo Dominici, Italy
Leonard M. Eisenberg, USA
Georgina Ellison, UK
Alessandro Faroni, UK
F. J. Fernández-Avilés, Spain
Jess Frith, Australia
Ji-Dong Fu, USA
Manuela E. Gomes, Portugal
Cristina Grange, Italy
Stan Gronthos, Australia
Hugo Guerrero-Cazares, USA
Jacob H. Hanna, Israel
David A. Hart, Canada
Alexandra Harvey, Australia
Yohei Hayashi, Japan
Tong-Chuan He, USA
Xiao J. Huang, China
Thomas Ichim, USA
Joseph Itskovitz-Eldor, Israel
Elena Jones, UK
Christian Jorgensen, France
Oswaldo Keith Okamoto, Brazil
Alexander Kleger, Germany
Diana Klein, Germany
Valerie Kouskoff, UK
Andrzej Lange, Poland
Laura Lasagni, Italy
Robert B. Levy, USA
Renke Li, Canada
Tao-Sheng Li, Japan
Shinn-Zong Lin, Taiwan
Risheng Ma, USA
Yupo Ma, USA
Marcin Majka, Poland
Giuseppe Mandraffino, Italy
Athanasios Mantalaris, UK
Cinzia Marchese, Italy
Katia Mareschi, Italy
Hector Mayani, Mexico
Jason S. Meyer, USA
Eva Mezey, USA
Susanna Miettinen, Finland
Toshio Miki, USA
Claudia Montero-Menei, France
Christian Morsczeck, Germany
Patricia Murray, UK
Federico Mussano, Italy
Mustapha Najimi, Belgium
Norimasa Nakamura, Japan
Bryony A. Nayagam, Australia
Karim Nayernia, UK
Krisztian Nemeth, USA
Francesco Onida, Italy
Sue O'Shea, USA
Gianpaolo Papaccio, Italy
Kishore B. S. Pasumarthi, Canada
Yuriy Petrenko, Czech Republic
Alessandra Pisciotta, Italy
Stefan Przyborski, UK
Bruno Pèault, USA
Peter J. Quesenberry, USA
Pranela Rameshwar, USA
Francisco J. Rodríguez-Lozano, Spain
Bernard A. J. Roelen, Netherlands
Alessandro Rosa, Italy
Peter Rubin, USA
Hannele T. Ruohola-Baker, USA
Benedetto Sacchetti, Italy
Ghasem Hosseini Salekdeh, Iran
Antonio Salgado, Portugal
Fermin Sanchez-Guijo, Spain
Anna Sarnowska, Poland
Heinrich Sauer, Germany
Coralie Sengenes, France
Dario Siniscalco, Italy
Shimon Slavin, Israel
Sieghart Sopper, Austria
Valeria Sorrenti, Italy
Giorgio Stassi, Italy
Ann Steele, USA
Alexander Storch, Germany
Bodo Eckehard Strauer, Germany
Hirotaka Suga, Japan
Gareth Sullivan, Norway
Masatoshi Suzuki, USA
Kenichi Tamama, USA
Corrado Tarella, Italy
Nina J.E.E. Tirnitz-Parker, Australia
Daniele Torella, Italy
Hung-Fat Tse, Hong Kong
Marc L. Turner, UK
Aijun Wang, USA
Darius Widera, UK
Bettina Wilm, UK
Dominik Wolf, Austria
Wasco Wruck, Germany

Qingzhong Xiao, UK
Takao Yasuhara, Japan
Zhaohui Ye, USA
Holm Zaehres, Germany
Elias T. Zambidis, USA
Ludovic Zimmerlin, USA
Ewa K. Zuba-Surma, Poland
Eder Zucconi, Brazil
Maurizio Zuccotti, Italy
Nicole Isolde zur Nieden, USA

Contents

Stem Cells in Cancer Progression and Therapy
Hua Tan, Weijun Su, and Xing-Ding Zhang
Editorial (2 pages), Article ID 3507604, Volume 2019 (2019)

Pyroptosis of MCF7 Cells Induced by the Secreted Factors of hUCMSCs
Yang Jiao, Hongbo Zhao, Guodong Chen, Xiongbo Sang, Luhan Yang, Zongliu Hou, Wei Si, and Bingrong Zheng
Research Article (12 pages), Article ID 5912194, Volume 2018 (2019)

Synaptic Plasticity of Human Umbilical Cord Mesenchymal Stem Cell Differentiating into Neuron-like Cells In Vitro Induced by Edaravone
Yunpeng Shi, Chengrui Nan, Zhongjie Yan, Liqiang Liu, Jingjing Zhou, Zongmao Zhao, and Depei Li
Research Article (11 pages), Article ID 5304279, Volume 2018 (2019)

Differentiation Potential of Human Wharton's Jelly-Derived Mesenchymal Stem Cells and Paracrine Signaling Interaction Contribute to Improve the In Vitro Maturation of Mouse Cumulus Oocyte Complexes
Martin Maldonado, Tianhua Huang, Jianying Chen, and Ying Zhong
Research Article (8 pages), Article ID 7609284, Volume 2018 (2019)

Integrated Genome-Wide Analysis of Gene Expression and DNA Copy Number Variations Highlights Stem Cell-Related Pathways in Small Cell Esophageal Carcinoma
Di Liu, Xinyan Xu, Junmiao Wen, Liyi Xie, Junhua Zhang, Yuxin Shen, Guoliang Jiang, Jiayan Chen, and Min Fan
Research Article (8 pages), Article ID 3481783, Volume 2018 (2019)

Human Bone Marrow Mesenchymal Stem Cells Promote Gastric Cancer Growth via Regulating *c-Myc*
Bin Chen, Jing Yu, Qianqian Wang, Yuanyuan Zhao, Li Sun, Changgen Xu, Xiangdong Zhao, Bo Shen, Mei Wang, Wenrong Xu, and Wei Zhu
Research Article (11 pages), Article ID 9501747, Volume 2018 (2019)

Hindawi
Stem Cells International
Volume 2019, Article ID 3507604, 2 pages
https://doi.org/10.1155/2019/3507604

Editorial

Stem Cells in Cancer Progression and Therapy

Hua Tan,[1] **Weijun Su**,[2] **and Xing-Ding Zhang**[3]

[1]*School of Biomedical Informatics, The University of Texas Health Science Center at Houston, Houston, TX 77030, USA*
[2]*School of Medicine, Nankai University, Tianjin 300071, China*
[3]*School of Medicine, Sun Yat-sen University, Guangzhou, Guangdong 510080, China*

Correspondence should be addressed to Hua Tan; hua.tan@uth.tmc.edu

Received 25 February 2019; Accepted 25 February 2019; Published 5 March 2019

Copyright © 2019 Hua Tan et al. This is an open access article distributed under the Creative Commons Attribution License, which permits unrestricted use, distribution, and reproduction in any medium, provided the original work is properly cited.

Stem cells have been widely studied in the fields of cancer biology. Yet, many fundamental questions regarding the specific roles of stem cell in cancer progression and therapy remain elusive, impeding the effective clinical translation of stem cell research. On the one hand, cancer stem cells (CSCs), which represent a small population within tumors, with potential to differentiate into heterogeneous tumor cell colonies, are suggested to be responsible for therapy resistance and tumor recurrence. On the other hand, stem cells can be used to treat hematological malignancies through bone marrow transplantation by replenishing hematopoietic stem cells (HSCs). Stem cells play different roles in particular contexts.

Since first discovered in acute myeloid leukemia (AML) by $CD34^+/CD38^-$ biomarkers in 1997, CSCs attracted intensive efforts of research. Following the first evidence of CSCs existing in human cortical glial tumors, CSCs were identified in diverse human tumor tissues, including the breast, colon, and pancreas. Basically, CSCs display distinct biophysiological properties and responses to various treatments, compared to terminally differentiated cancer (TDC) cells. Therapeutic paradigm targeting on CSCs rather than bulk tumor cells (i.e., the TDCs) proved to be more potent in shrinking tumors.

The continuing advancement of molecular and cellular biology, especially the rapid progress in next-generation sequencing techniques and cancer genomics analysis approaches, is making therapeutics targeting CSCs more precise and effective. The single-cell sequencing technology and spatial transcriptomics become increasingly popular and powerful in profiling individual cells with genetic and epigenetic hierarchy. Versatile gene editing techniques such as CRISPR/Cas9 have also been harnessed to study CSCs in human tumors. Collectively, the molecular signatures of CSCs as well as CSC-initiated tumor cell lineage, such as gene mutation, gene and protein expression, microRNA regulations, DNA methylation, and histone modification, can be discerned and even edited in an unprecedentedly high resolution, which provides a unique opportunity for designing targeted and immune-based therapies.

Cancer has long been considered as a genetic disease, where genetic evolution of cancer cells shapes the tumor progression. Gene mutation is a stochastic process and hence results in unsynchronized mutation patterns in cells. Meanwhile, epigenetic markers changed dramatically over tumor evolution. Therefore, cancer cells in a tumor form a dynamic ecosystem of multiple colonies with heterogeneity in molecular signatures. Some of the colonies exemplify stem-like cell properties and are suggested to sustain the growth and expansion of the whole system. This complex and ever-changing system can be depicted and simulated by mathematical models. During the past years, mathematical models have played a critical role in generating and testing hypothesis regarding cancer progression. Tumor growth under various conditions including drug treatment has been well addressed by computational models. Vital biological processes, such as CSC lineage commitment, genetic evolution, oncogenic signaling cascades, neovascularization, and tumor cell-microenvironment interactions, have been carefully investigated. Systems biology approaches integrating experimental data, bioinformatics analysis, and computational model are expected to play an increasingly significant

role in studying CSC-initiated and driven human cancer progression. The challenging part is to generate adequate yet nonredundant biomedical data at various scales (spatial and temporal) for model construction, calibration, and validation, towards enhancing the prediction capabilities of the in silico models.

While CSCs are deemed culprit of most therapy resistance and cancer relapse, stem cells derived from normal tissues can be leveraged to treat human malignancies. Via transplantation, HSCs were used to treat leukemia by replenishing the diminished blood cell population. Neural stem cells and human umbilical cord blood-derived mesenchymal stem cells (MSCs) were genetically transformed to treat gliomas. In these stem cell-based anticancer therapies, engineered stem cells stably express cancer suppressor genes or function as nanomedicine carriers to deliver cytotoxic agents targeting cancer cells. Strikingly, stem cells are also found to play an important role in cancer immunotherapy, by continuously replenishing the exhausted anticancer T-cells. Despite technique advancement, challenges existed. In particular, due to incomplete interpretation of the underlying molecular mechanisms, the treatment efficacy and durability of human cancers remain suboptimal in many cases. Additionally, the risk of tumorigenic transformation of the transplanted stem cells cannot be ignored. Upon being recruited into tumor microenvironment, stem cells might be educated into "cancer-favored" and reciprocally fuel tumor cells. These multifaceted interactions between stem cells and cancer cells should be taken into account while considering antitumor therapy with stem cells.

In the current special issue, we have solicited research articles and reviews that are aimed at addressing the biological and clinical questions regarding CSC-driven tumor progression and cancer treatment resistance and stem cell-based anticancer therapy. We stress on the molecular basis of how CSCs adapt to sustain the tumor progression under both physiological and stiff conditions such as local hypoxia and anticancer drug delivery. We also desire work exploring biological processes under stem cell transplantation therapy, such as how the stem cells home to the local environment, differentiate into progeny tumor cells, and/or exert paracrine effects.

B. Chen et al. explored the potential safety issues in the application of human bone marrow mesenchymal stem cells (hBM-MSCs) to regenerative medicine and tissue engineering. They revealed that hBM-MSC-conditioned medium (hBM-MSC-CM) promotes gastric cancer development via upregulation of c-Myc by both *in vitro* and *in vivo* experiments, which may be a potential risk factor and/or a therapeutic target for clinical applications.

D. Liu et al. conducted an integrative genome-wide analysis on gene expression and DNA copy number variations in a rare but aggressive malignancy—primary small-cell esophageal carcinoma (SCEC). They carried out a de novo expression array on three matched sets of primary SCEC and adjacent normal tissue samples procured from their institutional tissue bank. Stem cell-related pathways, WNT and Notch signaling, were shown to play significant roles in SCEC in this study.

M. Maldonado et al. studied the impact of human Wharton's jelly-derived MSCs (hWJ-MSCs) in *in vitro* maturation (IVM) of cumulus oocyte complexes (COCs). They demonstrated that hWJ-MSCs' differentiation potential and the presence of coordinated paracrine interaction between the stem cells and COCs are two prerequisites for the hWJ-MSCs to improve the IVM of COCs. Under appropriate conditions, the paracrine factors produced in the coculture system with DMEM-F12 may help develop synthetic media for desired *in vitro* culture of COCs. This work stands for a good attempt to research the paracrine effect imposed by stem cells on the cultured cells, especially using novel WJ-derived stem cells. The strategy and conclusions may have ramifications for cancer treatment via stem cell transplantation.

Y. Shi et al. addressed the differentiation of human umbilical cord mesenchymal stem cells (hUC-MSCs) into neuron-like cells. Working on human umbilical cord tissue, they proved that edaravone, a low-molecular antioxidative agent, can dose-dependently induce hUC-MSCs to differentiate into neuron-like cells. This study provides a novel method for neural-lineage induction from MSCs and demonstrates the potential applications of MSCs in regenerative medicine.

Y. Jiao et al. investigated the mechanisms underlying hUC-MSC-based cancer therapy. They evaluated the effect of secreted factors of hUC-MSCs on the breast cancer cell line MCF7 in terms of morphological changes, cell viability, cell cycle, apoptosis, DNA fragmentation, and interleukin-1β (IL-1β) secretion and confirmed that the secreted factors of hUC-MSCs could cause MCF7 cell death by inducing pyroptosis. Their results may enable the community to better understand the effect of hUC-MSCs on cell-based breast cancer therapy, as well as its associated molecular basis.

While this special issue represents an exciting start point to address the fundamental questions regarding stem cells in cancer biology and therapy, many challenges regarding the clinical effectiveness and biosafety still remain to be conquered, as mentioned above. We appeal more intense attention and participation in this promising field in the future, especially the involvement of new concepts and technologies such as single-cell sequencing, spatial transcriptomics, gene editing, and immunotherapy in the stem cell-related cancer research. We expect a new era in which stem cells can be elaborately tuned to fight for cancers, with detrimental effects trimmed and merits maximized.

Conflicts of Interest

The authors declare that there is no conflict of interest regarding the publication of this editorial article.

Hua Tan
Weijun Su
Xing-Ding Zhang

Hindawi
Stem Cells International
Volume 2018, Article ID 5912194, 12 pages
https://doi.org/10.1155/2018/5912194

Research Article

Pyroptosis of MCF7 Cells Induced by the Secreted Factors of hUCMSCs

Yang Jiao,[1,2] Hongbo Zhao,[2] Guodong Chen,[1] Xiongbo Sang,[1] Luhan Yang,[1] Zongliu Hou,[3] Wei Si,[4] and Bingrong Zheng[1]

[1]*School of Medicine, Yunnan University, Kunming, 650091 Yunnan, China*
[2]*Yunnan Key Laboratory of Stem Cell and Regenerative Medicine, Institute of Molecular and Clinical medicine, Kunming Medical University, Kunming, 650500 Yunnan, China*
[3]*Yan'an Hospital of Kunming City, Kunming, 650051 Yunnan, China*
[4]*Yunnan Key Laboratory of Primate Biomedical Research, Institute of Primate Translational Medicine, Kunming University of Science and Technology, Kunming, 650500 Yunnan, China*

Correspondence should be addressed to Zongliu Hou; hzl579@163.com, Wei Si; siwei76@hotmail.com, and Bingrong Zheng; zhengbr@ynu.edu.cn

Received 14 June 2018; Revised 22 August 2018; Accepted 16 September 2018; Published 11 November 2018

Guest Editor: Hua Tan

Copyright © 2018 Yang Jiao et al. This is an open access article distributed under the Creative Commons Attribution License, which permits unrestricted use, distribution, and reproduction in any medium, provided the original work is properly cited.

Human umbilical cord mesenchymal stem cells (hUCMSCs) are superior to other sources of mesenchymal stem/stromal cells (MSCs), and they are used as a novel tool for cell-based cancer therapy. However, the mechanism underlying hUCMSC-induced cancer cell death is not clear. In the present study, we aimed to evaluate the effect of secreted factors of hUCMSCs on the breast cancer cell line MCF7 by exposing them to the conditioned medium (CM) of hUCMSCs. We evaluated the morphological changes, cell viability, cell cycle, apoptosis, DNA fragmentation, and interleukin-1β (IL-1β) secretion of CM-exposed MCF7 cells. The results showed that the secreted factors of hUCMSCs could cause MCF7 cell death by inducing pyroptosis. We also sequenced the total RNA, and the differentially expressed genes (DEGs) were subjected to the Kyoto Encyclopedia of Genes and Genomes (KEGG) pathway analysis. A total of 2597 (1822 upregulated and 775 downregulated) genes were identified and 14 pathways were significantly enriched. The results showed that the expression of the pyroptosis-related genes *NLRP1* and *CASP4* and the inflammation-related pathways changed significantly in MCF7 cells exposed to the CM. To the best of our knowledge, this study is the first to report that the secreted factors of hUCMSCs can cause MCF7 cell pyroptosis. Furthermore, it is the first to examine the global gene expression in MCF7 cells exposed to CM. These results will provide valuable information for further studies on the mechanism of MCF7 cell pyroptosis induced by the secreted factors of hUCMSCs. It will also help understand the effect of hUCMSCs on cell-based breast cancer therapy.

1. Introduction

Globally, breast cancer is the leading type of cancer among women, affecting approximately 2.1 million women [1] and resulting in 533,600 deaths in 2015 [2]. In China, there has been an increase in the incidence of breast cancer, and it is expected to account for 15% of new cancer cases [3]. Treatments for breast cancer include radiation therapy and surgery, followed by the administration of hormone-blocking agents, chemotherapy, and the use of monoclonal antibodies [4]. However, as breast cancers are classified by several grading systems, and as each of these can affect the prognosis and treatment response, a new effective treatment for breast cancer is necessary.

Pyroptosis is a type of programmed cell death and is distinct from the immunologically silent apoptotic cell death, which is caspase-1 dependent [5]. The activity of caspase-1 can result in the maturation of IL-1β and IL-18 and cleave gasdermin D to induce pore opening and pyroptosis [6]. Furthermore, inflammasomes are important for caspase-1 activity [7] and are composed of either AIM2-like receptor, tripartite motif-containing proteins, or the members of the

nucleotide-binding domain, leucine-rich containing (NLR) family. The morphological changes during pyroptosis include plasma membrane rupture, water influx, cellular swelling, osmotic lysis, and proinflammatory cellular content release [8]. Furthermore, pyroptosis is different from apoptosis in terms of DNA cleavage, nuclear condensation, and nuclear integrity [8, 9].

Mesenchymal stem cells (MSCs) have received extensive attention as a new tool for cancer treatment. Human umbilical cord mesenchymal stem cells (hUCMSCs) are isolated from the human umbilical cord Wharton's jelly. The effects of hUCMSCs on cancer have been extensively studied. Han et al. [10] reported that hUCMSCs can induce apoptosis in PC-3 prostate cancer cells. Leng et al. [11] found that hUCMSCs can inhibit breast cancer progression by inducing tumor cell death and suppressing angiogenesis in mice. However, the mechanism underlying hUCMSC-induced cancer cell death is not clear. As secreted factors of hUCMCSs can inhibit cancer progression by inducing tumor cell death [12, 13], in the present study, we aimed to evaluate the effect of secreted factors of hUCMSCs on the breast cancer cell line MCF7, and we performed RNA-sequencing (RNA-Seq) to explore the genes and pathways involved in this process.

2. Materials and Methods

2.1. Cell Culture. The breast cancer cell line MCF7 used in the present study was obtained from the Kunming Cell Bank of the Chinese Academy of Sciences. It was maintained in Dulbecco's modified Eagle medium (DMEM) [containing 4.5 g/L glucose, L-glutamine, and 110 mg/L sodium pyruvate (Gibco by Thermo Fisher Scientific™, Suzhou, China)] supplemented with 10% fetal bovine serum (FBS, Gibco by Life Technologies™, Australia), 100 mg/L penicillin, and 100 mg/L streptomycin (Gibco by Life Technologies™, NY, USA) at 37°C with 5% CO_2.

The hUCMSCs were obtained from the human umbilical cord Wharton's jelly by the tissue explant technique [14]. The umbilical cords were donated for study after informed patient consent and ethical approval by the Medical Ethics Committee of Yunnan University Medical School.

The hUCMSCs were cultured in Minimum Essential Medium Alpha Modification (αMEM, Hyclone by Thermo Scientific™, Beijing, China) supplemented with 10 ng/mL fibroblast growth factor basic protein (bFGF; Merck Millipore, Darmstadt, Germany), 100 mg/L penicillin, and 100 mg/L streptomycin at 37°C with 5% CO_2. The identity of hUCMSCs was confirmed by the expression of mesenchymal cell surface markers CD105, CD90, CD44, and CK18 and by the nonexpression of CD45, HLA-DR, and CD31 (Additional file 1). The hUCMSCs were used before the eighth passage.

2.2. Exposure of MCF7 Cells to hUCMSC-Conditioned Medium. The hUCMSCs were cultured in plastic flasks (25 cm^2, Corning, NY, USA). After 48 h (when the cells were approximately 90% confluent), the hUCMSCs cultured medium was collected and filter-sterilized using a 0.22 μm Millex-GP Filter Unit (Millipore, Carrigtwohill, Tullagreen, Ireland). MCF7 cells at a density of 10^5 cells/mL were seeded in 6-well plates (Corning, NY, USA) containing normal medium and cultured overnight. Subsequently, the medium was replaced with hUCMSC-conditioned medium (hUCMSC-CM). The hUCMSC-CM was prepared by gradually increasing the ratio of hUCMSC cultured medium to fresh medium (10% hUCMSC-cultured medium + 90% fresh medium, 20% hUCMSC-cultured medium + 80% fresh medium, 40% hUCMSC-cultured medium + 60% fresh medium, 60% hUCMSC-cultured medium + 40% fresh medium, 80% hUCMSC-cultured medium + 20% fresh medium, and 100% hUCMSC-cultured medium). The changes in MCF7 cell morphology were recorded and photographed on days 1, 2, 3, 4, and 5 using inverted phase contrast optics (LEICA DFC420C). The ratio of 80% hUCMSC-cultured medium and 20% fresh medium was chosen for further analysis as MCF7 cells exhibited obvious morphological changes and these changes were most synchronous in this medium.

2.3. MTS Analysis for Cell Viability. MCF7 cells were seeded at a seeding density of 5×10^3 cells/well in 96-well plates (Corning, NY, USA) containing normal medium and cultured overnight. Subsequently, the medium was replaced with hUCMSC-CM (treatment) and fresh medium (control). The cell viability rate was evaluated using the CellTiter 96 Aqueous One Solution Cell Proliferation Assay kit (Promega, USA) on days 1, 2, 3, 4, and 5 after the replacement of medium according to the protocol of the manufacturer. Briefly, before the assay, 20 μL of CellTiter 96 Aqueous One Solution Reagent was added into each well of the 96-well assay plate containing the samples in 100 μL of culture medium, and the plate was then incubated at 37°C with 5% CO_2. After 3 h, the absorbance was recorded at 490 nm.

2.4. Flow Cytometric Analysis for Cell Cycle. The control and MCF7 cells exposed to hUCMSC-CM for 48 h were collected after trypsin digestion without EDTA (Solarbio, Beijing, China) and fixed in ice-cold 70% ethanol overnight. The fixed cells were stained with 50 μg/mL propidium iodide (PI, CWBIAO, Beijing, China) in phosphate-buffered saline (PBS) containing 0.1% Triton X-100 and 50 μg/mL RNase and then analyzed using the CyFlow Space (Partec) and FloMax 2.82 software.

2.5. Annexin V-FITC/PI Analysis. The percent of apoptotic cells was determined using the Annexin V-FITC/PI Apoptosis Detection kit (CWBIO, Beijing, China). Briefly, the control and MCF7 cells exposed to hUCMSC-CM for 48 or 72 h were collected after trypsin digestion without EDTA and then washed with cold PBS and resuspended in binding buffer at a concentration of 10^6 cells/mL. The cells were incubated at 37°C with 5 μL of Annexin V-fluorescein isothiocyanate (FITC) and 10 μL of propidium iodide for 10 min and analyzed with the CyFlow Space (Partec) and FloMax 2.82 software.

2.6. Terminal Deoxynucleotidyl Transferase dUTP Nick-End Labeling (TUNEL) Assay. The fragmentation of DNA was analyzed using the DeadEnd fluorometric TUNEL assay kit

(KeyGEN BioTECH, Nanjing, China) according to the protocol of the manufacturer. The control and MCF7 cells exposed to hUCMSC-CM for 72 h were fixed in 4% methanol-free formaldehyde solution in PBS for 30 min at 4°C and treated with proteinase K for 30 min at 37°C. Subsequently, the cells were treated with terminal deoxyribonucleotidyl transferase (TdT) containing biotin-11-dUTP for 1 h at 37°C in the dark and then treated with streptavidin-fluorescein for 30 min at 37°C in the dark. Finally, the cells were added to the medium containing 4′,6-diamidino-2-phenylindole and visualized under inverted phase contrast optics (LEICA DFC420C) after 10 min.

2.7. Quantification of Secreted IL-1β by the ELISA. The quantification of IL-1β secreted by MCF7 cells was carried out using the Human IL-1β/IL-1f2 Valukine™ ELISA Kit (NOVUS, Taiwan, China) according to the instructions of the manufacturer. The media from control MCF7 and MCF7 exposed to hUCMSC-CM were collected on days 0, 1, 2, 3, 4, and 5 and stored at −80°C for the enzyme-linked immunosorbent assay (ELISA).

2.8. RNA Sequencing. The control and MCF7 cells exposed to hUCMSC-CM (10^6 cells/mL) were harvested (three biological replicates), and the total RNA was extracted using TRIzol™ reagent (Invitrogen, Carlsbad, USA). The RNA quality and quantity were determined using the RNA Nano 6000 Kit for the Agilent 2100 Bioanalyzer system, and the samples were stored at −80°C until further use. The total RNA (10 μg) of each sample was used to construct the cDNA libraries. A total of six samples were sequenced using the BGISEQ-500 platform.

2.9. Bioinformatics Analysis. The raw reads were filtered using the internal software SOAPnuke to obtain clean reads [15]. The clean reads were then mapped with the reference genome using HISAT [16]. Gene expression was calculated as the number of uniquely mapped reads per kilobase of exon fragments per million mappable reads (FPKM) with RSEM [17]. Based on gene expression, the differentially expressed genes (DEGs) were analyzed using the DEGseq algorithms [18]. For the analysis, a q value of ≤0.001 and an absolute value of $\log_2$ ratio ≥ 1 were used to verify the significance of differences in gene expression. Based on the DEGs, the pathway functional analysis was performed using the clusterProfiler package [19]. The enrichment analysis was carried out by the hypergeometric test with a threshold value of 0.05 based on the KEGG database.

2.10. Validation of Gene Expression by the Quantitative Real-Time Polymerase Chain Reaction. MCF7 cells were cultured in hUCMSC-CM, and after 48 h, the total RNA from the cells was extracted using TRIzol™ reagent (Invitrogen, Carlsbad, USA). The quality and quantity of RNA were determined using the Nano-300 (Allsheng). All samples were then treated with the PrimeScript™ RT Reagent Kit with gDNA Eraser (Takara, China) to synthesize the first-stand cDNA. The primer sequences were designed using the PrimerQuest Tool (http://www.idtdna.com/primerquest/Home/Index), and the sequences are presented in Table 1. The quantitative real-time polymerase chain reaction (q-PCR) was performed using the BIO-RAD CFX96™ Real-Time System using FastStart Universal SYBR Green Master (Roche, Mannheim, Germany). Relative quantification was performed by the comparative Ct ($2^{-\triangle\triangle Ct}$) method.

Table 1: Primer sequences for quantitative real-time polymerase chain reaction.

Primers	NCBI ID	Primer sequences
Bcl2	NM_000633.2	S: 5′ TTTCTCATGGCTGTCCTTCAG GGT 3′ A: 5′ AGGTCTGGCTTCATACCACAG GTT 3′
HIF1A	NM_001530.3	S: 5′ GTCTGCAACATGGAAGGTA TTG 3′ A: 5′ GCAGGTCATAGGTGGTTTCT 3′
NF-κB	NM_002502.5	S: 5′ GAAGATTGAGCGGCCTGTAA 3′ A: 5′ TGTCTTCCACCAGAGGGTA ATA 3′
BIRC3	NM_001165.4	S: 5′ CAAGCCAGTTACCCTCATC TAC 3′ A: 5′ CTGAATGGTCTTCTCCAGG TTC 3′

2.11. Statistical Analyses. The statistical analyses were performed using Microsoft excel 2007 and R 3.5.1, and graphs were drawn using the GraphPad Prism 5 software and R 3.5.1. P values <0.05 were considered statistically significant.

3. Results

3.1. Effects of hUCMSC-CM on MCF7 Morphology. We cultured MCF7 cells in different ratios of hUCMSC-cultured medium to fresh medium (Additional file 2). We found that even 10% hUCMSC-cultured medium and 90% fresh medium can cause MCF7 cells pore-induced plasma membrane invagination and then death. However, the number of dead cells was very small, no more than 50%. With an increase in the proportion of hUCMSC-cultured medium, the phenomenon of pore-induced plasma membrane invagination was more obvious and the number of dead cells increased. In the medium of 80% hUCMSC-cultured medium and 20% fresh medium, MCF7 cells showed obvious morphological changes and these changes were the most synchronous. Although MCF7 cells cultured in 100% hUCMSC-cultured medium have the same morphological changes and synchronization, the cells died too quickly. Therefore, we chose the ratio of 80% hUCMSC-cultured medium and 20% fresh medium for further analysis.

We observed a striking difference in the shape of MCF7 cells exposed to hUCMSC-CM and that of control MCF7 cells (Figure 1). The control MCF7 cells grew very well and continued to maintain their typical morphology, that is, the

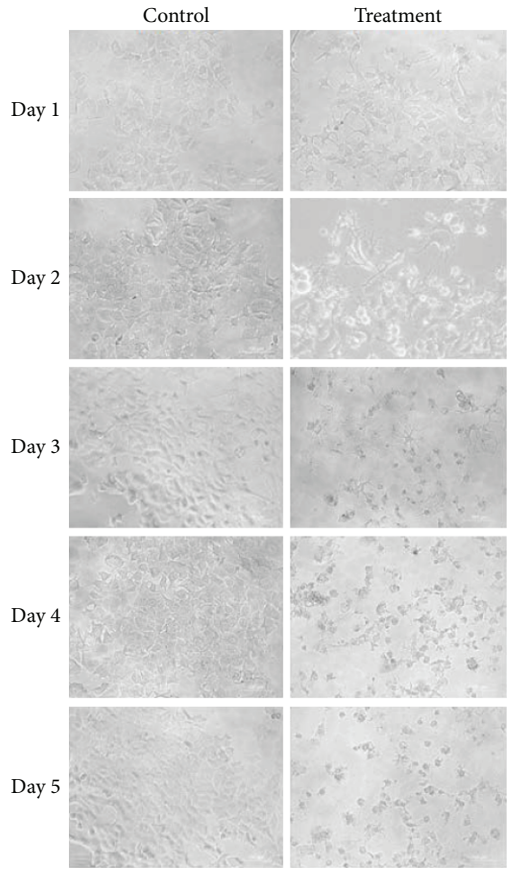

Figure 1: Comparative analysis of morphological changes in MCF7 cells exposed to hUCMSC-CM and control cells. Images were obtained on days 1, 2, 3, 4, and 5. Representative micrographs from at least three independent experiments are shown. All images were acquired at 20x magnification.

cell membrane was intact, the nucleus was not obvious, and the cells were polygonal and arranged orderly. However, MCF7 cells exposed to hUCMSC-CM gradually died, that is, the cells exhibited pore-induced plasma membrane invagination but still mainly intact at 24 h after the replacement of medium, and then the cells exhibited swelling at 48 h, and then the plasma membrane showed obvious ruptures, but the nucleus remained condense and the nuclear integrity was not compromised at 72 h.

3.2. Secreted Factors of hUCMSCs Caused MCF7 Cell Death but Did Not Change the Cell Cycle Significantly. We determined the cell viability daily for 5 d after treatment. Compared with that of the control cells, the viability of MCF7 cells exposed to hUCMSC-CM decreased marginally on the first day and then decreased continually in the following days (Figure 2(a)). To verify whether the decrease in cell viability was caused by cell cycle arrest, the cell cycle of MCF7 cells at 48 h after the exposure to hUCMSC-CM was evaluated. The hUCMSC-CM-treated cells showed a marginal decrease in the G0/G1 ($51.14 \pm 7.27\%$), S ($9.10 \pm 5.01\%$), and G2/M phases ($10.45 \pm 2.80\%$) when compared with those of the control cells ($55.96 \pm 11.69\%$, $14.01 \pm 4.58\%$, and $21.73 \pm 8.90\%$, respectively) (Figure 2(b)); these cell cycle changes were not significant (Figure 2(c)). Therefore, the decrease in cell viability was due to an increase in the number of dead cells but not due to cell cycle arrest.

3.3. Secreted Factors of hUCMSCs Caused MCF7 Cells Death through the Pyroptosis Pathway. To elucidate how the secreted factors of hUCMSCs caused MCF7 cell death, we performed the Annexin V-FITC/PI analysis. The results showed that in the control cells, there was an increase in the number of early apoptotic and late apoptotic cells with time ($P < 0.05$). In the hUCMSC-CM-treated cells, the results showed that there was no obvious change in the FITC+/PI− quadrant, but there was an increase in the FITC+/PI+ quadrant, from 1.96% at 24 h to 9.26% at 72 h ($q < 0.05$). However, significant increases occurred in the FITC−/PI+ quadrant. It was only 2.31% at 24 h after the replacement of medium, which increased to 13.76% at 48 h and 71.12% at 72 h (Figure 3). Therefore, we conclude that the death of MCF7 cells exposed to hUCMSC-CM was not mainly mediated by apoptosis, and the increases occurred in the FITC−/PI+ quadrant due to the rupture of plasma membrane.

As the morphological changes in MCF7 cells exposed to hUCMSC-CM were similar to those of pyroptotic cells described in the literature and the pyroptotic cells can be stained by PI [8], we further performed TUNEL staining and quantified secreted IL-1β to verify MCF7 cell death through the pyroptosis pathway. TUNEL staining labels DNA fragments. Like apoptotic cells, pyroptotic cells undergo DNA fragmentation and is stained positively with TUNEL [20]. The results showed that the control cells were negative for TUNEL staining, but MCF7 cells exposed to hUCMSC-CM were TUNEL positive (Figure 4(a)). The ELISA results showed that there was only a negligible amount of IL-1β in the medium of control cells (no more than 5 pg/mL), which gradually decreased. However, in the medium of hUCMSC-CM-treated cells, the initial concentration of IL-1β (25 pg/mL) was higher than that of the control. Subsequently, the concentration of IL-1β gradually increased, which doubled on day 5 (Figure 4(b)). These results suggest that the normal MCF7 cells do not secrete IL-1β, but MCF7 cells exposed to hUCMSC-CM secrete IL-1β, which is characteristic of pyroptotic cells [21]. Therefore, we conclude that the secreted factors of hUCMSCs caused MCF7 cell death through the pyroptosis pathway.

3.4. DEGs Were Analyzed and 14 Significant Pathways Were Detected according to RNA-Seq Data. The RNA samples from MCF7 cells, both control and treated cells (the data were obtained from three biological replications), were sequenced using the BGISEQ-500 platform. On an average, approximately 23.99 Mb reads per sample were generated and 18,174 genes were detected. Furthermore, 23.93 Mb clean reads were obtained after filtering the data. The average mapping ratio of clean reads with reference human genome was 94.63%, and the uniformity of the mapping results for each sample suggested that the samples were comparable.

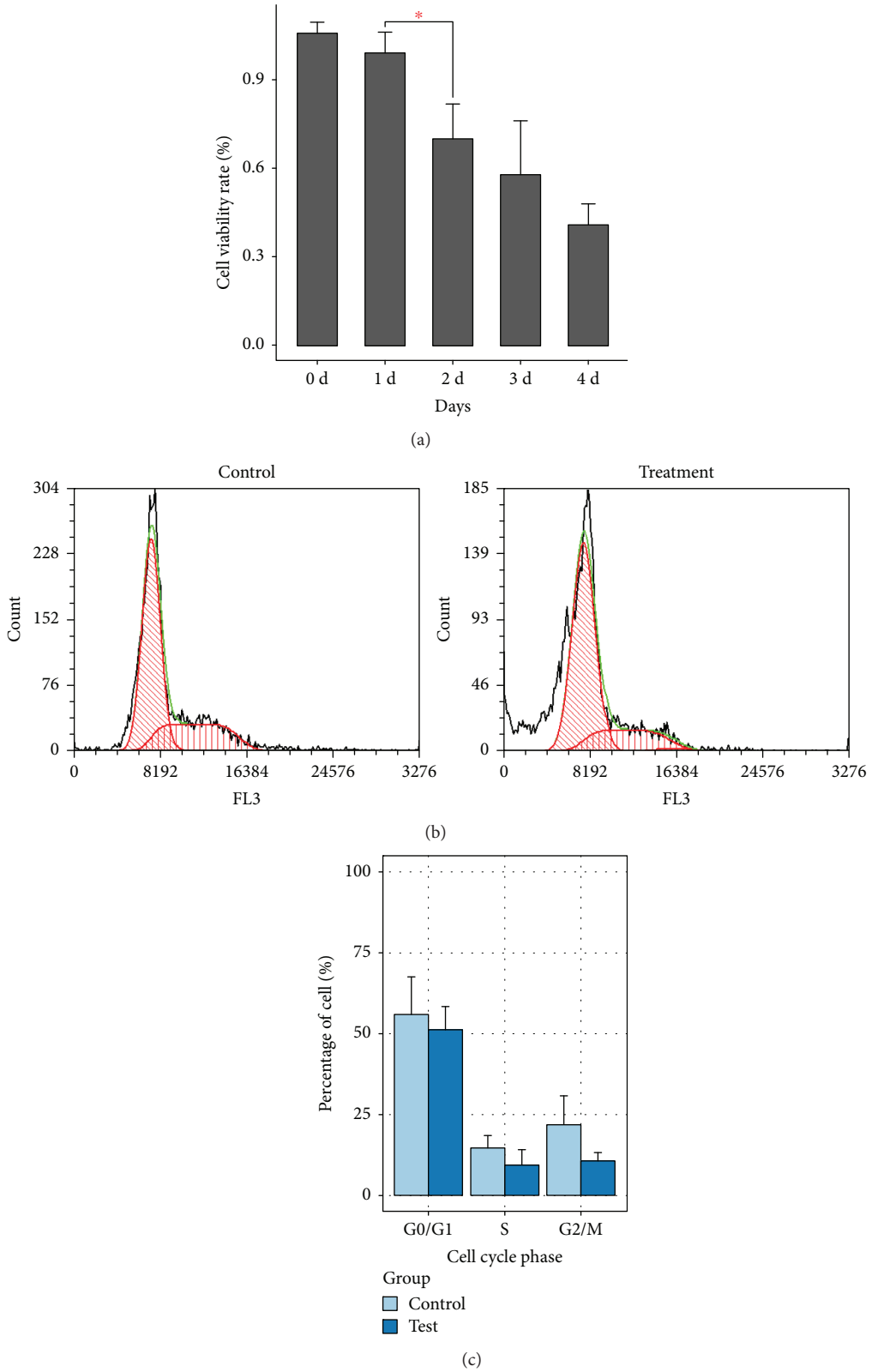

Figure 2: Cell viability and cell cycle analyses of MCF7 cells exposed to hUCMSC-CM (a) Effect of hUCMSC-CM on cell viability of MCF7 cells. x-axis represents days MCF7 cells exposed to hUCMSC-CM. y-axis represents cell viability rate. Cell viability rate = (the average OD of treatment group/the average OD of control group)*100%. Results were measured using MTS proliferation method. Experiments were carried out in triplicate and repeated 3 times. $^*P < 0.05$. (b) Flow cytometric analysis for cell cycle of MCF7 cells exposed to hUCMSC-CM. Treatment cells were collected after 48 h, cultured in hUCMSC-CM, and stained with PI. (c) Quantitative analysis for cell cycle. Data were presented as mean ± SD of three independent experiments. hUCMSCs: human umbilical cord mesenchymal stem cells.

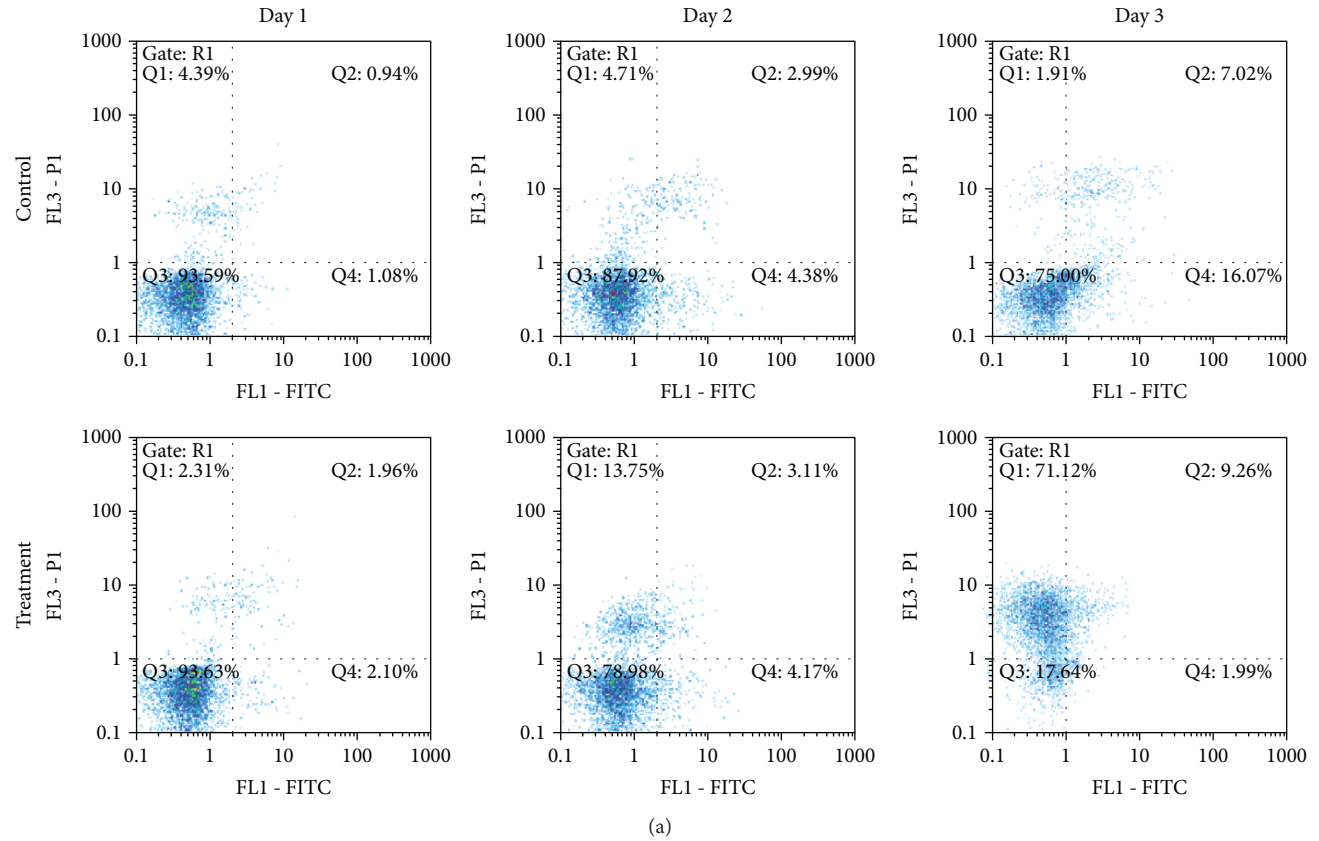

(a)

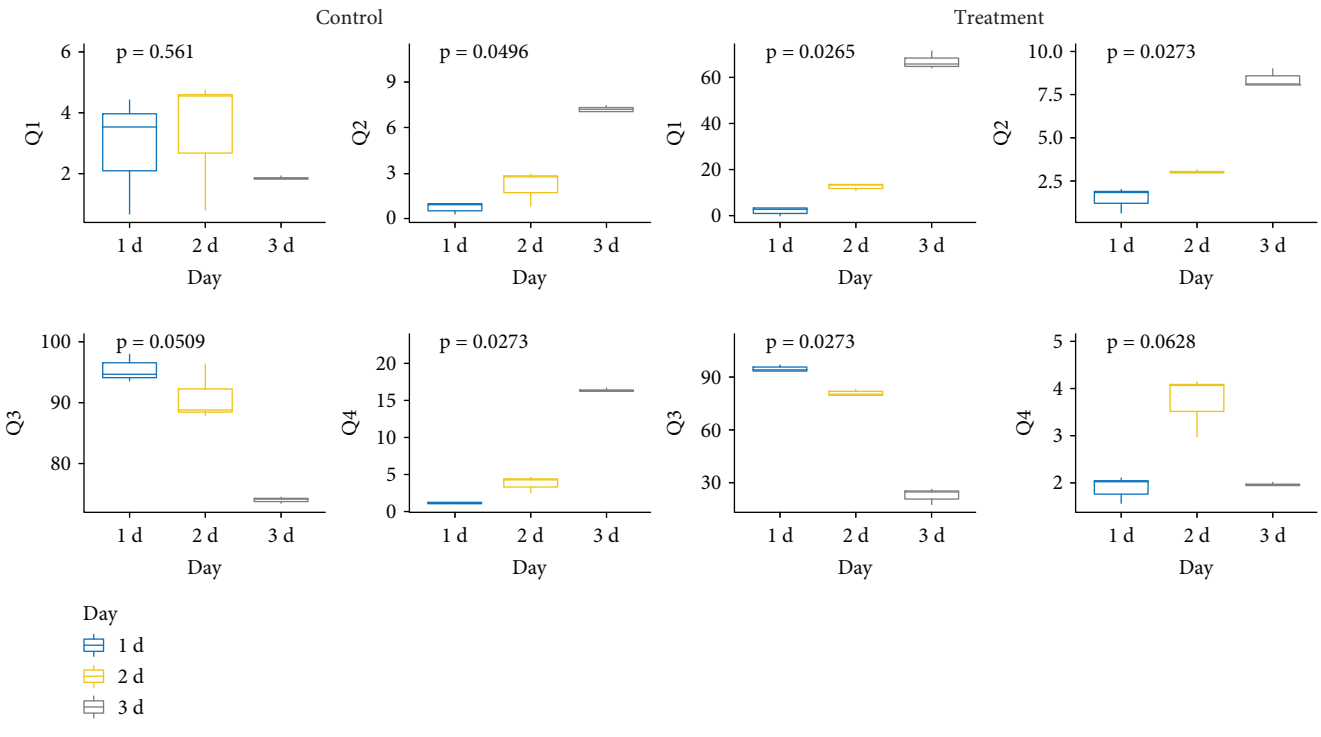

(b)

Figure 3: Flow cytometric analysis using Annexin V-FITC/PI. (a) Flow cytometry results of Annexin V-FITC/PI staining. Cells were collected on days 1, 2, and 3 after being exposed to hUCMSC-CM, respectively, and stained with 5 μL each of Annexin V-FITC and 10 μL PI. (b) Quantitative analysis for the Annexin V-FITC/PI results. Data were presented as mean ± SD of three independent experiments.

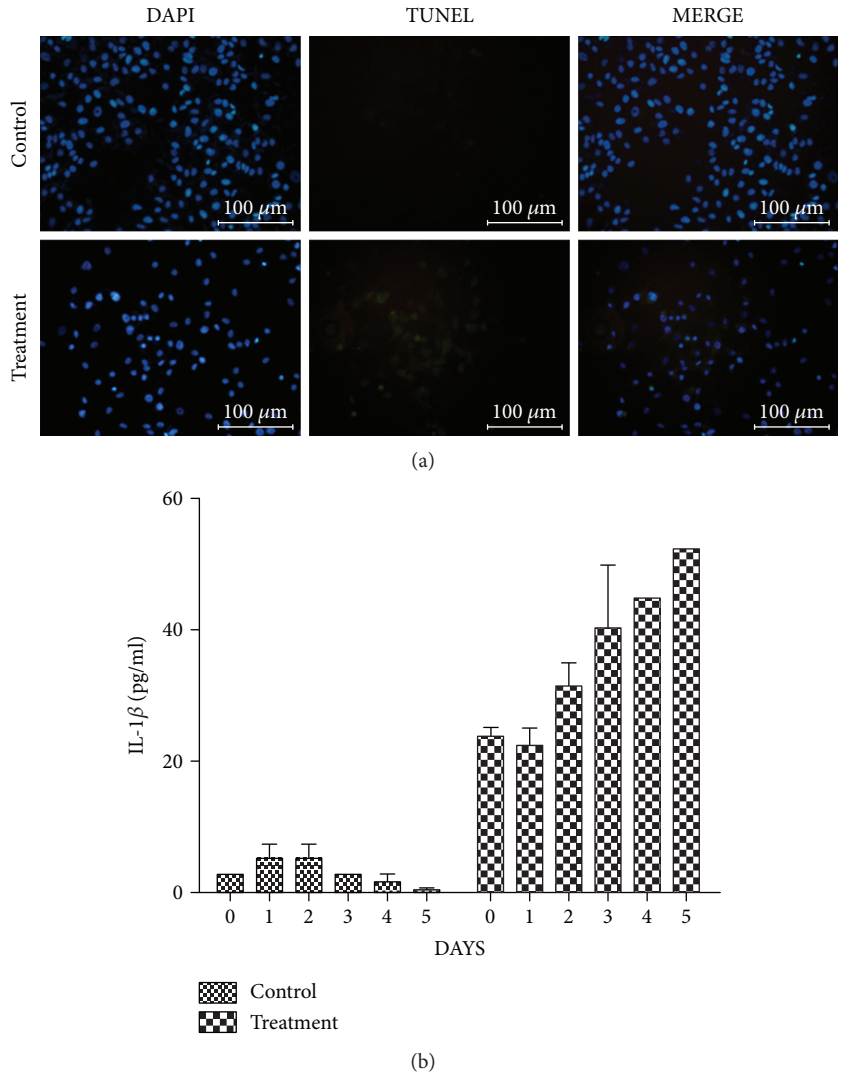

Figure 4: MCF7 cell assessment using TUNEL staining and secreted IL1β assay. (a) TUNEL assay for MCF7 cells at 72 h following exposure to hUCMSC-CM. (b) The concentration of secreted IL1β from MCF7 cells on days 0, 1, 2, 3, 4, and 5 following exposure to hUCMSC-CM. The experiment was repeated three times. $n = 3$.

In order to find DEGs, gene expression of each sample was calculated as FPKM with RSEM and the DEGs were identified using the DEGseq algorithms. A total of 1822 up- and 775 downregulated genes were identified ($|\log_2$ (fold change)$| > 1$, q value ≤ 0.001). The genes *NLRP1*, *CASP4*, *TLR2*, *TLR6*, *NFκB*, *HIF1A*, and *BIRC3* were significantly upregulated, and the *Bcl2* gene was significantly downregulated (Table 2). To validate gene expression, we randomly chose the upregulated genes *HIF-1A*, *NF-κB*, and *BIRC3* and the downregulated gene *Bcl2* to do the q-PCR. The specificity of q-PCR primers was confirmed by regular PCR (Additional file 3). Hypoxia-inducible factor1-alpha (HIF-1A) is a master transcriptional regulator of cellular and developmental response to hypoxia [22]. Nuclear factor kappa-light-chain-enhancer of activated B cells (NF-κB) is a protein complex that controls transcription of DNA, cytokine production, and cell survival. It is involved in cellular responses to stimuli and plays a key role in regulating the immune response to infection [23]. Baculoviral IAP repeat-containing protein 3 (BIRC3) is a member of the inhibitor of apoptosis family that inhibits apoptosis by interfering with the activation of caspases [24]. The *Bcl2* gene is a member of the *Bcl2* family of regulator proteins that regulate cell death, by either inducing (proapoptotic) or inhibiting (antiapoptotic) apoptosis [25]. The q-PCR results showed that differential gene expression was consistent with the RNA-Seq results (Figure 5(a)).

To identify the associated biological functions, the DEGs were subjected to the KEGG pathway analysis. The pathway functional enrichment results (Figure 5(b)) showed that there are 14 significant pathways ($P < 0.05$), including alcoholism, systemic lupus erythematosus, estrogen signaling pathway, *Staphylococcus aureus* infection, AGE-RAGE signaling pathway in diabetic complications,

Table 2: List of differentially expressed genes in MCF7 cells exposed to hUCMSC-CM.

Symbol	Gene ID	Length (bp)	Control expression	Treatment expression	log2 ratio (treatment/control)	q value
NLRP1	22,861	5491	20	102	2.35	8.40E-15
CASP4	837	1319	75	253	1.75	7.10E-24
TLR2	7097	8147	61.43	142.99	1.22	5.10E-09
TLR6	10,333	6683	60.31	124.52	1.04	1.12E-06
NFκB	4791	3067	6298	14,367	1.19	0
HIF1A	3091	4070	5694	19,529	1.78	0
BIRC3	330	5174	227.6	2297.57	3.33	0
Bcl2	596	5191	1546.17	383	−2.02	1.35E-164

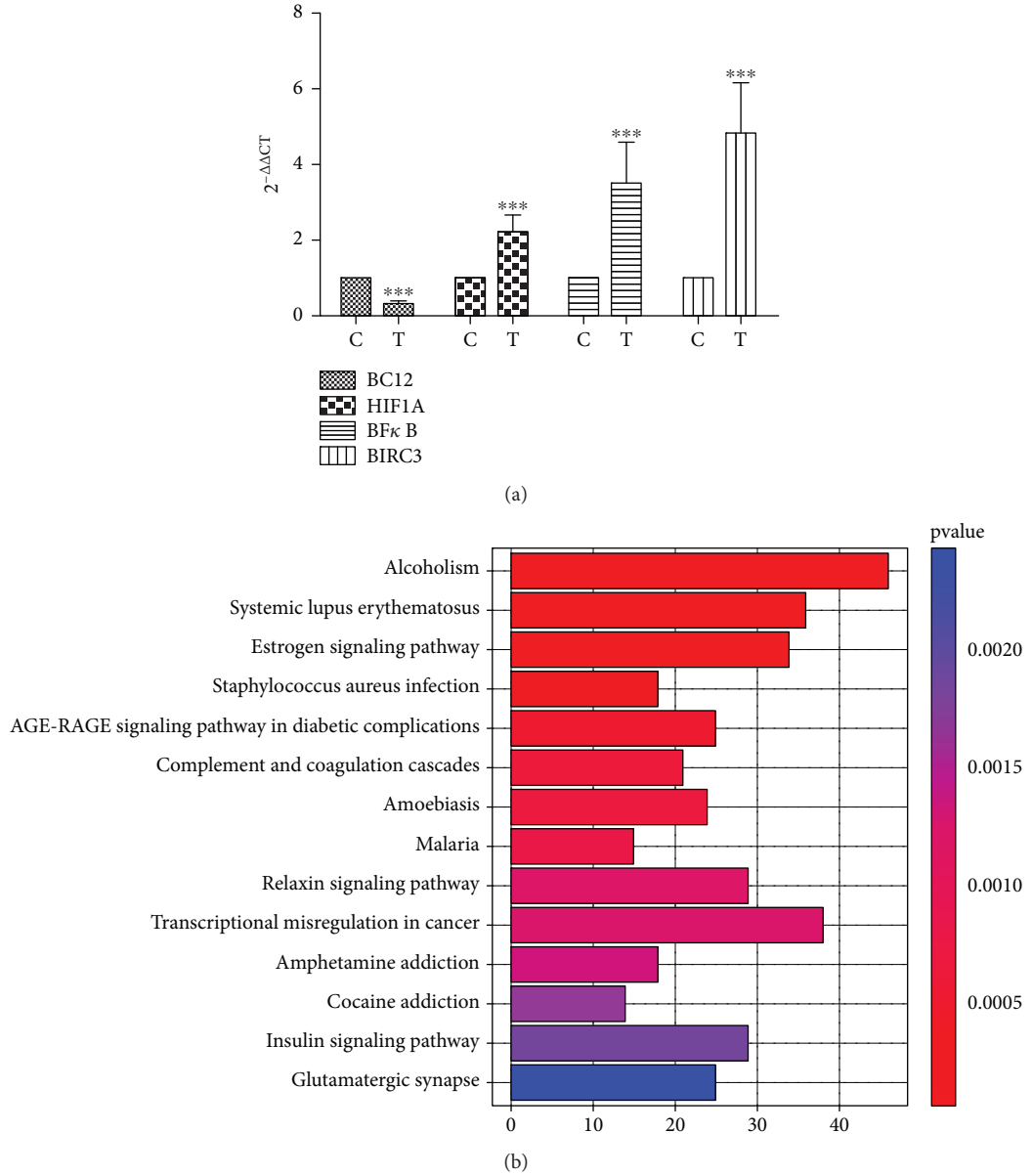

Figure 5: Gene expression and KEGG pathway analysis. (a) Validation of selected genes from DEGs by q-PCR. Data are presented as Ct ($2^{-\Delta\Delta Ct}$) relative to control. Data are presented as mean ± S.D. $n = 3$. $^{*}P < 0.05$, $^{**}P < 0.01$, and $^{***}P < 0.001$. C: control group; T: treatment group. (b) The significant KEGG pathways ($P < 0.001$). x-axis represents number of genes. y-axis represents pathways.

complement and coagulation cascades, amoebiasis, malaria, relaxin signaling pathway, transcriptional misregulation in cancer, amphetamine addiction, cocaine addiction, insulin signaling pathway, and glutamatergic synapse.

4. Discussion

The MSCs are multipotent stromal cells, which can be obtained from the bone marrow [26], adipose tissue [27], umbilical cord tissue, and umbilical cord blood [28]. In terms of therapeutic applications, the hUCMSCs have some beneficial properties when compared with those of other MSCs. These properties include large-cell number at harvest, low immunogenicity, propagated without feeder cells, stored after birth without significant risks to the donor, and absence of ethical dispute. In vivo, the MSCs exhibit oriented migration to the site of tumor, and they inhibit tumor growth and metastasis [11, 29, 30]. Therefore, the MSCs have been considered potential biological vehicles for tumor-targeted delivery of therapeutic genes [31–33]. In vitro, the effects of MSCs on cancer cells have been studied either by coculturing cancer cells with MSCs or by culturing cancer cells in CM, prepared using fresh medium and medium in which MSCs were cultured for several days. In the present study, we cultured MCF7 cells in hUCMSC-CM to study their effects. To the best of our knowledge, we report for the first time that the secreted factors of hUCMSCs can induce MCF7 cell pyroptosis. We also examined gene expression in MCF7 cells exposed to CM by RNA-Seq.

The changes in the morphology of MCF7 cells exposed to hUCMSC-CM revealed the characteristics of pyroptosis, that is, they had a permeable membrane which was initially intact, which was followed by cell swelling, rapid expansion, and finally rupture [34]. During this process, the nucleus of MCF7 cells exposed to hUCMSC-CM condensed and the DNA fragmented. As the plasma membrane ruptured, the cells were detected by PI staining [8]. As apoptotic cells, the pyroptosis cells were TUNEL positive [20]. And also, we found an obvious increase in the amount of IL-1β in the medium of MCF7 cells exposed to hUCMSC-CM. To summarize, we considered that MCF7 cells exposed to hUCMSC-CM were undergoing pyroptosis [21]. In the present study, MCF7 cells exposed to hUCMSC-CM showed swelling at 48 h and ruptured at 72 h. Therefore, the viability of MCF7 cells decreased 48 h after the replacement of medium. The treated cells showed no obvious changes in cell cycle. This indicates that hUCMSC-CM cannot arrest the cell cycle of MCF7 cells.

The RNA-Seq results revealed that 1822 and 775 genes were up- and downregulated in MCF7 cells exposed to hUCMSC-CM, respectively, compared with those of the control MCF7 cells. According to the KEGG analysis, we identified 14 significant pathways. We further classified these pathways according to the KEGG PATHWAY Database (http://www.genome.jp/kegg/pathway.html). We found that they are mainly related to the immune system, endocrine system, nervous system, and the diseases associated with these systems. The results showed that certain substances in hUCMSC-CM could cause inflammatory reaction and immune response in MCF7 cells. Whereas, some substances can cause endocrine system disorder, which is mainly induced by estrogen, relaxin, or glycometabolism, and some other substances can cause behavioral responses in MCF7 cells on exposure to addictive substances.

Interestingly, we found that the *NLRP1* gene was significantly upregulated. Nucleotide-binding, leucine-rich repeat pyrin domain-containing protein 1 (*NLRP1*) is a member of the NOD-like receptor (NLR) family and plays an important role in cell pyroptosis. As an important natural immune molecule, NLRP1 can identify pathogen-associated molecular patterns and risk molecular models as a pattern recognition receptor [35]. In humans, *NLRP1* has the ability to activate *caspase-1* by interacting directly with procaspase-1 or by recruiting adaptor protein ASC and then recruiting procaspase-1 to form a complex known as inflammasome [36]. Activated *caspase-1* can help in the maturation of pro-IL-1β and pro-IL-18 [37], causing inflammation to promote pyroptosis [38]. According to the RNA-Seq results, *caspase-1* was neither up- nor downregulated. This indicates that *caspase-1* may affect pyroptosis by activating procaspase-1 and not by increasing the transcriptional product. However, *caspase-4*, a member of a cysteine protease family called caspases, was significantly upregulated. In humans, *caspase-4* functions as the receptor of lipopolysaccharide (LPS) [39], which is found in the outer membrane of gram-negative bacteria and can induce pyroptosis [6]. When LPS binds to caspase-4, caspase-4 undergoes oligomerization, leading to caspase-1-induced maturation of IL-1β and IL-18, thereby mediating pyroptosis [40]. The significant upregulation of *caspase-4* shows that *caspase-4* might play an important role in the inflammation and pyroptosis of MCF7 cells induced by hUCMSC-CM. From the KEGG analysis, we found that systemic lupus erythematosus (SLE) is the second significant pathway. It is an autoimmune disease and is confirmed to be associated with the NLR family members, such as *NLRP1* and *NLRP3*. We also found that the assembly of inflammasomes is induced by NLR [41, 42]. Excessive inflammasome activation can promote excessive release of IL-1β and IL-18, causing autoinflammatory disorders and the subsequent development of autoimmune diseases, such as SLE [42]. Therefore, the enrichment of this pathway confirms that when MCF7 cells are cultured in hUCMSC-CM, they are subjected to inflammation.

TLR2, the other receptor related to initial immunization, was significantly upregulated. TLR2 is a member of the Toll-like receptor (TLR) family. It is expressed on the surface of certain cells, recognizes pathogen-associated molecular patterns and mediates the production of cytokines necessary for the development of effective immunity [43]. TLR2 can bind to a wide range of exogenous ligands, including lipoproteins, lipoteichoic acid, peptidoglycan, zymosan, lipoarabinomannan, glycosylphosphatidylinositol, phenol-soluble modulin, and glycolipids [44], thereby mediating host immune response against gram-positive bacteria [45]. This function of TLR2 is unique in its ability to form TLR2/TLR1 or TLR2/TLR6 heterodimer [46]. The TLR2-ligand interactions activate MyD88 signaling, which then activates proinflammatory transcription factors, such as

NF-κB and the PI3K/AKT pathway [47]. NF-κB translocates into the nucleus to regulate the production of inflammatory cytokines, such as IL-1β, IL-6, IL-8, and IL-12 [44]. The stimulation by TLR2-ligands alone without a second signal can promote IL-1β release but cannot induce cell death [48]. From the results of RNA-Seq, we also found that the expression of TLR6 and NF-κB was significantly upregulated. This indicates that the inflammation caused by TLR2 is not the major pathway that induces MCF7 cell pyroptosis but might play an important role in response to the stimulation of secreted factors of hUCMSCs and assist in MCF7 cell death. From the KEGG analysis, *Staphylococcus aureus* infection was found to be the fourth significant pathway. *Staphylococcus aureus* is a gram-positive bacterium and can be recognized by *TLR2*, indicating that *TLR2* is indeed an important gene in the death of MCF7 cells exposed to hUCMSC-CM.

Hypoxia-inducible factor1-alpha (HIF-1A) is a master transcriptional regulator of cellular and developmental response to hypoxia [22]. The activity of HIF-1A is directly regulated by cellular oxygen levels [49], and under hypoxic condition, *HIF-1A* transcription is often significantly upregulated [50, 51]. According to the RNA-Seq result, the expression of *HIF-1A* was upregulated. This indicates that when MCF7 cells are cultured in hUCMSC-CM, a hypoxic environment is created within the cells. Jorgensen et al. [34] found mitochondria with collapsed cristae in pyroptotic cells. Mitochondria are the major site of ROS production. They have a four-layer structure, and ROS generation mainly occurs at the electron transport chain (ETC) located on the inner mitochondrial membrane, which folds inward to form a ridge-like shape and called cristae, during the process of oxidative phosphorylation (OXPHOS) [52]. Therefore, the collapsed cristae could lead to reduction in ROS production [53], thereby causing hypoxia in cells. In fact, hypoxia causes pyroptosis. Wu et al. found hypoxia-reoxygenation injury can induce pyroptosis in HK2 cells [54]. In addition, Qiu et al. demonstrated that stimulation of H9C2 cardiomyocytes with high glucose and hypoxia/reoxygenation increased NLRP3 inflammasome activation and pyroptosis [55]. Furthermore, as autophagic suppression of ROS can limit ROS-modulated caspase-1 activation to inhibit inflammasome activity [56], hypoxia also might be a negative feedback mechanism in response to high inflammation within MCF7 cells. Recent studies have demonstrated that the expression of *HIF-1A* is regulated by the NF-κB [57], and *HIF-1A* restricts NF-κB transcriptional activity, thereby preventing inflammation and controlling the innate immune response [58, 59]. This indicates that the upregulation of *HIF-1A* in MCF7 cells exposed to hUCMSC-CM might be a negative feedback mechanism activated in response to high inflammation inside MCF7 cells.

There are a few limitations to this study. We selected only one breast cancer cell line to validate the expression of key genes. The use of MCF7 cells started in 1973, and they are widely used due to their exquisite hormone sensitivity [60]. However, the breast cancer cell lines have different subtypes, in which the expression of key genes should be validated. Furthermore, we only studied gene expression in pyroptotic MCF7 cells by RNA-Seq. Further analysis should be carried out for a deeper understanding.

5. Conclusions

The present study demonstrates that the secreted factors of hUCMSCs can promote inflammatory response and pyroptosis in MCF7 cells. Therefore, the inflammation- and hypoxia-related genes and pathways play an important role in MCF7 cell pyroptosis. Although further studies are necessary to characterize the interaction of these genes and pathways, our data provides valuable data for further studies in this direction.

Data Availability

The datasets generated and analyzed in the current study are included in within the article. The raw data of the RNA-Seq analysis will be provided by the corresponding author on request.

Conflicts of Interest

The authors declare that there is no conflict of interest regarding the publication of this article.

Authors' Contributions

Yang Jiao, Hongbo Zhao, and Guodong Chen have contributed equally to this work.

Acknowledgments

We thank the Department of Obstetrics and Gynecology of the Chenggong branch of Yan'an Hospital of Kunming for helping in the collection of human umbilical cord. Also, we would like to thank Editage (http://www.editage.com) for English language editing. This work was supported by the Major Science and Technology Projects of Yunnan Province (grant number 2018ZF007-05), the National Natural Science Foundation of China (grant number 81560043), the Foreign Cooperation Project of Yunnan Province (grant number 2018IA045), and the Joint Special Funds for the Department of Science and Technology of Yunnan Province-Kunming Medical University (grant number 2017FE468 (-011)).

Supplementary Materials

Supplementary 1. Additional file 1: flow cytometry analysis of mesenchymal stem cells surface markers. The flow cytometry analysis shows expression of CD105, CD90, CD44, and CK18 and nonexpression of CD 45, HLA-DR, and CD31 on the hUCMSC surface.

Supplementary 2. Additional file 2: confirm the phenotype using gradually increased ratio of hUCMSC-medium to fresh medium. Control: 100% fresh medium, treatment 1: 10% hUCMSC-medium + 90% fresh medium, treatment 2: 20% hUCMSC-medium + 80% fresh medium, treatment 3: 40%

hUCMSC-medium + 60% fresh medium, treatment 4: 60% hUCMSC-medium + 40% fresh medium, treatment 5: 80% hUCMSC-medium + 20% fresh medium, treatment 6: 100% hUCMSC-medium.

Supplementary 3. Additional file 3: confirm the specificity of q-PCR primers using regular PCR. DNA marker: DL2000.

References

[1] T. Vos, C. Allen, M. Arora et al., "Global, regional, and national incidence, prevalence, and years lived with disability for 310 diseases and injuries, 1990–2015: a systematic analysis for the Global Burden of Disease Study 2015," *The Lancet*, vol. 388, no. 10053, pp. 1545–1602, 2016.

[2] H. Wang, M. Naghavi, C. Allen et al., "Global, regional, and national life expectancy, all-cause mortality, and cause-specific mortality for 249 causes of death, 1980–2015: a systematic analysis for the Global Burden of Disease Study 2015," *The Lancet*, vol. 388, no. 10053, pp. 1459–1544, 2016.

[3] W. Chen, R. Zheng, P. D. Baade et al., "Cancer statistics in China, 2015," *CA: a Cancer Journal for Clinicians*, vol. 66, no. 2, pp. 115–132, 2016.

[4] M. D. Holmes, W. Y. Chen, L. Li, E. Hertzmark, D. Spiegelman, and S. E. Hankinson, "Aspirin intake and survival after breast cancer," *Journal of Clinical Oncology*, vol. 28, no. 9, pp. 1467–1472, 2010.

[5] T. Bergsbaken, S. L. Fink, and B. T. Cookson, "Pyroptosis: host cell death and inflammation," *Nature Reviews Microbiology*, vol. 7, no. 2, pp. 99–109, 2009.

[6] N. Kayagaki, I. B. Stowe, B. L. Lee et al., "Caspase-11 cleaves gasdermin D for non-canonical inflammasome signalling," *Nature*, vol. 526, no. 7575, pp. 666–671, 2015.

[7] P. Broz and V. M. Dixit, "Inflammasomes: mechanism of assembly, regulation and signalling," *Nature Reviews Immunology*, vol. 16, no. 7, pp. 407–420, 2016.

[8] S. L. Fink and B. T. Cookson, "Caspase-1-dependent pore formation during pyroptosis leads to osmotic lysis of infected host macrophages," *Cellular Microbiology*, vol. 8, no. 11, pp. 1812–1825, 2006.

[9] A. B. Molofsky, B. G. Byrne, N. N. Whitfield et al., "Cytosolic recognition of flagellin by mouse macrophages restricts Legionella pneumophila infection," *Journal of Experimental Medicine*, vol. 203, no. 4, pp. 1093–1104, 2006.

[10] I. Han, M. Yun, E. O. Kim, B. Kim, M. H. Jung, and S. H. Kim, "Umbilical cord tissue-derived mesenchymal stem cells induce apoptosis in PC-3 prostate cancer cells through activation of JNK and downregulation of PI3K/AKT signaling," *Stem Cell Research & Therapy*, vol. 5, no. 2, p. 54, 2014.

[11] L. Leng, Y. Wang, N. He et al., "Molecular imaging for assessment of mesenchymal stem cells mediated breast cancer therapy," *Biomaterials*, vol. 35, no. 19, pp. 5162–5170, 2014.

[12] K. Gauthaman, F. C. Yee, S. Cheyyatraivendran, A. Biswas, M. Choolani, and A. Bongso, "Human umbilical cord Wharton's jelly stem cell (hWJSC) extracts inhibit cancer cell growth in vitro," *Journal of Cellular Biochemistry*, vol. 113, no. 6, pp. 2027–2039, 2012.

[13] L. Mercatali, F. La Manna, G. Miserocchi et al., "Tumor-stroma crosstalk in bone tissue: the osteoclastogenic potential of a breast cancer cell line in a co-culture system and the role of EGFR inhibition," *International Journal of Molecular Sciences*, vol. 18, no. 8, 2017.

[14] O. K. Lee, T. K. Kuo, W. M. Chen, K. D. Lee, S. L. Hsieh, and T. H. Chen, "Isolation of multipotent mesenchymal stem cells from umbilical cord blood," *Blood*, vol. 103, no. 5, pp. 1669–1675, 2004.

[15] Y. Chen, Y. Chen, C. Shi et al., "SOAPnuke: a MapReduce acceleration-supported software for integrated quality control and preprocessing of high-throughput sequencing data," *GigaScience*, vol. 7, no. 1, pp. 1–6, 2018.

[16] D. Kim, B. Langmead, and S. L. Salzberg, "HISAT: a fast spliced aligner with low memory requirements," *Nature Methods*, vol. 12, no. 4, pp. 357–360, 2015.

[17] B. Li and C. N. Dewey, "RSEM: accurate transcript quantification from RNA-Seq data with or without a reference genome," *BMC Bioinformatics*, vol. 12, no. 1, p. 323, 2011.

[18] L. Wang, Z. Feng, X. Wang, X. Wang, and X. Zhang, "DEGseq: an R package for identifying differentially expressed genes from RNA-seq data," *Bioinformatics*, vol. 26, no. 1, pp. 136–138, 2010.

[19] G. Yu, L. G. Wang, Y. Han, and Q. Y. He, "clusterProfiler: an R package for comparing biological themes among gene clusters," *OMICS: A Journal of Integrative Biology*, vol. 16, no. 5, pp. 284–287, 2012.

[20] K. Labbe and M. Saleh, "Cell death in the host response to infection," *Cell Death and Differentiation*, vol. 15, no. 9, pp. 1339–1349, 2008.

[21] I. Jorgensen, M. Rayamajhi, and E. A. Miao, "Programmed cell death as a defence against infection," *Nature Reviews Immunology*, vol. 17, no. 3, pp. 151–164, 2017.

[22] N. V. Iyer, L. E. Kotch, F. Agani et al., "Cellular and developmental control of O2 homeostasis by hypoxia-inducible factor 1 alpha," *Genes and Development*, vol. 12, no. 2, pp. 149–162, 1998.

[23] T. D. Gilmore, "Introduction to NF-kappaB: players, pathways, perspectives," *Oncogene*, vol. 25, no. 51, pp. 6680–6684, 2006.

[24] P. Listen, N. Roy, K. Tamai et al., "Suppression of apoptosis in mammalian cells by NAIP and a related family of IAP genes," *Nature*, vol. 379, no. 6563, pp. 349–353, 1996.

[25] Y. Tsujimoto, L. Finger, J. Yunis, P. Nowell, and C. Croce, "Cloning of the chromosome breakpoint of neoplastic B cells with the t(14;18) chromosome translocation," *Science*, vol. 226, no. 4678, pp. 1097–1099, 1984.

[26] C. A. Gregory, D. J. Prockop, and J. L. Spees, "Non-hematopoietic bone marrow stem cells: molecular control of expansion and differentiation," *Experimental Cell Research*, vol. 306, no. 2, pp. 330–335, 2005.

[27] B. Bunnell, M. Flaat, C. Gagliardi, B. Patel, and C. Ripoll, "Adipose-derived stem cells: isolation, expansion and differentiation," *Methods*, vol. 45, no. 2, pp. 115–120, 2008.

[28] D. Thierry, R. Traineau, M. Adam et al., "Hematopoietic stem cell potential from umbilical cord blood," *Nouvelle Revue Française d'Hématologie*, vol. 32, no. 6, pp. 439-440, 1990.

[29] R. S. Rachakatla, F. Marini, M. L. Weiss, M. Tamura, and D. Troyer, "Development of human umbilical cord matrix stem cell-based gene therapy for experimental lung tumors," *Cancer Gene Therapy*, vol. 14, no. 10, pp. 828–835, 2007.

[30] R. J. Tang, S. N. Shen, X. Y. Zhao et al., "Mesenchymal stem cells-regulated Treg cells suppress colitis-associated colorectal cancer," *Stem Cell Research & Therapy*, vol. 6, no. 1, p. 71, 2015.

[31] C. J. Shen, T. F. Chan, C. C. Chen, Y. C. Hsu, C. Y. Long, and C. S. Lai, "Human umbilical cord matrix-derived stem cells expressing interferon-β gene inhibit breast cancer cells via apoptosis," *Oncotarget*, vol. 7, no. 23, pp. 34172–34179, 2016.

[32] Y. Yu, Y. Liu, C. Zong et al., "Mesenchymal stem cells with Sirt1 overexpression suppress breast tumor growth via chemokine-dependent natural killer cells recruitment," *Scientific Reports*, vol. 6, no. 1, 2016.

[33] P. F. Yu, Y. Huang, Y. Y. Han et al., *Oncogene*, vol. 36, no. 4, pp. 482–490, 2017.

[34] I. Jorgensen, Y. Zhang, B. A. Krantz, and E. A. Miao, "Pyroptosis triggers pore-induced intracellular traps (PITs) that capture bacteria and lead to their clearance by efferocytosis," *Journal of Experimental Medicine*, vol. 213, no. 10, pp. 2113–2128, 2016.

[35] T. D. Kanneganti, M. Lamkanfi, and G. Nunez, "Intracellular NOD-like receptors in host defense and disease," *Immunity*, vol. 27, no. 4, pp. 549–559, 2007.

[36] F. Martinon and J. Tschopp, "NLRs join TLRs as innate sensors of pathogens," *Trends in Immunology*, vol. 26, no. 8, pp. 447–454, 2005.

[37] J. Yuan, A. Najafov, and B. F. Py, "Roles of caspases in necrotic cell death," *Cell*, vol. 167, no. 7, pp. 1693–1704, 2016.

[38] M. R. de Zoete, N. W. Palm, S. Zhu, and R. A. Flavell, "Inflammasomes," *Cold Spring Harbor Perspectives in Biology*, vol. 6, no. 12, 2014.

[39] J. Shi, Y. Zhao, Y. Wang et al., "Inflammatory caspases are innate immune receptors for intracellular LPS," *Nature*, vol. 514, no. 7521, pp. 187–192, 2014.

[40] E. Viganò, C. E. Diamond, R. Spreafico, A. Balachander, R. M. Sobota, and A. Mortellaro, "Human caspase-4 and caspase-5 regulate the one-step non-canonical inflammasome activation in monocytes," *Nature Communications*, vol. 6, no. 1, p. 8761, 2015.

[41] P. J. Shaw, M. F. McDermott, and T. D. Kanneganti, "Inflammasomes and autoimmunity," *Trends in Molecular Medicine*, vol. 17, no. 2, pp. 57–64, 2011.

[42] C. A. Yang and B. L. Chiang, "Inflammasomes and human autoimmunity: a comprehensive review," *Journal of Autoimmunity*, vol. 61, pp. 1–8, 2015.

[43] V. Bagheri, A. Askari, M. K. Arababadi, and D. Kennedy, "Can Toll-like receptor (TLR) 2 be considered as a new target for immunotherapy against hepatitis B infection?," *Human Immunology*, vol. 75, no. 6, pp. 549–554, 2014.

[44] Y. Liu, H. Yin, M. Zhao, and Q. Lu, "TLR2 and TLR4 in autoimmune diseases: a comprehensive review," *Clinical Reviews in Allergy and Immunology*, vol. 47, no. 2, pp. 136–147, 2014.

[45] S. Borrello, C. Nicolò, G. Delogu, F. Pandolfi, and F. Ria, "TLR2: a crossroads between infections and autoimmunity?," *International Journal of Immunopathology and Pharmacology*, vol. 24, no. 3, pp. 549–556, 2011.

[46] K. Farhat, S. Riekenberg, H. Heine et al., "Heterodimerization of TLR2 with TLR1 or TLR6 expands the ligand spectrum but does not lead to differential signaling," *Journal of Leukocyte Biology*, vol. 83, no. 3, pp. 692–701, 2008.

[47] B. Liang, R. Chen, T. Wang et al., "Myeloid differentiation factor 88 promotes growth and metastasis of human hepatocellular carcinoma," *Clinical Cancer Research*, vol. 19, no. 11, pp. 2905–2916, 2013.

[48] M. G. Netea, C. A. Nold-Petry, M. F. Nold et al., "Differential requirement for the activation of the inflammasome for processing and release of IL-1β in monocytes and macrophages," *Blood*, vol. 113, no. 10, pp. 2324–2335, 2009.

[49] G. L. Semenza, "Regulation of mammalian O2homeostasis by hypoxia-inducible factor 1," *Annual Review of Cell and Developmental Biology*, vol. 15, no. 1, pp. 551–578, 1999.

[50] L. A. Palmer, G. L. Semenza, M. H. Stoler, and R. A. Johns, "Hypoxia induces type II NOS gene expression in pulmonary artery endothelial cells via HIF-1," *American Journal of Physiology-Lung Cellular and Molecular Physiology*, vol. 274, no. 2, pp. L212–L219, 1998.

[51] R. H. Wenger, I. Kvietiko, A. Rolfs, M. Gassmann, and H. H. Marti, "Hypoxia-inducible factor-1α is regulated at the post-mRNA level," *Kidney International*, vol. 51, no. 2, pp. 560–563, 1997.

[52] X. Li, P. Fang, J. Mai, E. T. Choi, H. Wang, and X.-f. Yang, "Targeting mitochondrial reactive oxygen species as novel therapy for inflammatory diseases and cancers," *Journal of Hematology & Oncology*, vol. 6, no. 1, p. 19, 2013.

[53] N. R. Madamanchi and M. S. Runge, "Mitochondrial dysfunction in atherosclerosis," *Circulation Research*, vol. 100, no. 4, pp. 460–473, 2007.

[54] H. Wu, T. Huang, L. Ying et al., "MiR-155 is involved in renal ischemia-reperfusion injury via direct targeting of FoxO3a and regulating renal tubular cell pyroptosis," *Cellular Physiology and Biochemistry*, vol. 40, no. 6, pp. 1692–1705, 2016.

[55] Z. Qiu, S. Lei, B. Zhao et al., "NLRP3 inflammasome activation-mediated pyroptosis aggravates myocardial ischemia/reperfusion injury in diabetic rats," *Oxidative Medicine and Cellular Longevity*, vol. 2017, Article ID 9743280, 17 pages, 2017.

[56] T. Suzuki and G. Nunez, "A role for Nod-like receptors in autophagy induced byShigellainfection," *Autophagy*, vol. 4, no. 1, pp. 73–75, 2008.

[57] P. van Uden, N. S. Kenneth, and S. Rocha, "Regulation of hypoxia-inducible factor-1α by NF-κB," *Biochemical Journal*, vol. 412, no. 3, pp. 477–484, 2008.

[58] D. Bandarra, J. Biddlestone, S. Mudie, H. A. J. Müller, and S. Rocha, "HIF-1α restricts NF-κB-dependent gene expression to control innate immunity signals," *Disease Models & Mechanisms*, vol. 8, no. 2, pp. 169–181, 2015.

[59] F. Hu, R. Mu, J. Zhu et al., "Hypoxia and hypoxia-inducible factor-1α provoke toll-like receptor signalling-induced inflammation in rheumatoid arthritis," *Annals of the Rheumatic Diseases*, vol. 73, no. 5, pp. 928–936, 2014.

[60] D. L. Holliday and V. Speirs, "Choosing the right cell line for breast cancer research," *Breast Cancer Research*, vol. 13, no. 4, p. 215, 2011.

Hindawi
Stem Cells International
Volume 2018, Article ID 5304279, 11 pages
https://doi.org/10.1155/2018/5304279

Research Article

Synaptic Plasticity of Human Umbilical Cord Mesenchymal Stem Cell Differentiating into Neuron-like Cells In Vitro Induced by Edaravone

Yunpeng Shi,[1,2] Chengrui Nan,[1,2] Zhongjie Yan,[1,2] Liqiang Liu,[1,2] Jingjing Zhou,[3] Zongmao Zhao,[1,2] and Depei Li[3]

[1]*Department of Neurosurgery, The Second Hospital of Hebei Medical University, Shijiazhuang, Hebei 050000, China*
[2]*Neuroscience Research Center, Hebei Medical University, Shijiazhuang, Hebei 050000, China*
[3]*Department of Anesthesiology and Critical Care, The University of Texas MD Anderson Cancer Center, Houston, TX 77030, USA*

Correspondence should be addressed to Zongmao Zhao; zzm692017@sina.com

Received 27 April 2018; Revised 2 August 2018; Accepted 14 August 2018; Published 28 October 2018

Academic Editor: Weijun Su

Copyright © 2018 Yunpeng Shi et al. This is an open access article distributed under the Creative Commons Attribution License, which permits unrestricted use, distribution, and reproduction in any medium, provided the original work is properly cited.

Objective. The human umbilical cord mesenchymal stem cells (hUMSCs) are characterized with the potential ability to differentiate to several types of cells. Edaravone has been demonstrated to prevent the hUMSCs from the oxidative damage, especially its ability in antioxidative stress. We hypothesized that Edaravone induces the hUMSCs into the neuron-like cells. *Methods*. The hUMSCs were obtained from the human umbilical cord tissue. The differentiation of hUMSCs was induced by Edaravone with three different doses: 0.65 mg/ml, 1.31 mg/ml, and 2.62 mg/ml. Flow cytometry was used to detect the cell markers. Protein and mRNA levels of nestin, neuron-specific enolase (NSE), and glial fibrillary acidic protein (GFAP) were detected by Western blot and RT-PCR. The expression of synaptophysin (SYN), growth-associated protein 43 (GAP43), and postsynaptic density 95 (PSD95) was detected by Real-Time PCR. *Results*. As long as the prolongation of the culture, the hUMSCs displayed with the long strips or long fusiform to fat and then characterized with the radial helix growth. By using flow cytometry, the cultured hUMSCs at the 3rd, 5th, and 10th passages were expressed with CD73, CD90, and CD105 but not CD11b, CD19, CD34, CD45, and HLA-DR. Most of the hUMSCs cultured with Edaravone exhibited typical nerve-immediately characters including the cell body contraction, increased refraction, and protruding one or more elongated protrusions, which were not found in the control group without addition of Edaravone. NSE, nestin, and GFAP were positive in these neuron-like cells. Edaravone dose-dependently increased expression levels of NSE, nestin, and GFAP. After replacement of maintenance fluid, neuron-like cells continued to be cultured for five days. These neuron-like cells were positive for SYN, PSD95, and GAP43. *Conclusion*. Edaravone can dose-dependently induce hUMSCs to differentiate into neuron-like cells that expressed the neuronal markers including NSE, nestin, and GFAP and synaptic makers such as SYN, PSD95, and GAP43.

1. Introduction

Stem cells are characterized with self-renewal ability and multidirectional differentiation potential. For example, bone marrow, umbilical cord, and epidermis [1–3] were able to differentiate into various functional cells induced by different approaches [4]. In particular, mesenchymal stem cells (MSCs), as one of pluripotent stem cells, have been demonstrated to be capable to differentiate into pluripotent cells [5] including vascular endothelial cells [6], neuron-like cells [7, 8], corneal endothelial cell [9], and hepatocyte-like cells [10]. The differentiation ability probably explains why MSCs have been reported to play important roles in neuronal protection from the oxidative stress, inhibition of ischemia-induced necrosis, and apoptosis [11]. These evidences indicate the probability that the induction of MSC differentiation for neuronal protection would be an effective method for eliminating brain ischemia injury in a clinical setting. The human umbilical cord MSCs (hUMSCs) have the advantages of simple convenient preparation, feasible

source, nontraumatic risk of infection, and its low immunogenicity and immunosuppression, so the hUMSCs turn to be an ideal source used as the engineering cells in studying stem cell differentiation.

Edaravone, a low-molecular weight agent, can scavenge oxygen free radicals and decrease the ability of the xanthine oxidase and hypoxanthine oxidase and reduce the formation of prostacyclin, thus enhance the tissue antioxidative capacity [12]. Edaravone can penetrate the blood-brain barrier, and it has been used in clinic to decrease the ischemia-induced injury in the brain such as acute cerebral infarction, cerebral hemorrhage, and even amyotrophic lateral sclerosis [13]. The early treatment of acute cerebral infarction with Edaravone can prevent the reduction of cerebral blood flow around the lesion area and increase the neuronal antioxidant ability. More importantly, Edaravone was reported to prevent the MSC damage from hypoxia and activate the potential for angiogenesis [14], but it is not known whether Edaravone can induce the differentiation of hUMSCs into the neuronal-like cells that would be explained as another mechanisms underlying its benefits to treat ischemia-induced neuronal injury. The aim of this study was to observe the effects of Edaravone on the differentiation of hUMSCs into neuron-like cells and to further explore the possible mechanisms.

As the main part of the neuron transmission of information, synapses are the structural basis of the interconnected transmission of information between neurons. It is the basic structure and functional unit of the neural loop. The establishment and maintenance of synapses depend on the corresponding expression of many genes. The number and density of synaptophysin (SYN) can indirectly reflect the number and density of synapses [15]. GAP43 (growth-associated protein 43) is closely related to axonal growth and is a key factor for axonal growth and elongation [16]. PSD95 (Postsynaptic density protein 95) is the most important scaffold protein on the postsynaptic membrane, which plays an important role in the process of synapse formation. We use Edaravone to induce hUMSCs to differentiate into nerve-like cells. We continue to culture the cells and detect the expression of specific synapse markers, SYN, GAP43, and PSD95, which lays the foundation for further cell electrophysiological study.

2. Materials and Methods

2.1. Materials and Chemicals. The umbilical cord was obtained from the Department of Obstetrics and Gynecology of the Second Affiliated Hospital of Hebei Medical University. All the participants signed the relevant consent letter to use the umbilical cord for the present research. The following reagents were obtained commercially: Edaravone (packing: 20 g, purity: 99.7%, batch no.: A06-131204) was provided by Jilin Province Boda Pharmaceutical Co. Ltd. FBS (BI, Israel); L-DMEM/F-12, H-DMEM/F-12 (GIBCO, Grand Island, USA); EDTA and DMSO (Sigma-Aldrich Co. LLC., St. Louis, MO 63178,USA); FITC-CD19, FITC-CD34, PE-CD11b, PE-CD73, PE-CD90, PE-CD45, and PE-CD105 (Becton, Dickinson and Company, Franklin Lakes, New Jersey 07417-1880); PS immunohistochemistry kit (Beijing Zhongshan Golden Bridge Company, China); Taq PCR star mix (Genstar, China); EasyScript First-Strand cDNA synthesis supermix (TransGen Biotech, China); TB Green™ Premix Ex Taq™ II (Tli RNaseH Plus) (TaKaRa Japan); cell *RIPA* Lysis Buffer and phenylmethylsulfonyl fluoride (Solarbio, Beijing, China); polyclonal antibodies of neuron-specific enolase (NSE) and nestin (OriGene, USA); glial fibrillary acidic protein (GFAP) and glyceraldehyde-3-phosphate dehydrogenase (Affbiotech, USA); and polyclonal antibodies of synaptophysin, growth-associated protein 43, and postsynaptic density 95 (Abways, China).

2.2. Isolation and Culture of hUMSCs. The obtained umbilical cords were placed in H-DMEM/F12 culture medium under aseptic conditions, stored at 4°C, and then timely transported to a cell culture room to carry out the following steps. Each umbilical cord was rinsed thoroughly with D-Hank's medium. After removing the blood sample, umbilical artery, and umbilical vein, the umbilical cord mesenchymal tissue was cut into pieces of 1 mm^3 in size, digested with 0.2% collagenase II, and placed in a culture flask containing 2 ng/ml EGF, 20% FBS, 25 mM L-Glu, and 100 U/ml penicillin-streptomycin mixture at 37°C with 5% CO_2 and saturation humidity to obtain primary cells. Half of the culture medium was replaced every 24 h, and it was replenished every 3 days. When the cells achieved 80–90% confluency, the medium was removed, and cells were rinsed two times with PBS and then digested with trypsin (0.25%)–EDTA (0.2 g/l) into single cells for passaging at the ratio of 1 : 3. The culture medium was H-DMEM/F12 containing 100 U/ml of a penicillin-streptomycin mixture and 10% FBS.

2.3. Analysis of Cellular Phenotype of hUMSCs. In the logarithmic phase of growth, hUMSCs were digested with trypsin and rinsed with PBS, and then, the single cell suspension was aliquot into 10 tubes at 1×10^6 cells/tube. Separately, mouse anti-human monoclonal antibodies (5 μl/each) against CD11-PE, CD45-PE, CD73-PE, CD90-PE, CD105-PE, HLA-DR-PE, CD19-FITC, and CD34-FITC were added to the 8 tubes, while anti-mouse IgG1-PE and anti-mouse IgG1-FITC (each 7 μl) were added to the other two tubes as isotype controls. After mixing the contents thoroughly, the tubes were incubated at 4°C for 30 min. Thereafter, the cells were rinsed with PBS and then centrifuged. The supernatant was discarded, and the cells were resuspended with 400 μl of PBS for the followed analysis by flow cytometry.

2.4. Differentiation of hUMSCs into Neuron-like Cells. The hUMSCs were obtained at the 3rd passage of cells according to the logarithmic growth phase. The hUMSCs were separated into four groups including three groups treated with different dose of Edaravone (low-dose, LH; medium-dose, MD; and high-dose, HD) and one control group (Con). MSCs were placed in a cell culture chamber. When about 80% of the cells adhered to the wall, the whole culture solution was discarded. Neurobasal medium containing 50 ng/ml bFGF was first induced for 24 hours. After washing with PBS, LD, MD, and HD groups were, respectively, added with Edaravone concentrations of 0.65 mg/ml, 1.31 mg/ml, and

2.62 mg/ml for incubation with the Neurobasal medium. Then, the hUMSCs were induced in the incubator, and the morphological changes of the cells were observed by inverted phase contrast microscope.

2.5. Calculation of Positive Rate of Neuron-like Cells. Under the inverted microscope, 3 nonoverlapping fields were randomly selected; the total cell number and the number of neuron-like cells were counted, and the rate of neuron-like cells were calculated.

2.6. Immunochemistry Analysis. After incubation with Edaravone for 12 h, expression levels of neuronal-specific proteins NSE, nestin, and GFAP were detected by immunocytochemistry as follows. The cells were rinsed with PBS gently and fixed with 4% paraformaldehyde for 20 min at room temperature followed by the rinses with PBS three times for 5 min each time. The cell membranes were disrupted with 0.5% Triton-X-100 in PBS for 15 min at room temperature away from light and then incubated with 3% H_2O_2 at room temperature for 5 min. The cells were blocked by the normal goat serum at room temperature for 15 min. The blocked cells were induced by the primary antibodies against NSE, nestin, and GFAP at 4°C overnight. On the second day, the appropriate biotinylated secondary antibody was added for incubation at room temperature for 15 min, then followed by horseradish peroxidase-conjugated streptavidin at room temperature for 15 min. Finally, the cells were stained with freshly prepared DAB for 1 min and counterstained with hematoxylin before finally rinsed repeatedly with water. Under the inverted microscope, 3 nonoverlapping fields were randomly selected; the total cell number and the number of neuron-like cells were counted and the rate of neuron-like cells calculated.

2.7. RT-PCR Analysis. Total RNA was extracted by TRIpure Reagent (Aidlab Biotechnologies Co. Ltd., China) following the manufacturer's instructions and quantified with an Ultramicro ultraviolet visible light meter (Gene Company Limited, China). cDNA was synthesized from total RNA with EasyScript First-Strand cDNA synthesis supermix (TransGen Biotech, China) following the manufacturer's instructions. Semiquantitative PCR was performed using Taq PCR star mix (Genstar, China) with the following reaction conditions: 1 cycle of 94°C for 3 min; 30 cycles of 94°C for 30 s, T_m (°C) for 30 s, and 72°C for 30 s; and a final extension at 72°C for 10 min. A 10 μl of each PCR product was analyzed by electrophoresis, and the gene expression levels were calculated using GAPDH as the internal control. The primers were designed using Primer 5.0 software and are shown: nestin: F-TCCA GAAACTCAAGCACCACT and R-TCCACCGTATCTTC CCACCT 342 bp, NSE: F-GGCACTCTACCAGGACTTTG and R-GCGATGACTCACCATAACCC 286 bp, GFAP: F-GTCCATGTGGAGCTTGAC and R-CATTGAGCAGGTC CTGGTAC 406 bp, and GAPDH: F-AGAAGGCTGGGGCT CATTTG and R-AGGGGCCATCCACAGTCTTC 258 bp.

2.8. Western Blot Analysis. Cell lysates were prepared with cell *RIPA* Lysis Buffer and phenylmethylsulfonyl fluoride, and protein concentrations were determined with an Ultramicro ultraviolet visible light meter (Gene Company limited, China).Total protein (16 μg) of each lysate was electrophoresed in 10% SDS-PAGE gel and transferred to a polyvinylidene fluoride (PVDF) membrane (Solarbio, Beijing, China). The membranes were blocked by 10% nonfat milk for 2 h at room temperature and incubated with GFAP, nestin, and NSE primary antibodies at 4°C overnight. After rinsing with PBS for 10 min, the membranes were incubated with anti-rabbit IgG (1 : 2000, Affbiotech, USA) for 2 h at room temperature and visualized by Supersignal West Pico Chemiluminescent Substrate (Thermo Scientific, USA) using the Image alphaEaseFC system (Alpha Innotech, USA).

2.9. Continuous Culture of Neuron-like Cells. We chose a group of cells with the highest positive rate of nerve cell markers and stable expression. After 24 hours of induction, we clean it with PBS, replace the maintenance fluid, and continue training for five days. The maintenance fluid is formulated with Neurobasal medium containing 2% B27 and 50 ng/ml bFGF. The inverted phase contrast microscope dynamically observed the morphological changes of each group.

2.10. Real-Time PCR Analysis. Total RNA was extracted by TRIpure Reagent (Aidlab Biotechnologies Co. Ltd, China) following the manufacturer's instructions and quantified with Ultramicro ultraviolet visible light meter (Gene Company Limited, China). cDNA was synthesized from total RNA with EasyScript First-Strand cDNA synthesis supermix (TransGen Biotech, China) following the manufacturer's instructions. Real-Time PCR was performed using TB Green™ Premix Ex Taq™ II (Tli RNaseH Plus) by TaKaRa. The gene expression levels were calculated using GAPDH as the internal control. The primers were designed using Primer 5.0 software and are shown: SYN: F–CACTACTAC AGAGGGAAAATGAATG and R-CACGGTGCCCAGAC AGGT 108 bp, GAP43: F-GAAGGGGGAGGGTGATGC and R-CTTGGAGGACGGCGAGTTAT 130 bp, PSD95: F-GCGGAGCAACCCCAAAAG and R-GATGAACCCAA TGTCGTCGG 196 bp, and GAPDH: F-ACGGATTTGGT CGTATTGGG and R-GATGAACCCAATGTCGTCGG 210 bp.

2.11. Statistical Analysis. All the data were expressed as mean ± s.e. SPSS19.0 was used for statistical analysis. One-way ANOVA was used in three or more group comparison followed by SNK method within two separate groups. $P < 0.05$ was considered to be significantly different.

3. Results

3.1. Growth and Morphological Changes of hUMSCs. Primary cultured cells were passaged at the ratio of 1 : 1. After 12 hours of passage, most of the cells adhered to growth, and the cells were elongated or long fusiform (Figure 1(a)). With the increase of incubation time, the cells gradually became longer and adhered completely, and the morphology became flat. Cell growth was rapid, in about 5 days after passage can be completely adhere to the wall and grow. The cells had radial or spiral growth according to the ratio of 1 : 2 or 1 : 3 subculture. Continue to culture, the cells were overlapped

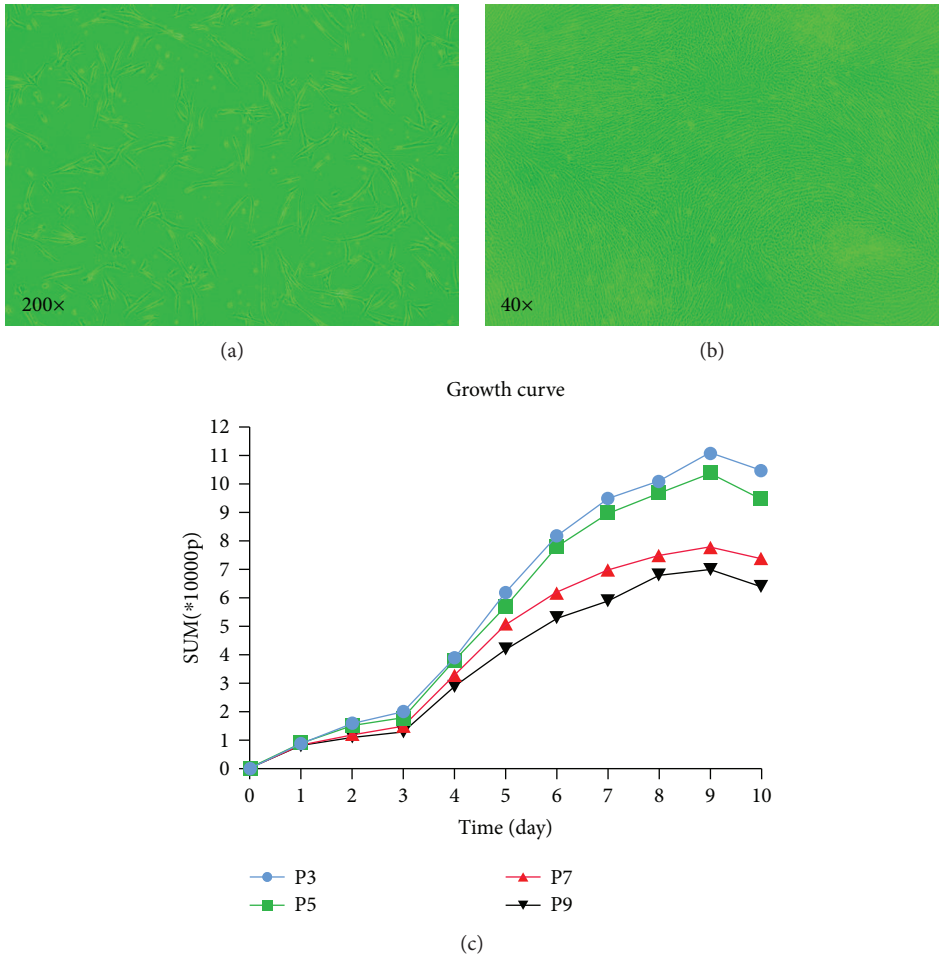

Figure 1: (a) (200x) Cells were elongated or long fusiform. (b) (40x) The cells were spirally divergent. (c) The growth curve of the 3rd, 5th, 7th, and 9th passage cells.

showing the spiral divergent growth around the center, and the local density was increased (Figure 1(b)). The cells were cultured until the ninth passage, and the cell homogeneity and growth were good. Because of the relatively small number of the 1st and 2nd passage (P1 and P2) cells and the good growth condition of the 3rd passage (P3) cells, we selected the 3rd passage hUMSCs with good growth status. The growth curve is plotted in Figure 1(c).

3.2. Cellular Phenotype of hUMSCs. We detected the cell phenotype of the 2nd, 5th, and 10th passages of hUMSCs by flow cytometry and found that all generations of cells tested coexpressed CD105, CD90, and CD73 but not CD11b, CD34, CD19, CD45, and histocompatibility antigen HLA-DR (MHC-II) (Figure 2).

3.3. Morphological and Quantitative Changes of Neuron-like Cells in Each Group. The hUMSC incubation with Edaravone showed the morphological properties of neuron-like cells. After 1 h incubation with low dose of Edaravone, the hUMSCs were presented with the sporadic cell body contraction, the enhanced refraction, and the cell morphology which turned into a long oval or round and out of one or more elongated processes (Figure 3(a)). After 4 h, the number of protrusions increased, and the length of protrusions and the number of bifurcations increased. 12 h later, about 50% of the cells had the above changes; adjacent cells protruding protuberances will gradually intertwine connected into a network. The percentage of neuron-like cells reached the peak at 24 hours. The hUMSCs in the MD group were presented with obvious changes after adding Edaravone for 1 hour. In the MD group at 12 hours, the percentage of neuron-like cells reached the peak, which was much earlier than the LD group. In the HD group, a large number of cells became neuron-like cells at 1 hour; neuron-like cells reached a peak at 4 hours (Figure 3(b)) and remained at high rates of change until 24 hours. Blank group was the control group. There was no significant change in 24 h after continuous observation. Under the inverted microscope, 3 nonoverlapping visual fields were randomly selected; the total number of cells and the number of neuron-like cells were counted, and the rate of neuron-like cells was calculated. The result was expressed by mean ± s.e. The curve of the rate of neuron-like cells in each group is shown in Figure 4. There was significant difference in the positive rate between each group, $P < 0.01$. The cells in the HD group

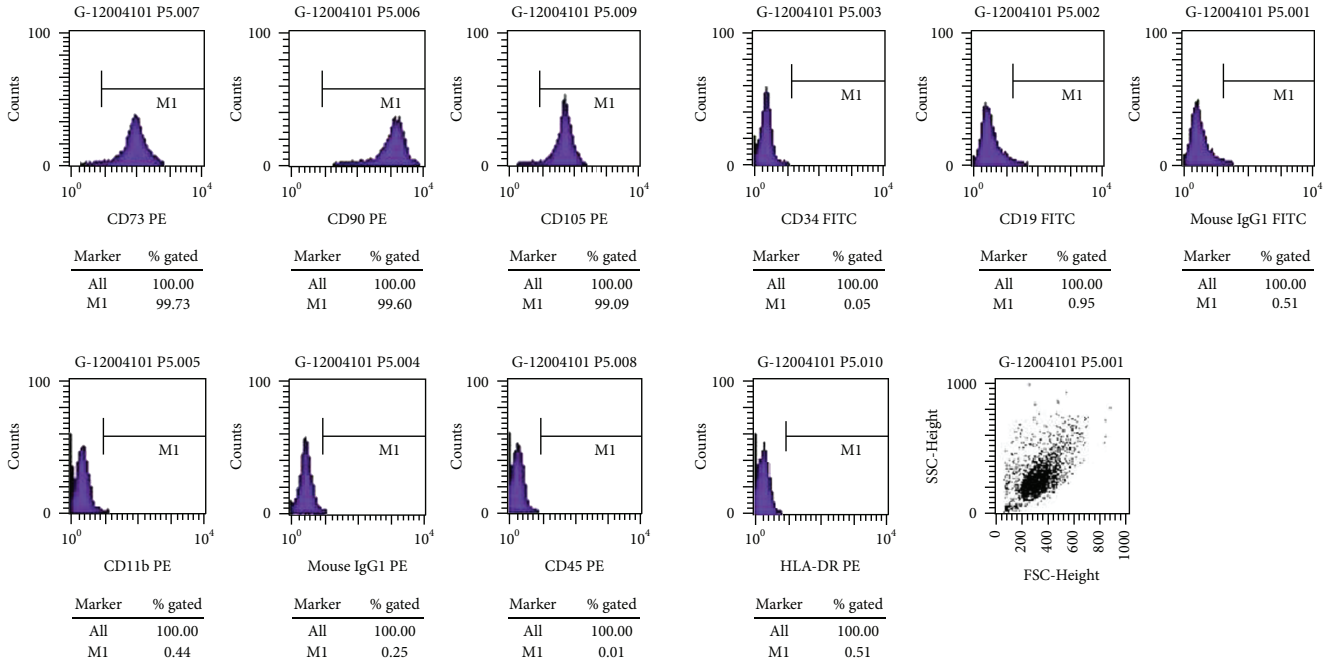

Figure 2: Cellular phenotype of hUMSCs detected by flow cytometry.

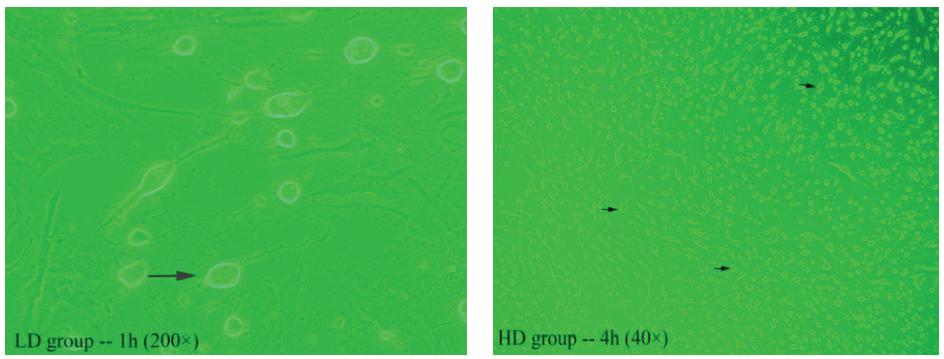

(a) (b)

Figure 3: (a) (200x) Arrowheads show neuron-like cells. (b) (40x) A large number of neuron-like cells, arrowheads show neuron-like cells.

changed the most rapidly and maintained at a relatively high positive rate.

3.4. Result of Immunochemistry Analysis. The neurological markers were detected after different concentrations of Edaravone incubation for 12 hours. As shown in Figure 5, brown cell bodies and the purple nucleus were nestin, NSE, or GFAP-positive cells. By contrast, no cells positively expressed these markers in the control group. Under the inverted microscope, 3 nonoverlapping visual fields were randomly selected; the total number of cells and the number of neuron-like cells were counted, and the rate of neuron-like cells was calculated. After 12 hours of induction, the positive rate of neuronal markers in each group is shown in Figure 6. The result was expressed by mean ± s.e. Differences in expression levels of nestin, GFAP, and NSE between any two groups were significant ($P < 0.05$). The results showed that the expression of nerve markers in the HD group was the most.

3.5. RT-PCR Analysis Results of the HD Group. The highest positive rate and stable expression of each nerve cell marker were detected in the HD group (2.62 mg/ml). Therefore, we use semiquantitative RT-PCR to detect the expression of mRNA in the HD group. According to the induction time, the groups were divided into blank, 2 h, 4 h, 6 h, 12 h, and 24 h. Through statistical neural marker expression amount and reference, to calculate the neural marker expression level, the result was expressed by mean ± s.e. RT-PCR results of NSE, nestin, GFAP, and GAPDH at each time point are shown in (Figure 7).

3.6. Western Blot Analysis Results of the HD Group. We use Western blot analysis to detect the expression of protein in the HD group. According to the induction time, the groups

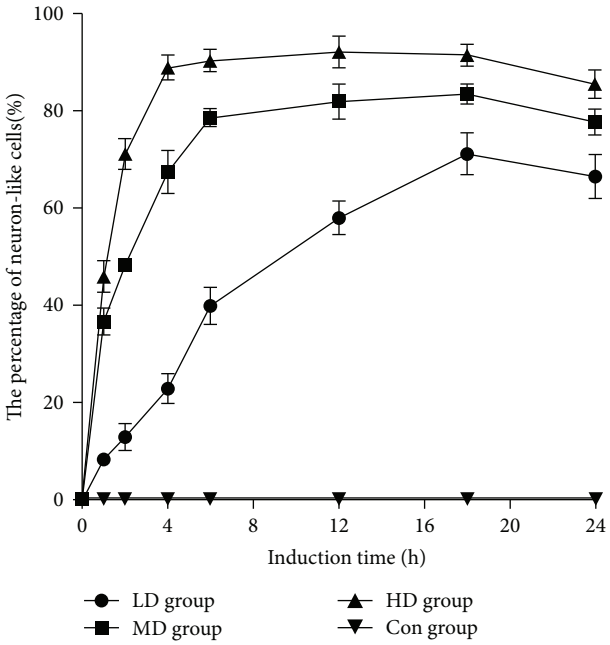

Figure 4: The percentage of neuron-like cells in each group was changed with the induction time.

were divided into blank, 2 h, 4 h, 6 h, 12 h, and 24 h. Through statistical neural marker expression amount and reference, to calculate the neural marker expression level, the result was expressed by mean ± s.e. Western blot results of NSE, nestin, GFAP, and GAPDH at each time point are shown in Figure 8.

3.7. Real-Time PCR Analysis Results of Specific Synapse Marker. We use Real-Time PCR to detect the expression of mRNA in the HD group. After replacement of maintenance fluid, nerve-like cells continued to be cultured for five days. According to maintenance culture time, the groups were divided into blank, 1 d, 2 d, 3 d, 4 d, and 5 d. Through statistical synaptic marker expression amount and reference, to calculate the synaptic markers expression level, the result was expressed by mean ± s.e. SYN, PSD95, and GAP43 at each time point are shown in Figure 9.

4. Discussion

With the rapid development of stem cell therapy research, stem cell transplantation is considered to be a potential treatment. At the same time, mesenchymal stem cells as a new source of cell therapy are of concern to a large number of scholars and researchers [17, 18]. In theory, pluripotent embryonic stem cells and the inner layer of blastocysts are the ideal cell transplantation option. However, the application of these cells is ethically restricted and has teratogenicity and tumorigenicity. MSC can have in vitro long-term survival and constantly amplify and induce differentiation into nerve, vascular endothelium, myocardial, corneal endothelium, cartilage, islet, and other functional cells [5]. The nervous system has little ability to repair itself after being damaged, so the nerve cells that are targeted by neural tissue engineering may be able to repair the damaged nerve tissue. Previous studies have shown that bone marrow MSCs, neural stem cells, adipose MSC, umbilical cord MSC, umbilical cord blood MSC, and placental stem cells from different species and sources can be used for the treatment of neurological diseases. Shen et al. [19] report the treatment of ischemic or some degenerative disease caused by nervous system dysfunction; mesenchymal stem cells can provide a stable source of nutrition and reflect its multidirectional differentiation potential. At the same time, MSC do not appear to decrease with the number of passages, and there is no risk of differentiation with time [20]. This conclusion has been demonstrated in models of intracerebral hemorrhage and Parkinson's disease in rats and spinal cord injury in primates [21, 22]. Previous adult stem cell research mostly focused on bone marrow-derived mesenchymal stem cells. There are limitations and defects in bone marrow MSC because of limited number and difficulty in obtaining. The number and differentiation potential of bone marrow mesenchymal stem cells will decrease with age. At present, human umbilical cord mesenchymal stem cells (hUMSCs) are popular cells in cell culture. hUMSCs have the advantages of strong proliferative ability, low immunogenicity, stable amplification in vitro, wide source, without any ethical restriction, and can be divided into multiple germ layers. At present, there is no study on the differentiation of human umbilical cord mesenchymal stem cells induced by Edaravone. Therefore, we used Edaravone to induce human umbilical cord mesenchymal stem cells. More experiments show that under certain conditions of culture, hUMSCs spontaneously tend to differentiate into neuron-like cells and have a good protective effect of neurons [23]. At this stage, the use of cell therapy in the treatment of neurological diseases is divided into the following two methods [24, 25]. One is the purpose of the cells through a variety of ways into the body, relying on its own differentiation potential, and the impact of the environment plays a therapeutic effect. In another method, cells are first differentiated into cells of interest by various means and then into the body to play a therapeutic effect.

The most reported method of induction into nerve cells is divided into three kinds: cell nutrition factor, antioxidant, and nerve cell coculture method. In general, the main factors of cell nutrition are bFGF, transforming growth factor-β, and BDNF. Antioxidants are mainly DMSO, compound or single herb, or active ingredients of traditional Chinese medicine. The neural cell coculture method is to coculture MSCs with neural cells. There are also reports that microRNA-124 can also regulate the directional differentiation of MSCs to neurons [26]. These neuron-like cells can express a variety of neurological markers, such as nesin, GFAP, NSE, NF-H, and MAP-2. In this study, different concentrations of Edaravone were used to induce hUMSCs. It was found that the astigmatism of hUMSCs became stronger, and the cells protruded elongated protrusions, which had the morphological characteristics of neuron-like cells. The results of immunocytochemistry showed that NSE, GFAP, and nestin were positive, and the induction efficiency of 2.62 mg/ml group was significant. The results of RT-PCR and Western blot showed that the expressions of NSE, GFAP, and nestin in the induced group were significantly higher than those in the blank

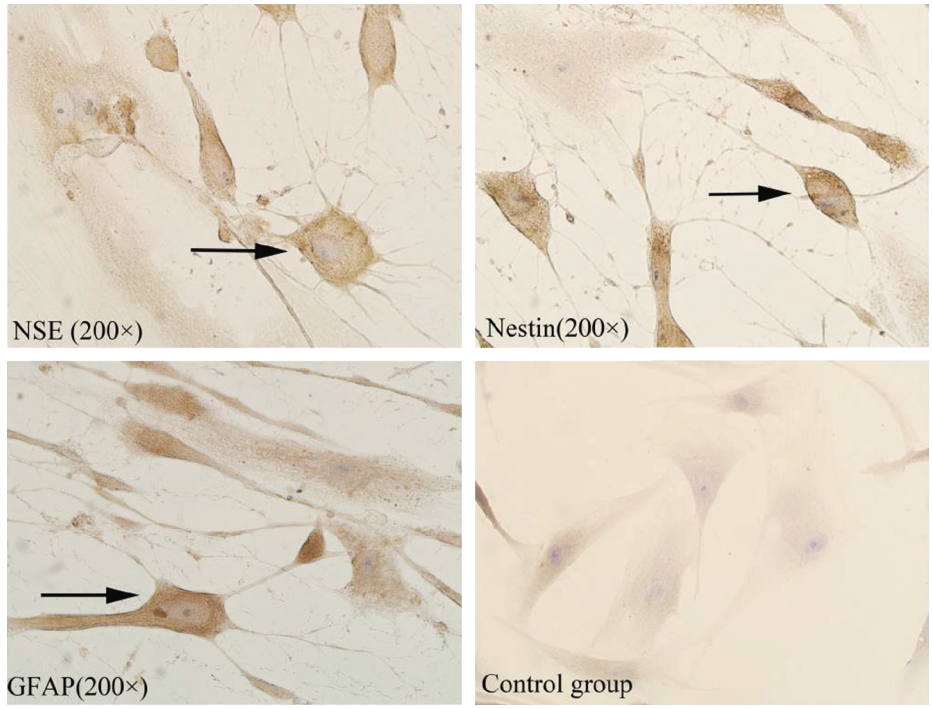

Figure 5: Immunohistochemical staining of neuron-like cells in treatment groups for NSE, nestin, and GFAP, respectively. The arrows in figures indicate neuron-like cells.

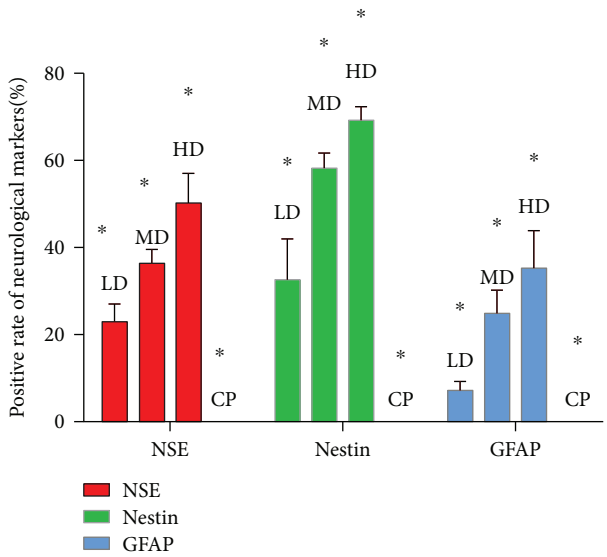

Figure 6: After 12 hours of induction, the positive rate of neuronal markers in each group.

control group. And 2.62 mg/ml is the higher concentration available, close to its maximum solubility in L-DMEM [27]. This study demonstrates that Edaravone can effectively induce hUMSCs to differentiate into neuron-like cells and the concentration of 2.62 mg/ml for the appropriate induction concentration.

The mechanism of each induction method is also different, such as bFGF induction mechanism as a neurotrophic factor in promoting cell mitosis in the process of simulation of embryonic neural cell growth microenvironment, thus leading to hUMSC differentiation into nerve cells. The induction mechanism of coculture may be related to the secretion of various nerve growth factors from various nerve cells. In this growing microenvironment, hUMSCs tend to differentiate into neuron-like cells, also providing the conditions for axonal development [28, 29]. Tetramethylpyrazine can promote the differentiation of hUMSCs into neuron-like cells by inhibiting the expression of Ca2+ signaling, promoting the increase of cAMP content in the second messenger and changing the expression of MEK-ERK signaling pathway [30]. Chemical antioxidant β-mercaptoethanol is also regulating the second messenger cAMP content, thus initiating the PKA pathway to promote MSC differentiation [31]. In recent years, with the development of biological tissue engineering technology, some scholars have proposed that using certain cell scaffold compounds can promote the differentiation of MSCs [32]. Edaravone is widely used in the treatment of ischemic stroke and a variety of spinal cord injury. Edaravone has the effect of reducing cerebral edema, improving cerebral ischemic symptoms, protecting brain tissue, and so on. It is a kind of oxygen free radical scavenger with good curative effect. Edaravone has antioxidant, antiischemia and reperfusion injury, antifibrosis, inhibition of nerve cell damage, and other effects; it can inhibit the peroxidation to protect the brain cells [33]. Edaravone is a kind of brain protective agent, which can reduce the death of nerve cells. In brain hemorrhage and cerebral infarction experiments, it can inhibit the decrease of local cerebral blood flow around the infarct. We hope to use cell transplantation to

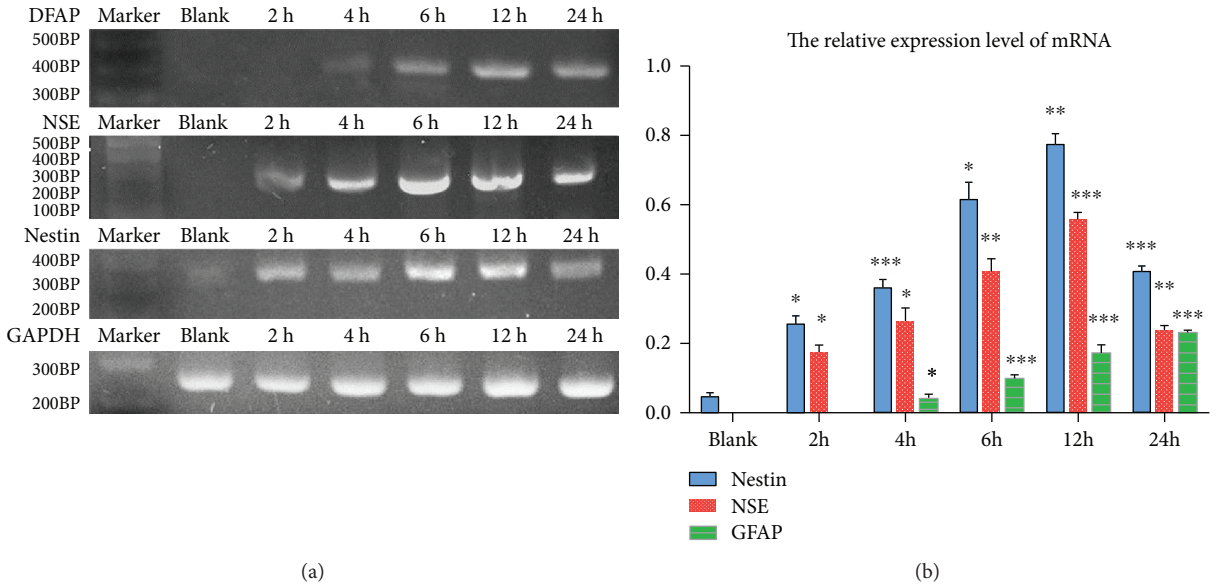

Figure 7: (a) Result of semiquantitative RT-PCR. (b) Relative expression level of mRNA.

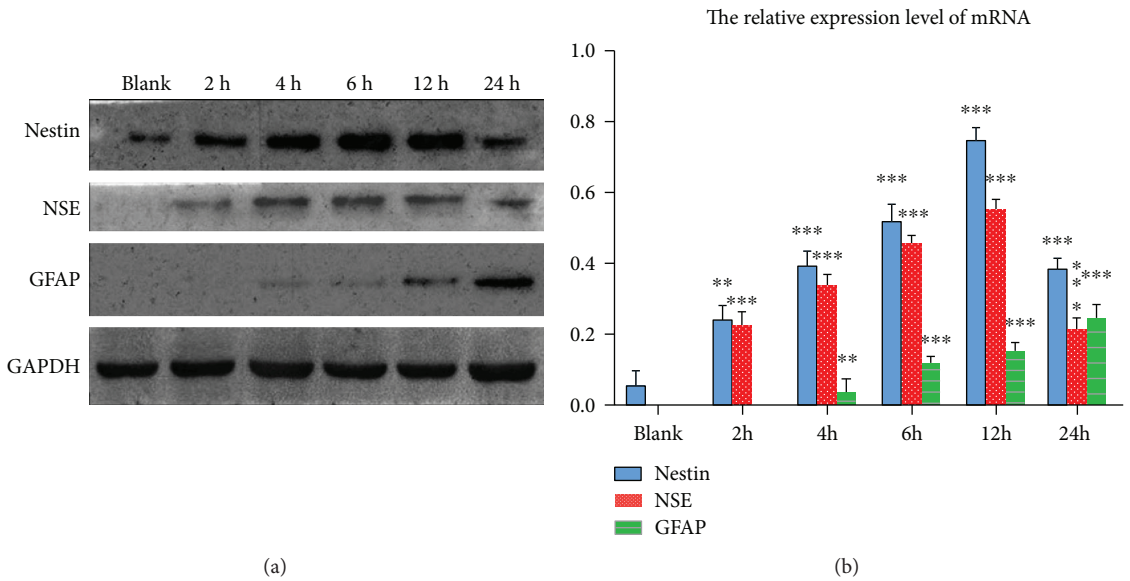

Figure 8: (a) Result of Western blot. (b) Relative expression level of protein.

improve the neuron injury caused by brain injury, bleeding, infarction, and the adverse effects of Parkinson's disease, amyotrophic lateral sclerosis, and other degenerative diseases. We look forward that cells derived from Edaravone can also play a role in brain protection, providing cell support for the next further experiments. Therefore, in this study, we used Edaravone to induce hUMSCs to differentiate into neuron-like cells. At the same time, it was found that those neuron-like cells induced by Edaravone had the electrophysiological basis for neuronal cells [34]. However, the induction mechanism of Edaravone is still unclear at this stage. Weissmann et al. [35] and other studies have shown that in the growth and development of nerve cells, the cytoskeleton played a key role. Doherty [36] and other studies have pointed out that in the development of nerve cells, Shh signaling pathway has an important role; it can be conducive to the survival of nerve cells in the microenvironment. The next research direction is whether the Shh signaling pathway and cytoskeleton play an important role in the induction of hUMSCs into neuron-like cells by Edaravone.

Synaptic plasticity has long been recognized as the basis of neurocognitive biology. Many studies have found that memory can be preserved for a long time by the brain at the synapse level [37]. The existing proteins are modified to give signals to the nucleus. So a specific gene is expressed. Gene products are transported to synapses, and new proteins are synthesized locally, thus establishing new synapses and forming new information transfer functions [38]. This

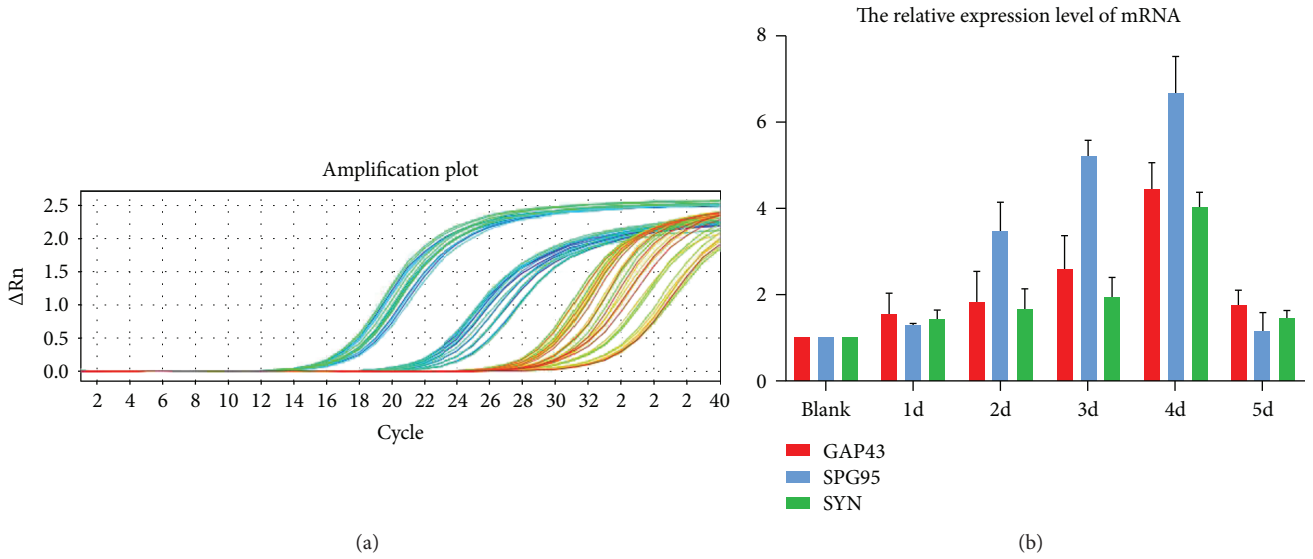

Figure 9: (a) Result of Real-Time PCR. (b) Relative expression level of mRNA.

process is called synaptic plasticity. Changes in synaptic markers can reflect changes in morphological plasticity. Synaptophysin (SYN), as one of the most important markers of synaptogenesis, plays an important role in the process of synaptogenesis and differentiation [39]. Postsynaptic density 95 is mainly involved in maintaining synaptic structure and plays an important role in the regulation of synapse morphology [40]. Growth-associated protein 43 (GAP43), as a specific phosphorylated protein, is mainly located in the presynaptic membrane of neurons. It is widely involved in the development, differentiation, and regeneration of the nervous system and is closely related to the formation and plasticity of synapses [41]. Therefore, we examined the expression levels of SYN, GAP43, and postsynaptic density 95. However, whether the obtained neuron-like cells have synapses capable of transmitting information needs further neuro-electrophysiological studies.

At the same time, hUMSCs cannot only directly inhibit the growth of some tumors in vivo and in vitro but also easily accept foreign gene modification and have the characteristics of target migration to tumor tissue, damaged tissue, and chronic inflammatory response sites. We would like to discuss whether the cells can also have the characteristics of nerve cell protection and tumor cell apoptosis by using eukaryotic cell transfection. There are also many difficulties in introducing nerve cells which are differentiated into cells into the body and have a therapeutic effect. In the next days, we still need to continue efforts.

Data Availability

The data used to support the findings of this study are included within the article.

Conflicts of Interest

The authors declare that they have no conflicts of interest.

Acknowledgments

This research was supported by the National Natural Science Foundation of China (81870984, 81401032) and the Hebei Provincial Natural Science Foundation (H2015206309).

References

[1] A. Bongso, C. Y. Fong, and K. Gauthaman, "Taking stem cells to the clinic: major challenges," *Journal of Cellular Biochemistry*, vol. 105, no. 6, pp. 1352–1360, 2008.

[2] M. L. Weiss and D. L. Troyer, "Stem cells in the umbilical cord," *Stem Cell Reviews*, vol. 2, no. 2, pp. 155–162, 2006.

[3] T. J. Sun, R. Tao, Y. Q. Han, G. Xu, J. Liu, and Y. F. Han, "Wnt3a promotes human umbilical cord mesenchymal stem cells to differentiate into epidermal-like cells," *European Review for Medical and Pharmacological Sciences*, vol. 19, no. 1, pp. 86–91, 2015.

[4] M. Makridakis, M. G. Roubelakis, and A. Vlahou, "Stem cells: insights into the secretome," *Biochimica et Biophysica Acta (BBA) - Proteins and Proteomics*, vol. 1834, no. 11, pp. 2380–2384, 2013.

[5] A. J. Friedenstein, J. F. Gorskaja, and N. N. Kulagina, "Fibroblast precursors in normal and irradiated mouse hematopoietic organs," *Experimental Hematology*, vol. 4, no. 5, pp. 267–274, 1976.

[6] J. Li-shan, Z. Yun, Z. Ya, Z. Jian, Z. Ting, and Y. Xiangming, "In vitro induced differentiation of mesenchymal stem cells from bone marrow mesenchymal stem cells into vascular endothelial cells," *Chinese Journal of Tissue Engineering Research*, vol. 13, no. 19, pp. 3698–3702, 2009.

[7] W. Jin, Y. P. Xu, A. H. Yang, and Y. Q. Xing, "In vitro induction and differentiation of umbilical cord mesenchymal stem cells into neuron-like cells by all-trans retinoic acid," *International Journal of Ophthalmology*, vol. 8, no. 2, pp. 250–256, 2015.

[8] L. Guo, L. Wang, L. Wang et al., "Resveratrol induces differentiation of human umbilical cord mesenchymal stem cells into neuron-like cells," *Stem Cells International*, vol. 2017, Article ID 1651325, 7 pages, 2017.

[9] N. C. Joyce, D. L. Harris, V. Markov, Z. Zhang, and B. Saitta, "Potential of human umbilical cord blood mesenchymal stem cells to heal damaged corneal endothelium," *Molecular Vision*, vol. 18, pp. 547–564, 2012.

[10] Y. Sun, F. Duan, and X. Chen, "Inducing differentiation of human umbilical cord blood mesenchymal stem cells into hepatocyte-like cells in vitro," *Chinese Journal of Gastroenterology and Hepatology*, vol. 13, pp. 239–243, 2004.

[11] D. Kong, J. Zhu, Q. Liu et al., "Mesenchymal stem cells protect neurons against hypoxic-ischemic injury via inhibiting parthanatos, necroptosis, and apoptosis, but not autophagy," *Cellular and Molecular Neurobiology*, vol. 37, no. 2, pp. 303–313, 2017.

[12] Z. Yin, H. Xu, and N. Yuan, "Clinical evaluation of edaravone in removal of free redicals and treatment for brain edema after intracerebral hemorrhage," *Journal of Apoplexy and Nervous Diseases*, vol. 25, no. 3, pp. 313–315, 2008.

[13] K. Abe, M. Aoki, S. Tsuji et al., "Safety and efficacy of edaravone in well defined patients with amyotrophic lateral sclerosis: a randomised, double-blind, placebo-controlled trial," *The Lancet Neurology*, vol. 16, no. 7, pp. 505–512, 2017.

[14] G. W. Zhang, T. X. Gu, X. J. Sun et al., "Edaravone promotes activation of resident cardiac stem cells by transplanted mesenchymal stem cells in a rat myocardial infarction model," *The Journal of Thoracic and Cardiovascular Surgery*, vol. 152, no. 2, pp. 570–582, 2016.

[15] L. Siyu, W. Fengchang, X. Haixiong et al., "Biological features and differentiation of human umbilical cord mesenchymal stem cells at different passages," *Chinese Journal of Tissue Engineering Research*, vol. 21, no. 13, pp. 2015–2022, 2017.

[16] M. L. Weiss, S. Medicetty, A. R. Bledsoe et al., "Human umbilical cord matrix stem cells: preliminary characterization and effect of transplantation in a rodent model of Parkinson's disease," *Stem Cells*, vol. 24, no. 3, pp. 781–792, 2006.

[17] N. K. Satija, V. K. Singh, Y. K. Verma et al., "Mesenchymal stem cell-based therapy: a new paradigm in regenerative medicine," *Journal of Cellular and Molecular Medicine*, vol. 13, no. 11-12, pp. 4385–4402, 2009.

[18] E. Syková, P. Jendelová, L. Urdzíková, P. Lesný, and A. Hejcl, "Bone marrow stem cells and polymer hydrogels—two strategies for spinal cord injury repair," *Cellular and Molecular Neurobiology*, vol. 26, no. 7-8, pp. 1113–1129, 2006.

[19] J. Shen, A. Nair, R. Saxena, C. C. Zhang, J. Borrelli, and L. Tang, "Tissue engineering bone using autologous progenitor cells in the peritoneum," *PLoS One*, vol. 9, no. 3, article e93514, 2014.

[20] Z. Li, W. Zhao, W. Liu, Y. Zhou, J. Jia, and L. Yang, "Transplantation of placenta-derived mesenchymal stem cell-induced neural stem cells to treat spinal cord injury," *Neural Regeneration Research*, vol. 9, no. 24, pp. 2197–2204, 2014.

[21] A. Gugliandolo, P. Bramanti, and E. Mazzon, "Mesenchymal stem cell therapy in Parkinson's disease animal models," *Current Research in Translational Medicine*, vol. 65, no. 2, pp. 51–60, 2017.

[22] G. Ping, S. Zhan-sheng, W. Bo-min, L. Lian-xin, W. Fu, and M. Le-ming, "Transplantation of neuron-like cells from bone marrow mesenchymal stem cells for treatment of spinal cord injury," *Journal of Clinical Rehabilitative Tissue Engineering Research*, vol. 17, no. 23, pp. 4256–4263, 2013.

[23] Y. J. Zheng, L. Y. Hai, and L. Meng, "Differentiation and application of umbilical cord blood mesenchymal stem cells to neurons," *Chongqing Medicine*, vol. 43, no. 3, pp. 366–368, 2014.

[24] S. R. Cho, M. S. Yang, S. H. Yim et al., "Neurally induced umbilical cord blood cells modestly repair injured spinal cords," *NeuroReport*, vol. 19, no. 13, pp. 1259–1263, 2008.

[25] V. R. Dasari, K. K. Veeravalli, A. J. Tsung et al., "Neuronal apoptosis is inhibited by cord blood stem cells after spinal cord injury," *Journal of Neurotrauma*, vol. 26, no. 11, pp. 2057–2069, 2009.

[26] M. Mondanizadeh, E. Arefian, G. Mosayebi, M. Saidijam, B. Khansarinejad, and S. M. Hashemi, "MicroRNA-124 regulates neuronal differentiation of mesenchymal stem cells by targeting Sp1 mRNA," *Journal of Cellular Biochemistry*, vol. 116, no. 6, pp. 943–953, 2015.

[27] Z. Jian, *The Research of Supramolecular Complexes of Edaravone and Cyclodextrins*, Nanjing Normal University, 2011.

[28] R. J. Tolwani, P. S. Buckmaster, S. Varma et al., "BDNF overexpression increases dendrite complexity in hippocampal dentate gyrus," *Neuroscience*, vol. 114, no. 3, pp. 795–805, 2002.

[29] K. A. Trzaska, C. C. King, K. Y. Li et al., "Brain-derived neurotrophic factor facilitates maturation of mesenchymal stem cell-derived dopamine progenitors to functional neurons," *Journal of Neurochemistry*, vol. 110, no. 3, pp. 1058–1069, 2009.

[30] Y. Y. Liu, X. X. Zhao, H. B. Zhao, B. F. Ge, X. Y. Liu, and K. M. Chen, "Tetramethylpyrazine induces the differentiation of mouse bone marrow-derived mesenchymal stem cells into nerve cells mediated by Ca~(2+) signaling," *Journal of Gansu Agricultural University*, vol. 45, no. 2, pp. 1–5, 2010.

[31] W. Deng, M. Obrocka, I. Fischer, and D. J. Prockop, "In vitro differentiation of human marrow stromal cells into early progenitors of neural cells by conditions that increase intracellular cyclic AMP," *Biochemical and Biophysical Research Communications*, vol. 282, no. 1, pp. 148–152, 2001.

[32] W. Yue, F. Yan, Y. L. Zhang et al., "Differentiation of rat bone marrow mesenchymal stem cells into neuron-like cells in vitro and co-cultured with biological scaffold as transplantation carrier," *Medical Science Monitor*, vol. 22, pp. 1766–1772, 2016.

[33] N. Nakamoto, S. Tada, K. Kameyama et al., "A free radical scavenger, edaravone, attenuates steatosis and cell death via reducing inflammatory cytokine production in rat acute liver injury," *Free Radical Research*, vol. 37, no. 8, pp. 849–859, 2003.

[34] R. Zeng, Z. Hu, and W. Guo, "Electrophysiology study on differentiation of rat bone marrow stromal stem cells into neuron-like cells in vitro by edaravone," *Modern Practical Medicine*, vol. 21, no. 3, pp. 197–200, 2009.

[35] C. Weissmann, H. J. Reyher, A. Gauthier, H. J. Steinhoff, W. Junge, and R. Brandt, "Microtubule binding and trapping at the tip of neurites regulate tau motion in living neurons," *Traffic*, vol. 10, no. 11, pp. 1655–1668, 2009.

[36] D. Doherty, "Joubert syndrome: insights into brain development, cilium biology, and complex disease," *Seminars in Pediatric Neurology*, vol. 16, no. 3, pp. 143–154, 2009.

[37] C. H. Bailey, E. R. Kandel, and K. M. Harris, "Structural components of synaptic plasticity and memory consolidation," *Cold Spring Harbor Perspectives in Biology*, vol. 7, no. 7, article a021758, 2015.

[38] J. N. Bourne and K. M. Harris, "Nanoscale analysis of structural synaptic plasticity," *Current Opinion in Neurobiology*, vol. 22, no. 3, pp. 372–382, 2012.

[39] H. D. Guo, J. X. Tian, J. Zhu et al., "Electroacupuncture suppressed neuronal apoptosis and improved cognitive

impairment in the AD model rats possibly via downregulation of notch signaling pathway," *Evidence-Based Complementary and Alternative Medicine*, vol. 2015, Article ID 393569, 9 pages, 2015.

[40] Y. Jiang, B. Vaessen, T. Lenvik, M. Blackstad, M. Reyes, and C. M. Verfaillie, "Multipotent progenitor cells can be isolated from postnatal murine bone marrow, muscle, and brain," *Experimental Hematology*, vol. 30, no. 8, pp. 896–904, 2002.

[41] S. E. Smith, S. A. Figley, D. J. Schreyer, and P. G. Paterson, "Protein-energy malnutrition developing after global brain ischemia induces an atypical acute-phase response and hinders expression of GAP-43," *PLoS One*, vol. 9, no. 9, article e107570, 2014.

Hindawi
Stem Cells International
Volume 2018, Article ID 7609284, 8 pages
https://doi.org/10.1155/2018/7609284

Research Article

Differentiation Potential of Human Wharton's Jelly-Derived Mesenchymal Stem Cells and Paracrine Signaling Interaction Contribute to Improve the In Vitro Maturation of Mouse Cumulus Oocyte Complexes

Martin Maldonado, Tianhua Huang, Jianying Chen, and Ying Zhong

Reproductive Medicine & Genetics, Chengdu Jinjiang Hospital for Maternal & Child Health Care, Chengdu 610066, China

Correspondence should be addressed to Ying Zhong; yzhong2014@126.com

Received 5 June 2018; Revised 21 August 2018; Accepted 30 August 2018; Published 11 October 2018

Academic Editor: Hua Tan

Copyright © 2018 Martin Maldonado et al. This is an open access article distributed under the Creative Commons Attribution License, which permits unrestricted use, distribution, and reproduction in any medium, provided the original work is properly cited.

In vitro maturation (IVM) in cumulus oocyte complexes (COCs) can be improved by the presence of human Wharton's jelly-derived MSCs (hWJ-MSCs), under specific culture conditions. COCs were cultured in twelve different culture systems, composed of four stock media, stock media conditioned with hWJ-MSCs, and stock media in which the oocytes were indirectly cocultured with the hWJ-MSCs. The rates of maturation to meiosis II were compared among the groups. G2-PLUS and coculture with DMEM-F12 were the most efficient systems for the maturation of COCs. The fertilization rate and rate of development to the blastocyst stage were compared between these two groups. Moreover, hWJ-MSC-conditioned media showed no benefits for the COC-IVM. The analysis of OCT4 expression of hWJ-MSCs in G1-PLUS, TYH, and G2-PLUS showed a downregulation of OCT4 by 25.9, 24.7, and 6.6%, respectively, compared to that in hWJ-MSCs cultured in DMEM-F12. Finally, we have demonstrated that two prerequisites appeared to be necessary for the hWJ-MSCs to improve the IVM of COCs: hWJ-MSCs' differentiation potential and the presence of coordinated paracrine interaction between the stem cells and COCs. Under the appropriate conditions, the paracrine factors produced in the coculture system with DMEM-F12 may help to develop synthetic media for successful in vitro culture of COCs.

1. Background

In vitro maturation (IVM) in cumulus oocyte complexes (COCs) can be improved by the presence of human Wharton's jelly-derived MSCs (hWJ-MSCs), under specific culture conditions.

Mesenchymal stem cells (MSCs) are attractive candidates for cell-based therapeutic strategies, primarily due to their intrinsic ability to self-renew and undergo multipotential differentiation and because they are amenable to genetic manipulation [1–3].

In a coculture, MSCs not only provide a target cell source with multipotent differentiation capacity but can also act as assisting cells to promote tissue homeostasis, metabolism, growth, and repair [4]. Their incorporation into coculture systems seems to be important for creating complex tissues or organs by cell-to-cell contact or/and through the delivery of soluble factors to the target cells.

Among the different types of MSCs, human Wharton's jelly-derived MSCs (hWJ-MSCs) appear to offer the best clinical advantages due to their unique beneficial characteristics [5]. hWJ-MSCs reprogram resident cells to favor tissue regeneration, attenuate wound inflammation, and inhibit fibrosis [6, 7]. They interact with host cells and influence the stem cell niche through differentiation and/or paracrine signaling mechanisms [6, 8, 9]. They are poor

antigen-presenting cells; do not express MHC class II or the costimulatory molecules CD40, CD40L, CD80, and CD86 [10, 11]; and are not prone to undergo malignant transformation [12, 13].

Many attempts have been made to grow immature oocytes *in vitro* [14–16]. The culture conditions used for *in vitro* maturation (IVM), which include various media types and hormone supplements, as well as the presence of cumulus cells, can significantly influence maturation rates and subsequent embryo development [14, 17–19].

Furthermore, during ovarian follicular development, several growth factors and cytokines act as intraovarian regulators *in vivo*, and in the follicle, the action of gonadotrophins is modulated by locally produced paracrine and autocrine growth factors [20, 21].

Scientific evidence indicates that the secretion of trophic, soluble, or immunomodulatory factors, known as paracrine signals, may represent the most important underlying mechanism of MSC effects [9, 22, 23].

Given the appropriate stimuli and local environment, MSCs not only can develop into various cell types in vitro and regenerate tissues in vivo, but they can also secrete a variety of cytokines and growth factors, such as MCP-1, VEGF-A, EGF, FGF-2, IL-6, LIF, and TGF-β [2, 24].

Since cytokines and growth factors are known to stimulate meiotic progress and the processes associated with IVM, the aim of the present study was to determine whether IVM in cumulus oocyte complexes (COCs) could be improved by the presence of hWJ-MSCs through nonspecific release of cytokines and soluble factors using conditioned medium or by paracrine signaling from hWJ-MSCs using indirect coculture conditions. However, the success of IVM of COCs in coculture also depends on the choice of a suitable medium to allow oocyte maturation and the survival and potency of the hWJ-MSCs. In this work, we have opted to use DMEM-F12, a defined combination of nutrients, growth factors, and hormones that supports stemness and the differentiation potential of MSCs; two commercially available culture media for culture of human embryos from after fertilization until the 8-cell stage (G1-PLUS); a medium for culture of human embryos from the 8-cell stage on day three until the blastocyst stage (G2-PLUS); and TYH, first reported as a medium for in vitro fertilization (IVF) of mouse eggs with epididymal spermatozoa, by Yoda et al. [25] and Toyoda et al. [26] in 1971.

2. Methods

2.1. Animals. Male and female Kunming mice were maintained in a specific-pathogen-free animal facility in individual ventilated cages and housed at 23°C under a 12-hour dark/light cycle. Water and food were given *ad libitum*. All animal work was performed using protocols approved by the Institutional Review Board of the Chengdu Jinjiang Maternity and Child Health Hospital.

The health conditions of mice were monitored daily. Prior to the experimental endpoint, mice experienced minimal pain or stress during routine handling and hormone administration.

No ill or dead mice were observed prior to the experimental endpoint. Mice were euthanized by cervical dislocation.

2.2. Oocyte Handling. Mouse COCs were retrieved from 6- to 8-week-old Kunming mice (Chengdu Da Suo Biology and Technology Company) by ovary puncture with a 28 G sterile needle under a stereomicroscope. COCs were isolated 48 hours after an intraperitoneal injection of 10 IU of pregnant mare serum gonadotropin (PMSG, Sigma Chemical Co., St. Louis, MO). G-MOPS™ PLUS was used for handling and manipulation of the oocytes outside the incubator. Groups of oocytes were separated and cultured in 12 different culture systems and divided into 3 experimental stages. The first experimental stage included the following stock media preparations: (a) DMEM-F12 (Gibco; Thermo Fisher Scientific Inc., Waltham, MA, USA), (b) G1-PLUS (Vitrolife), (c) G2-PLUS (Vitrolife), and (d) TYH medium (Table S1). The second experimental stage included the following types of hWJ-MSC-conditioned media: (e) conditioned-DMEM-F12, (f) conditioned-G1-PLUS, (g) conditioned-G2-PLUS, and (h) conditioned-TYH. The third experimental stage included the following types of coculture with hWJ-MSCs: (i) coculture in DMEM-F12, (j) coculture in G1-PLUS, (k) coculture in G2-PLUS, and (l) coculture in TYH. The maturation status was evaluated after 24 hours of in vitro culture at 37°C in 6% CO_2. Oocytes with polar bodies were considered mature MII oocytes.

For all the experimental assays in this study, DMEM-F12 was supplemented with 10% fetal bovine serum (FBS, Thermo Fisher Scientific).

2.3. Isolation and Culture of hWJ-MSCs. Protocols for sampling the human umbilical cord were approved by the Institutional Review Board of Chengdu Jinjiang Hospital for Maternal & Child Health Care, according to the principles expressed in the Declaration of Helsinki. All participants provided their written consent to participate in this study. Human umbilical cords were obtained from consenting patients delivering full-term infants by cesarean section. The procedures for culture of hWJ-MSCs were consistent with those of Huang et al., with minor modifications [27]. Briefly, the arteries and veins of each tissue were mechanically removed, and the subamniotic region of the Wharton jelly was transferred to a sterile container and diced into small fragments. The explants were transferred into 100 mm plates with fresh growth media containing DMEM-F12 (Gibco)/FBS. The cells were left undisturbed for 7 days in a 37° humidified incubator with 5% CO_2 to allow migration of cells from the explants. Thereafter, the tissue was removed, and the hWJ-MSCs were evenly redistributed by digesting them with TrypLE (Gibco). Fresh media (4-5 ml) were added every 2/3 days. Then, the cells (±90% confluence) were digested and replated at a 1 : 5 ratio.

We have previously assessed the phenotypic properties of hWJ-MSCs based on the immune response-related surface markers CD80, CD86, CD40, CD40L, HLA-1, and HLA-DR [12].

2.4. Preparation of Conditioned Media. hWJ-MSCs (80% confluence) were cultured for 24 hours with each one of the following media types: (a) DMEM-F12, (b) G1-PLUS, (c) G2-PLUS, or (d) TYH. Thereafter, the media were collected and immediately used for COC IVM.

2.5. Indirect Coculture of COCs with hWJ-MSCs. hWJ-MSCs were plated in 24.5 mm, 3 μm Transwel culture plates (Corning™, Inc.). COCs were allocated on the permeable polycarbonate membrane and coincubated with the hWJ-MSCs for 24 hours in the following media conditions: (a) hWJ-MSC-COCs-DMEM-F12, (b) hWJ-MSC-COCs-G1-PLUS, (c) hWJ-MSC-COCs-G2-PLUS, or (d) hWJ-MSC-COCs-TYH.

2.6. Quantitative Real-Time Polymerase Chain Reaction (qPCR) Assay. The OCT4 expression of hWJ-MSCs in the 4 coculture systems were analyzed by qPCR. The cells were homogenized, and the RNA was extracted with the TaKaRa MiniBEST Universal RNA Extraction Kit (TaKaRa Bio Inc.). The total RNA concentration and O.D. were assayed by UV spectrophotometry. Genomic DNA elimination was performed with TaKaRa RR047Q. qPCR was performed with 200 ng of target cDNA; OCT4 (forward, GTGTTCAGC CAAAAGACCATCT; reverse, GGCCTGCATGAGGGTT TCT) and β-actin (Table S2), which was used as a reference gene (forward, CCTCATGAAGATCCTCACCGA; reverse, TTGCCAATGGTGATGACCTGG), were evaluated using relative quantification with SYBR Premix Ex Taq™ (Takara RR420Q) using an ABI 7500 (Applied Biosystems, Foster City, CA). The data analyzed was collected from 3 different experiments and the samples were run in triplicate.

2.7. IVM and IVF. IVM, with standard and conditioned media, was performed in 50 μl microdrops of medium containing 10 COCs per microdrop, under mineral oil submersion for 24 hours at 37°C with 6% CO_2. For coculture, groups of ±50 COCs were cultured with hWJ-MSCs in the various combinations of media, as explained in Section 2.5. The oocytes were monitored for IVM by confocal microscopy at 0 and 24 hours.

IVF then was performed as follows. Briefly, epididymis tissues from Kunming mice were isolated and subjected to small cuts with scissors. The growth medium (1 ml of G2-PLUS or DMEM-F12) was added, and the mixture was incubated for 7 min at 37°C. Then, the supernatant was centrifuged at 650 ×g for 5 min and discarded. The remaining pellet was resuspended by pipetting with 1 ml of medium and incubated at 37°C for 1 hour (capacitation). A second centrifugation was performed, and 700 μl of the 800 μl of supernatant was discarded. The remaining volume contained the activated spermatozoa. Groups of oocytes ($n = 20$) were inseminated in 80 μl microdrops of the activated spermatozoa in G2-PLUS medium (under equilibrated mineral oil at 37°C in air with 6% CO_2). For IVF in coculture conditions, groups of oocytes ($n = 20$) were inseminated in 80 μl microdrops previously cultured with hWJ-MSCs in DMEM-F12 medium. At the time of insemination, the DMEM-F12 medium was replaced with the activated spermatozoa in DMEM-F12 medium. A portion of the oocytes from each treatment was incubated without spermatozoa to evaluate the incidence of spontaneous activation (data not shown). Six hours after insemination, the oocytes were gently cleaned by pipetting, and presumptive zygotes obtained from COCs were separately cultured *in vitro* for 5 days in G2-PLUS medium or cocultured with hWJ-MSCs in DMEM-F12 medium (37°C, in air with 6% CO_2). The proportion of the embryos at each stage was recorded at 24 hours, 48 hours, and after 5 days of *in vitro* culture.

2.8. Statistical Analysis. Statistical analysis was performed using Microsoft Office Excel 2010. The oocyte maturation, fertilization, and embryonic development rates were calculated using the Pearson chi-squared test. The qPCR data was analyzed with the two-tailed paired Student's t-test. A P value < 0.05 was considered to indicate statistical significance.

3. Results

3.1. IVM and IVF of COCs. A total of 2422 immature oocytes met the eligibility criteria for this study. The developmental competency of COCs is listed in Table 1.

Among the 12 culture systems analyzed in this work, G2-PLUS and coculture-DMEM-F12 were the most effective media conditions for IVM. Both showed no significant differences in their ability to improve oocyte maturation and were statistically different from the rest of the systems.

When the groups were compared according to media type (Figure 1), we noticed that conditioning DMEM-F12 (Figure 1(a)) and G2-PLUS (Figure 1(c)) with hWJ-MSCs yielded negative outcomes compared to those from stock media, suggesting that the release of unspecific soluble factors from hWJ-MSCs may have an adverse effect on the oocyte maturation. In conditioned-G1-PLUS (Figure 1(b)), IVM was not significantly different from the stock media. Moreover, no improvement was noted in conditioned-TYH culture (Figure 1(d)).

On the other hand, the coculture system in G1- and G2-PLUS media appeared to have detrimental effects on IVM (Figures 1(b) and 1(c)) compared to the effects of culture in stock media. Coculture in TYH showed no significant differences with stock media conditions (Figure 1(d)). However, the IVM of COCs in coculture with hWJ-MSC-DMEM-F12 was significantly improved compared to IVM in stock DMEM-F12 (Figure 1(a)).

We also analyzed the fertilization and developmental rates of oocytes cultured in G2-PLUS and cocultured with DMEM-F12 media. Although we noticed a modest improvement in the rate of development to the blastocyst stage in the coculture with DMEM-F12, the result was not significant at $P < 0.05$ (Table 1). Oocytes, either cultured in G2-PLUS or cocultured in DMEM-F12 media, cleaved and likely did not experience developmental arrest at the pronuclear stage.

3.2. Analysis of OCT4 Expression. The POU transcription factor OCT4 (Table S2), encoded by POU5F1, is critical for sustaining the self-renewal capacity of adult somatic stem cells [28, 29] and is considered a master regulator of pluripotency

Table 1: Developmental competency of COCs among the different culture systems.

Culture media	Total number of COCs	Polar bodies (number)	Polar bodies (%)	Number of cleaved oocytes (%)	Number of blastocyst stage (%)
DMEM-F12	199	81	40.7		
G1-PLUS	204	85	41.6		
G2-PLUS	199	115	57.8*	61 (53.04)	7 (11.48)
TYH	198	71	35.9		
Conditioned-DMEM-F12	200	56	28		
Conditioned-G1-PLUS	206	79	38.4		
Conditioned-G2-PLUS	204	69	33.8		
Conditioned-TYH	202	81	40.1		
Coculture-DMEM-F12	205	115	56.1*	58 (50.43)	8 (13.79)
Coculture-G1-PLUS	203	51	25.1		
Coculture-G2-PLUS	206	66	32		
Coculture-TYH	196	74	37.7		

Oocytes with polar bodies were considered mature MII oocytes. The fertilization rate and rate of development to the blastocyst stage were compared between G2-PLUS and coculture-DMEM-F12. *Both showed no significant differences in their ability to improve oocyte maturation and were statistically different from the rest of the systems. The data were analyzed by the chi-squared test. A value of $P < 0.05$ was considered statistically significant.

that controls lineage commitment [30]. We analyzed OCT4 expression of hWJ-MSCs, by qPCR in the 4 different stock media with the aim of verifying whether the specific media affected hWJ-MSC potency. Our data confirmed that the expression of OCT4 in hWJ-MSCs cultured on G1-PLUS, TYH, and G2-PLUS was downregulated by 25.9, 24.7, and 6.6%, respectively, compared to that in hWJ-MSCs cultured in DMEM-F12 (Figure 2). We also confirmed that the expression of OCT4 from hWJ-MSCs was not affected by the presence of COCs when cultured in DMEM-F12.

4. Discussion

Culture conditions, including the formulation of the base medium, supplementations, and the in vitro physical environment (such as the oxygen tension and presence of cumulus cells), all influence multiple events that are crucial to oocyte maturation and subsequent embryonic development [31, 32].

The culture media types have been shown to modulate not only the metabolism of oocytes [33] but also the maturation to MII, the kinetics of cell cycle progression, and spindle/chromatin organization [34, 35].

Scientific evidence suggests that gonadotropins, epidermal growth factor, and essential and nonessential amino acids improve the maturation of porcine oocytes [36, 37]. Human menopausal gonadotropin, pregnant mare serum gonadotropin, follicle-stimulating hormone (FSH), and luteinizing hormone, pyruvic acid, estradiol (E2), recombinant FSH, insulin, transferrin, and selenium have been included in the IVM media for human oocyte maturation [38–40]. Undefined protein sources, such as fetal bovine serum, human maternal serum, synthetic human serum, and human follicular and peritoneal fluid have also been used to supplement maturation media [41–43].

Although taurine and calcium lactates have been suggested as necessary components for IVM of mouse COCs [30], the two most efficient culture media (G2-PLUS and DMEM-F12) tested in this work lacked these compounds.

It is evident that there is no consensus on the adequate supplementation media for oocyte maturation as the postulated compounds and combinations stated above have yielded suboptimal results, thus reinforcing the idea that the in vitro culture conditions lack some crucial components.

One of the shortcomings in the type of culture system used to date has been the absence of somatic cell support.

The role of stem cells in coculture reaches beyond that of simply providing a favorable cell source with multipotent differentiation capacity. Whether serving in target or assisting roles, stem cells are pivotal in tissue growth, metabolism, maturation, and repair [44, 45].

Many kinds of exogenous growth factors are secreted by MSCs, some of which are important components of the follicle developmental microenvironment for appropriate "oocyte capacitation" or oocyte cytoplasmic development prior to maturation [20].

The present work supported the idea that remote cell signaling from hWJ-MSCs positively affects meiotic progression of COCs maintained in the same microenvironment with DMEM-F12, resulting in a defined combination of nutrients, growth factors, and hormones that supports oocyte maturation and the differentiation potential of MSCs.

Our data also suggest that the paracrine factors produced by hWJ-MSCs in DMEM-F12 helped cocultured COCs to reach levels of nuclear and cytoplasmic maturation similar to those seen in culture with G2-PLUS, a blastocyst culture medium with superior efficiency for IVM of immature oocytes [30]. However, the specific compounds produced by the hWJ-MSCs, such as cytokines and soluble and growth factors that might be involved in the regulation of oocyte maturation, need to be identified.

In addition, the beneficial effect of coculture did not require any direct contact between the hWJ-MSCs and COCs during IVM and IVF, as previously reported for

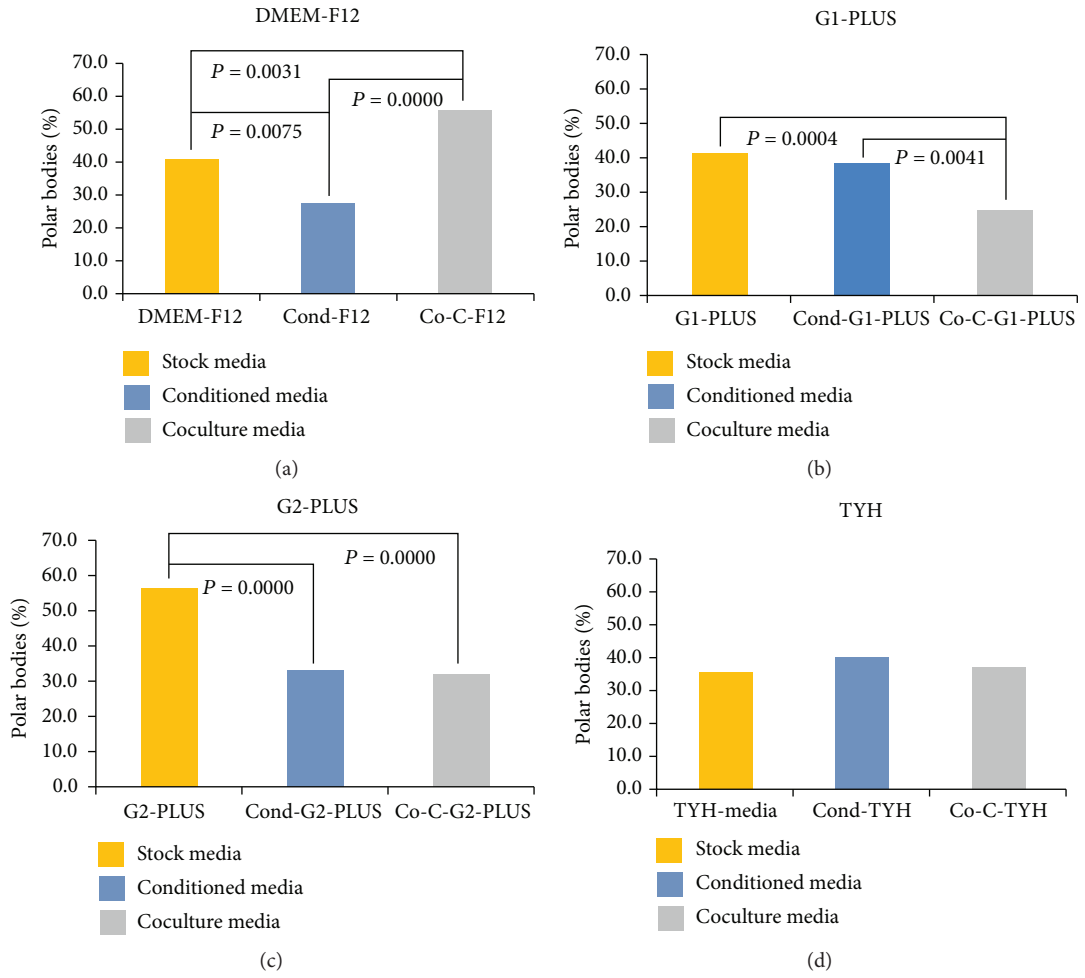

Figure 1: Comparison of IVM for COCs cultured in the same media: DMEM-F12 (a), G1-PLUS (b), G2-PLUS (c), and TYH (d). The data were analyzed by the chi-squared test. A value of $P < 0.05$ was considered statistically significant.

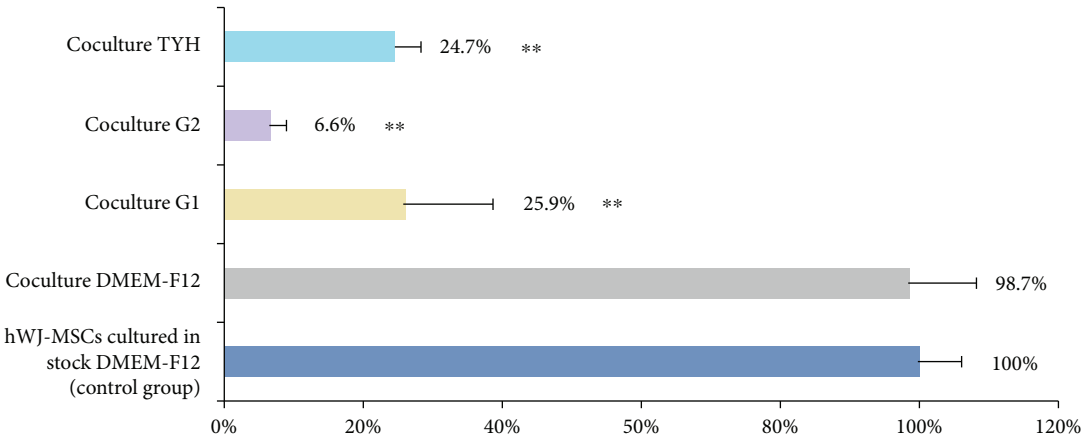

Figure 2: qPCR analysis of OCT4 in hWJ-MSCs cultured under the 4 coculture conditions. In G1-PLUS, TYH, and G2-PLUS, OCT4 expression was downregulated to 25.9, 24.7, and 6.6%, respectively, compared to the OCT4 level in hWJ-MSCs cultured in DMEM-F12. The expression of OCT4 from hWJ-MSCs was not affected by the presence of COCs when cultured in DMEM-F12 (control group). The data was analyzed with the two-tailed paired Student's t-test. A P value < 0.05 was considered to indicate statistical significance. $^{**}(P < 0.01)$ is the statistical significance compared with coculture-DMEM-F12.

bovine and mouse oocytes [46, 47], supporting the idea that cell-cell interaction occurs via soluble factors triggered by remote cell signaling.

The scientific evidence suggests that some of the positive effects of soluble factors secreted by hWJ-MSCs might be due to antioxidant properties, especially since it is now

recognized that exogenous antioxidants improve maturation *in vitro* in the cat [48] and specifically support the MI to MII transition in pig oocytes [49].

The above statements appear to be consistent with our results showing that the hWJ-MSC-conditioned medium had no positive effect on the IVM of COCs and suggest that coordinated paracrine signaling communication is required between the assisting (hWJ-MSCs) and the target cells (COCs).

We evaluated the fertilization rate and extended culture up to the blastocyst stage to detect the maturation and developmental competence of the oocytes, which should be better indicators than molecular markers or detailed morphological studies.

We also verified that oocytes, either cultured in G2-PLUS or cocultured in DMEM-F12 media, cleaved and likely did not experience developmental arrest at the pronuclear stage. Nonetheless, further studies should be conducted to ascertain the implantation and pregnancy potential of these embryos, and detailed analysis of their chromosomal status or genomic imprinting pattern should be performed.

OCT4 is a critical transcription factor for regulating the self-renewal and differentiation properties of ESCs [50] and its downregulation induces loss of pluripotency and dedifferentiation to the trophectoderm [51].

hWJ-MSCs constitutively express the early embryonic transcription factors Nanog, OCT4, Sox-2, Rex-1, and LIN28, indicating their multipotency and high self-renewal capacity [52, 53].

Moreover, the expression of the pluripotency genes, OCT4, Nanog, and Sox-2, was also reported for WJ-MSCs [52, 54, 55], although it was much lower than that in ESC [53]. Modest expression of pluripotency genes might explain why WJ-MSCs are not tumorigenic.

In our work, we have opted to analyze the pluripotency gene OCT4 as a tool for the identification of cell differentiation since up- or downregulation of OCT4 indicates loss of differentiation potential and stemness regardless of the expression of the other markers of pluripotency expressed in these cells.

We have already suggested that specific MSC media compositions are necessary for the hWJ-MSCs to positively interact with COCs and improve IVM, which is also correlated with the expression of OCT4 and consequently with the differentiation potential of the hWJ-MSCs. However, further investigation with different commercially available media formulations that support MSC culture will be required to support this idea.

Importantly, cell-cell interactions are seldom unidirectional, with both cell populations being affected in a coculture system. However, the rate at which COCs were cocultured with hWJ-MSCs in this study demonstrated that oocytes had no effect on the OCT4 expression of hWJ-MSCs; thus, the potency of the stem cells remained unaffected.

5. Conclusion

Our findings support the concept of cross-talk between hWJ-MSCs and COCs in indirect coculture. We have demonstrated that two prerequisites appear to be necessary for hWJ-MSCs to improve COC IVM: stem cell differentiation potential and paracrine signaling interaction with the COCs. The paracrine factors produced by hWJ-MSCs in the coculture system with the DMEM-F12 medium may guide the development of synthetic media for successful in vitro culture of COCs.

Data Availability

All data generated or analyzed during this study are included in this published article (and its supplementary information files).

Conflicts of Interest

The authors indicate no potential conflicts of interest.

Acknowledgments

This work was supported by the Chengdu Jinjiang Hospital for Maternal & Child Health Care, Chengdu, China.

Supplementary Materials

Table S1: TYH medium formulation. Table S2: list of primers. *(Supplementary Materials)*

References

[1] R. J. Deans and A. B. Moseley, "Mesenchymal stem cells: biology and potential clinical uses," *Experimental Hematology*, vol. 28, no. 8, pp. 875–884, 2000.

[2] A. I. Caplan and J. E. Dennis, "Mesenchymal stem cells as trophic mediators," *Journal of Cellular Biochemistry*, vol. 98, no. 5, pp. 1076–1084, 2006.

[3] M. Kassem, M. Kristiansen, and B. M. Abdallah, "Mesenchymal stem cells: cell biology and potential use in therapy," *Basic & Clinical Pharmacology & Toxicology*, vol. 95, no. 5, pp. 209–214, 2004.

[4] N. K. Paschos, W. E. Brown, R. Eswaramoorthy, J. C. Hu, and K. A. Athanasiou, "Advances in tissue engineering through stem cell-based co-culture," *Journal of Tissue Engineering and Regenerative Medicine*, vol. 9, no. 5, pp. 488–503, 2015.

[5] A. Bongso and C. Y. Fong, "The therapeutic potential, challenges and future clinical directions of stem cells from the Wharton's jelly of the human umbilical cord," *Stem Cell Reviews*, vol. 9, no. 2, pp. 226–240, 2013.

[6] M. Maldonado, T. Huang, L. Yang, L. Xu, and L. Ma, "Human umbilical cord Wharton jelly cells promote extra-pancreatic insulin formation and repair of renal damage in STZ-induced diabetic mice," *Cell Communication and Signaling*, vol. 15, no. 1, p. 43, 2017.

[7] W. M. Jackson, L. J. Nesti, and R. S. Tuan, "Mesenchymal stem cell therapy for attenuation of scar formation during wound healing," *Stem Cell Research & Therapy*, vol. 3, no. 3, p. 20, 2012.

[8] H. Li and X. Fu, "Mechanisms of action of mesenchymal stem cells in cutaneous wound repair and regeneration," *Cell and Tissue Research*, vol. 348, no. 3, pp. 371–377, 2012.

[9] A. M. Hocking and N. S. Gibran, "Mesenchymal stem cells: paracrine signaling and differentiation during cutaneous wound repair," *Experimental Cell Research*, vol. 316, no. 14, pp. 2213–2219, 2010.

[10] M. L. Weiss, C. Anderson, S. Medicetty et al., "Immune properties of human umbilical cord Wharton's jelly-derived cells," *Stem Cells*, vol. 26, no. 11, pp. 2865–2874, 2008.

[11] S. Liu, M. Yuan, K. Hou et al., "Immune characterization of mesenchymal stem cells in human umbilical cord Wharton's jelly and derived cartilage cells," *Cellular Immunology*, vol. 278, no. 1-2, pp. 35–44, 2012.

[12] Q. Tang, Q. Chen, X. Lai et al., "Malignant transformation potentials of human umbilical cord mesenchymal stem cells both spontaneously and via 3-methycholanthrene induction," *PLoS One*, vol. 8, no. 12, article e81844, 2013.

[13] A. Bongso, C. Y. Fong, and K. Gauthaman, "Taking stem cells to the clinic: major challenges," *Journal of Cellular Biochemistry*, vol. 105, no. 6, pp. 1352–1360, 2008.

[14] H. Miki, N. Ogonuki, K. Inoue, T. Baba, and A. Ogura, "Improvement of cumulus-free oocyte maturation in vitro and its application to microinsemination with primary spermatocytes in mice," *Journal of Reproduction and Development*, vol. 52, no. 2, pp. 239–248, 2006.

[15] N. Mousset-Simeón, P. Jouannet, L. Le Cointre, C. Coussieu, and C. Poirot, "Comparison of three in vitro culture systems for maturation of early preantral mouse ovarian follicles," *Zygote*, vol. 13, no. 2, pp. 167–175, 2005.

[16] S. Lenie, R. Cortvrindt, T. Adriaenssens, and J. Smitz, "A reproducible two-step culture system for isolated primary mouse ovarian follicles as single functional units," *Biology of Reproduction*, vol. 71, no. 5, pp. 1730–1738, 2004.

[17] H. Nakano and H. Kubo, "Study of the in vitro maturation of mouse oocytes induced by microinjection of maturation promoting factor (MPF)," *Journal of Assisted Reproduction and Genetics*, vol. 17, no. 1, pp. 67–73, 2000.

[18] B. C. A. Heng and N. S. Chye, "Investigations of oocyte in vitro maturation within a mouse model," *Zygote*, vol. 12, no. 1, pp. 1–18, 2004.

[19] R. De La Fuente, M. J. O'Brien, and J. J. Eppig, "Epidermal growth factor enhances preimplantation developmental competence of maturing mouse oocytes," *Human Reproduction*, vol. 14, no. 12, pp. 3060–3068, 1999.

[20] R. B. Gilchrist and J. G. Thompson, "Oocyte maturation: emerging concepts and technologies to improve developmental potential in vitro," *Theriogenology*, vol. 67, no. 1, pp. 6–15, 2007.

[21] M. Sakaguchi, T. Dominko, N. Yamauchi, M. L. Leibfried-Rutledge, T. Nagai, and N. L. First, "Possible mechanism for acceleration of meiotic progression of bovine follicular oocytes by growth factors in vitro," *Reproduction*, vol. 123, no. 1, pp. 135–142, 2002.

[22] G. Ren, X. Chen, F. Dong et al., "Concise review: mesenchymal stem cells and translational medicine: emerging issues," *Stem Cells Translational Medicine*, vol. 1, no. 1, pp. 51–58, 2012.

[23] K. Khosrotehrani, "Mesenchymal stem cell therapy in skin: why and what for?," *Experimental Dermatology*, vol. 22, no. 5, pp. 307–310, 2013.

[24] M. Heil, T. Ziegelhoeffer, B. Mees, and W. Schaper, "A different outlook on the role of bone marrow stem cells in vascular growth: bone marrow delivers software not hardware," *Circulation Research*, vol. 94, no. 5, pp. 573-574, 2004.

[25] Y. Yoda, M. Yokoyama, and T. Hosi, "Studies on the fertilization of mouse eggs in vitro. I. In vitro fertilization of eggs by fresh epididymal sperm," *The Japanese Journal of Animal Reproduction*, vol. 16, no. 4, pp. 147–151, 1971.

[26] Y. Toyoda, M. Yokoyama, and T. Hosi, "Studies on the fertilization of mouse eggs in vitro. II. Effects of in vitro preincubation of spermatozoa on time of sperm penetration of mouse eggs in vitro," *The Japanese Journal of Animal Reproduction*, vol. 16, no. 4, pp. 152–157, 1971.

[27] P. Huang, L. M. Lin, X. Y. Wu et al., "Differentiation of human umbilical cord Wharton's jelly-derived mesenchymal stem cells into germ-like cells in vitro," *Journal of Cellular Biochemistry*, vol. 109, pp. 747–754, 2010.

[28] M. H. Tai, C. C. Chang, M. Kiupel, J. D. Webster, L. K. Olson, and J. E. Trosko, "Oct4 expression in adult human stem cells: evidence in support of the stem cell theory of carcinogenesis," *Carcinogenesis*, vol. 26, no. 2, pp. 495–502, 2005.

[29] J. H. Kim, M. K. Jee, S. Y. Lee et al., "Regulation of adipose tissue stromal cells behaviors by endogenic Oct4 expression control," *PLoS One*, vol. 4, no. 9, article e7166, 2009.

[30] M. Kim, S. J. Hong, J. H. Lee, C. K. Min, K. J. Hwang, and R. W. Park, "Comparison of in vitro maturation media of immature oocytes: the effectiveness of blastocyst culture media," *Fertility and Sterility*, vol. 95, no. 2, pp. 554–557, 2011.

[31] J. J. M. van de Sandt, A. C. Schroeder, and J. J. Eppig, "Culture media for mouse oocyte maturation affect subsequent embryonic development," *Molecular Reproduction and Development*, vol. 25, no. 2, pp. 164–171, 1990.

[32] M. L. Sutton, R. B. Gilchrist, and J. G. Thompson, "Effects of in-vivo and in-vitro environments on the metabolism of the cumulus–oocyte complex and its influence on oocyte developmental capacity," *Human Reproduction Update*, vol. 9, no. 1, pp. 35–48, 2003.

[33] R. Roberts, S. Franks, and K. Hardy, "Culture environment modulates maturation and metabolism of human oocytes," *Human Reproduction*, vol. 17, no. 11, pp. 2950–2956, 2002.

[34] N. A. Cekleniak, C. M. H. Combelles, D. A. Ganz, J. Fung, D. F. Albertini, and C. Racowsky, "A novel system for in vitro maturation of human oocytes," *Fertility and Sterility*, vol. 75, no. 6, pp. 1185–1193, 2001.

[35] A. Trounson, C. Anderiesz, and G. Jones, "Maturation of human oocytes in vitro and their developmental competence," *Reproduction*, vol. 121, no. 1, pp. 51–75, 2001.

[36] M. M. Bevers and F. Izadyar, "Role of growth hormone and growth hormone receptor in oocyte maturation," *Molecular and Cellular Endocrinology*, vol. 197, no. 1-2, pp. 173–178, 2002.

[37] J. Y. Hong, H. Y. Yong, B. C. Lee, W. S. Hwang, J. M. Lim, and E. S. Lee, "Effects of amino acids on maturation, fertilization and embryo development of pig follicular oocytes in two IVM media," *Theriogenology*, vol. 62, no. 8, pp. 1473–1482, 2004.

[38] X. Zhang, A. Zerafa, J. Wong, D. T. Armstrong, and F. Khamsi, "Human menopausal gonadotropin during in vitro maturation of human oocytes retrieved from small follicles enhances in vitro fertilization and cleavage rates," *Fertility and Sterility*, vol. 59, no. 4, pp. 850–853, 1993.

[39] K. Cha, H. Chung, D. Lee et al., "Obstetric outcome of patients with polycystic ovary syndrome treated by in vitro maturation and in vitro fertilization-embryo transfer," *Fertility and Sterility*, vol. 83, no. 5, pp. 1461–1465, 2005.

[40] E. Isachenko, G. Rahimi, V. Isachenko, and F. Nawroth, "In-vitro maturation of germinal-vesicle oocytes and cryopreservation in metaphase I/II: a possible additional option to preserve fertility during ovarian tissue cryopreservation," *Reproductive BioMedicine Online*, vol. 8, no. 5, pp. 553–557, 2004.

[41] R.-C. Chian, W. M. Buckett, A. K. A. Jalil et al., "Natural-cycle in vitro fertilization combined with in vitro maturation of immature oocytes is a potential approach in infertility treatment," *Fertility and Sterility*, vol. 82, no. 6, pp. 1675–1678, 2004.

[42] A. L. Mikkelsen, "Strategies in human in-vitro maturation and their clinical outcome," *Reproductive BioMedicine Online*, vol. 10, no. 5, pp. 593–599, 2005.

[43] K. Y. Cha, J. J. Koo, J. J. Ko, D. H. Choi, S. Y. Han, and T. K. Yoon, "Pregnancy after in vitro fertilization of human follicular oocytes collected from nonstimulated cycles, their culture in vitro and their transfer in a donor oocyte program," *Fertility and Sterility*, vol. 55, no. 1, pp. 109–113, 1991.

[44] N. I. Kalinina, V. Y. Sysoeva, K. A. Rubina, Y. V. Parfenova, and V. A. Tkachuk, "Mesenchymal stem cells in tissue growth and repair," *Acta Naturae*, vol. 3, no. 4, pp. 30–37, 2011.

[45] N. Sato, L. Meijer, L. Skaltsounis, P. Greengard, and A. H. Brivanlou, "Maintenance of pluripotency in human and mouse embryonic stem cells through activation of Wnt signaling by a pharmacological GSK-3-specific inhibitor," *Nature Medicine*, vol. 10, no. 1, pp. 55–63, 2004.

[46] A. M. Luciano, V. Lodde, M. S. Beretta, S. Colleoni, A. Lauria, and S. Modina, "Developmental capability of denuded bovine oocyte in a co-culture system with intact cumulus-oocyte complexes: role of cumulus cells, cyclic adenosine $3'$,$5'$-monophosphate, and glutathione," *Molecular Reproduction and Development*, vol. 71, no. 3, pp. 389–397, 2005.

[47] L. Ge, D. Han, G. C. Lan et al., "Factors affecting the in vitro action of cumulus cells on the maturing mouse oocytes," *Molecular Reproduction and Development*, vol. 75, no. 1, pp. 136–142, 2008.

[48] P. Comizzoli, D. E. Wildt, and B. S. Pukazhenthi, "Overcoming poor in vitro nuclear maturation and developmental competence of domestic cat oocytes during the non-breeding season," *Reproduction*, vol. 126, no. 6, pp. 809–816, 2003.

[49] Y. Tao, B. Zhou, G. Xia, F. Wang, Z. Wu, and M. Fu, "Exposure to L-ascorbic acid or α-tocopherol facilitates the development of porcine denuded oocytes from metaphase I to metaphase II and prevents cumulus cells from fragmentation," *Reproduction in Domestic Animals*, vol. 39, no. 1, pp. 52–57, 2004.

[50] J. Nichols, B. Zevnik, K. Anastassiadis et al., "Formation of pluripotent stem cells in the mammalian embryo depends on the POU transcription factor Oct4," *Cell*, vol. 95, no. 3, pp. 379–391, 1998.

[51] H. Niwa, J. Miyazaki, and A. G. Smith, "Quantitative expression of Oct-3/4 defines differentiation, dedifferentiation or self-renewal of ES cells," *Nature Genetics*, vol. 24, no. 4, pp. 372–376, 2000.

[52] C. K. Tong, S. Vellasamy, B. Chong Tan et al., "Generation of mesenchymal stem cell from human umbilical cord tissue using a combination enzymatic and mechanical disassociation method," *Cell Biology International*, vol. 35, no. 3, pp. 221–226, 2011.

[53] C.-Y. Fong, L.-L. Chak, A. Biswas et al., "Human Wharton's jelly stem cells have unique transcriptome profiles compared to human embryonic stem cells and other mesenchymal stem cells," *Stem Cell Reviews and Reports*, vol. 7, no. 1, pp. 1–16, 2011.

[54] J. H. Yoon, E. Y. Roh, S. Shin et al., "Comparison of explant-derived and enzymatic digestion-derived MSCs and the growth factors from Wharton's jelly," *BioMed Research International*, vol. 2013, Article ID 428726, 8 pages, 2013.

[55] U. Nekanti, L. Mohanty, P. Venugopal, S. Balasubramanian, S. Totey, and M. Ta, "Optimization and scale-up of Wharton's jelly-derived mesenchymal stem cells for clinical applications," *Stem Cell Research*, vol. 5, no. 3, pp. 244–254, 2010.

Hindawi
Stem Cells International
Volume 2018, Article ID 3481783, 8 pages
https://doi.org/10.1155/2018/3481783

Research Article

Integrated Genome-Wide Analysis of Gene Expression and DNA Copy Number Variations Highlights Stem Cell-Related Pathways in Small Cell Esophageal Carcinoma

Di Liu,[1] Xinyan Xu,[1] Junmiao Wen,[1] Liyi Xie,[1] Junhua Zhang,[1] Yuxin Shen,[2] Guoliang Jiang,[1] Jiayan Chen ,[1] and Min Fan [1]

[1]*Department of Radiation Oncology, Fudan University Shanghai Cancer Center, Shanghai, China*
[2]*Department of Radiation Oncology, The Second Military Medical University, Shanghai, China*

Correspondence should be addressed to Jiayan Chen; chenjiayan2008@126.com and Min Fan; fanming1@yahoo.com

Received 17 March 2018; Accepted 2 July 2018; Published 30 August 2018

Academic Editor: Weijun Su

Copyright © 2018 Di Liu et al. This is an open access article distributed under the Creative Commons Attribution License, which permits unrestricted use, distribution, and reproduction in any medium, provided the original work is properly cited.

Purpose/Objectives. Primary small cell esophageal carcinoma (SCEC) represents a rare and aggressive malignancy without any prospective clinical trial or established treatment strategy at present. Although previous studies have indicated similarities between SCEC and small cell lung cancer (SCLC) in terms of their clinical manifestations, pathology, and morphology, very little genetic information is available on this highly malignant tumor. At present, patients with SCEC are staged and treated according to the guidelines established for SCLC. However, early recurrence and distant metastasis are common, and long-time survivors are rare. Current options available for patients with relapsed SCEC are fairly unsatisfactory, and their prognosis is generally poor. Novel therapeutic approaches against SCEC are therefore urgently needed and require a deeper understanding of the underlying genetic mechanisms. The current investigation aims to characterize the gene expression profile and copy number variations (CNVs) in SCEC to clarify molecular markers and pathways that may possess clinical significance. *Materials/Methods*. De novo expression array was carried out on three matched sets of primary SCEC and adjacent normal tissue samples procured from the institutional tissue bank, utilizing the Affymetrix HG U133 Plus 2.0 Array. After individual tissue normalization, the statistical software GeneSpring GX 12.5 was used to determine differentially expressed genes (DEGs) in the tumors relative to their paired normal tissues. Gene enrichments in addition to functional annotation and gene interaction networks were performed using DAVID 6.8 and STRING 10.0, respectively. A gene alteration was determined to be recurrent if it was observed in at least 2 samples. Chromosomes X and Y were not included in calculations as gender differences are a known source of analysis bias. The DEGs of at least one SCEC sample could be mapped to the CNV regions (fold change (FC) ≥ 2 and false discovery rate (FDR) < 0.01) after gene expression profiling by RefSeq Transcript ID. These overlapped genes were subjected to the functional annotation using DAVID 6.8. In order to elucidate the effect of CNV on mRNA expression, we integrated the genome-wide copy number data and gene expression in 3 paired samples. CNV-associated gene expression aberration (CNV-FC) was calculated for the recurrent DEGs using previously published integrated microarray data as reference. Pearson's correlation coefficient was employed to determine if there was a statistical correlation between the gene expression $\log_2$ ratios and their copy numbers using the SPSS 19.0 software. Genes that possessed CNV-FC ≥ 2 and $r \geq 0.6$ ($p < 0.05$) were determined to be genes potentially associated with cancer. *Results*. High-quality DNA and total RNA were first extracted from both SCEC and normal tissues. Microarray data showed significant upregulation in WNT gene sets and downregulation in the PTEN and notch gene sets in SCEC. Functional annotation showed that genes associated with DNA replication, mitosis, cell cycle, DNA repair, telomere maintenance, RB, and p53 pathways were significantly altered in SCEC compared to corresponding noncancerous tissues (Benjamini $p < 0.05$). Thirteen recurrent CNVs were found in all SCEC samples by array CGH. Chromosomal regions with gain were located in 14q11.2, and regions with loss were located in 4q22.3-23.3, 3q25.31-q29, 5p15.31-15.2, 8q21.11-24.3, and 9p23-13.1 in all samples. In two samples, the 14q11.2-32.33 region was amplified, whereas 3p26.3-25.3, 4p16.3-11, 4q11-22.3, 4q23-25, 8p23.3, and 16p13.3 were deleted. We further identified 306 genes that consistently differed in copy number and expression (194 upregulated and 112 downregulated) between the SCEC and noncancerous tissues in all three samples. These genes were significantly enriched with those involved in cell cycle, mitosis, DNA repair, P53 pathway,

and RB pathway, according to their functional annotation. These 306 DEGs also included network genes of the above pathways such as NUF2, CCNE2, NFIB, ETV5, KLF5, ATAD2, NDC80, and ZWINT. In addition, 39 individual DEGs demonstrated a minimum 2-fold copy number-associated expression change (median: 5.35, 95% CI: 4.53–16.98) and Pearson's correlation coefficient ≥ 0.6 ($p < 0.05$), of which PTP4A3 showed the highest correlation (CNV-FC = 21362.13; Pearson's correlation coefficient = 0.9983; $p = 0.037$). Two distinct groups of genes belonging to each SCEC and nonmalignant tissues were observed upon unsupervised two-way (genes and samples) hierarchical clustering. *Conclusions*. The current investigation is the first to produce data regarding the genomic signature of SCEC at the transcription level and in relation to CNVs. Our preliminary data indicate possible key roles of WNT and notch signaling in SCEC and overexpressed PTP4A3 as a potential therapeutic target. Further validation of our findings is warranted.

1. Introduction

Primary small cell esophagus carcinoma (SCEC) is a rapidly progressive, aggressive, and rare malignancy of a specific histological type. SCEC often manifests as early lymph node invasion or distant metastases, with patients often diagnosed only when they possess advanced disease, a phenomenon that inevitably leads to dismal clinical outcomes [1, 2]. Of all the different subtypes of esophageal malignancies that occur around the world, 0.5–2.8% of these comprises of SCEC [3]. However, the incidence is as high as 7.6% in the Chinese population [4] with increasing trend. China is a region endemic for esophageal malignancies, the absolute number of SCEC patients is still high. Information is scarce surrounding its underlying pathogenesis and progression, and thus, little is known regarding potential therapeutic targets.

Although previous studies have shown clinical, pathological, and morphological similarities between SCEC and small cell lung cancer (SCLC), the genetic basis of SCEC, a highly malignant tumor, is largely unknown. Since prospective clinical trials or standard treatments have not yet been established, patients with SCEC are staged and treated according to the guidelines for SCLC. Nevertheless, early recurrence and distant metastasis is common in SCEC and long-time survival is rare. In addition, SCEC patients with relapse respond inadequately to second line of treatment making their prognosis generally poor. Therefore, the identification of novel biomarkers to aid early diagnosis, enable the design of targeted therapeutics and prognostic evaluation of SCEC, is of high clinical significance.

The initiation and development of malignancies have been well established to be triggered by the accumulation of several genetic aberrations over a long period of time [5]. DNA copy number variations (CNVs) are characteristics of a myriad of human malignancies; however, their influence on gene expression has yet to be clarified. The availability and integration of gene expression microarray data and genome-wide array-based comparative genomic hybridization (aCGH) has supplied novel insights into the molecular pathogenesis behind differing genetic expression [6–9]. An improved understanding of the underlying genetic alterations in SCEC would be the foundation of novel, innovative therapies, which are urgently needed.

In the present study, SCEC tissues were first screened for significantly altered genomic regions and differentially expressed genes (DEGs) relative to normal tissues. This was followed by an analysis where we integrated both gene copy number and expression in order to identify potential correlations between the two. Finally, quantitative reverse transcription polymerase chain reaction (qRT-PCR) analysis was performed on ten representative DEGs in order to obtain validated results obtained via microarray analysis.

2. Materials and Methods

2.1. Tissue Processing, Genomic DNA, and Total RNA Extraction. Paired SCEC and adjacent noncancerous tissues from three surgical specimens were harvested surgically and frozen with liquid nitrogen, before being kept at −80°C in the tissue bank of Fudan University Shanghai Cancer Center (FUSCC). All three patients had middle thoracic SCEC stage III (based on the American Joint Committee on Cancer (6th edition) TNM staging system) or limited stage (based on the Veteran's Administration Lung Cancer Study Group, VALSG). The median age of all patients was 59 years (ranges from 56 to 67), with two of the three patients being female. All selected patients had not received any anticancer therapy before surgery nor were they afflicted with any other cancer type. Ethical approval was granted by the Human Research Ethics Committee of FUSCC prior to commencement of this study, and informed consent was procured from all patients before enrollment.

Frozen tissue blocks were first sectioned and subjected to cresyl violet or toluidine blue staining to visualize total RNA and genomic DNA (gDNA), respectively (Ambion, Austin, TX, USA). LMD (Leica Microsystems, Wetzlar, Germany) was used by pathologists to discern between malignant and nonmalignant cells in the tissue sections. Total RNA and gDNA were extracted with the help of commercially available kits and were performed based on to the manufacturer's instructions. Agilent's 2100 Bioanalyzer (Agilent Technologies, Palo Alto, CA) was used to confirm the purity, integrity, and concentration of total RNA (data not shown). RNA integrity was determined with the RIN software algorithm [10], and only samples with a RIN score of >7.5 were used for microarray experiments. High-quality RNA characteristics were samples that possessed low background noise and had distinct peaks representing 18S and 28S ribosomal RNA. 1% agarose gel electrophoresis was used to verify gDNA quality, while its concentration was quantified with a Nanodrop ND-1000 spectrophotometer (Nanodrop Technologies, Wilmington, DE).

2.2. Array CGH. Genomic abnormalities in the SCEC tissues were analyzed by Agilent aCGH G3 Human 4x180k Array.

The gDNA (500 ng) of cancerous and noncancerous samples was digested overnight at 37°C using the Rsa I and Alu I restriction site enzymes (Promega, Madison, WI). Cy5-/Cy3-dUTP fluorescent dyes were used to label both samples with the Agilent Genomic DNA Labeling Kit Plus (Agilent Technologies). The labeled gDNA products were purified with Microcon YM-30 filtration device (Millipore, Bedford, MA), and the yield of DNA and dye incorporation were quantified. CGH microarrays were used to hybridized mixtures of the labeled sample pairs (containing identical quantities of each malignant and nonmalignant samples) at 65°C for 24 hours. The slides were then rinsed with Agilent Oligo aCGH Wash Buffer 1 and 2 (Thermo Shandon, Waltham, MA, US) as per the manufacturer's instructions. Following washing, an Agilent microarray scanner was used to scan the slides. The Feature Extraction software version 10.7 was used to analyze raw data at the default CGH parameter settings (Agilent Technologies).

Array CGH data was processed as previously described. Briefly, putative CNV intervals contained in each sample were identified using CytoGenomics 2.7.8.0 (Agilent Technologies, Santa Clara, CA, US). Conversion of the Cy5/Cy3 ratios into $\log_2$-transformed values was then carried out with data corrections carried out using fuzzy zero and centralization corrections. Lastly, the ADM-2 algorithm was used to identify CNVs in individual SCEC samples at threshold 6 before proceeding to locate aberration frequencies. Additionally, the following aberration filters were applied: maximum number of aberration regions = 10000, minimum absolute average $\log_2$ ratio for region = 0.5, and minimum number of probes in region = 3. The analysis excluded chromosomes X and Y. Data on the original copy number was submitted to the NCBI's Gene Expression Omnibus (GEO) [11] and is accessible through the GEO Series accession number GSE111298. A recurrent variation was determined to be present if recurrence was observed in at least 2 of the 3 samples. Minimum common regions of recurrent variations in the 3 samples were analyzed, including the chromosomal positions and size of the aberrations.

2.3. Gene Expression Microarray Analysis. Gene expression profiling of the SCEC and noncancerous tissues was carried out with the Affymetrix HG U133 Plus 2.0 Array (Affymetrix, Santa Clara, CA). The GeneChip 3'IVT Express Kit (Affymetrix, Santa Clara, CA, US) was used to amplify, label, and purify total RNAs as per the manufacturer's protocols. Biotin-labeled cRNA was hybridized at 45°C for 16 hours, and the gene chips were rinsed and stained with streptavidin-phycoerythrin (Molecular Probes) with the GeneChip Fluidics Workstation 450 (Affymetrix). A confocal laser scanner (GeneArray Scanner 3000) was utilized to scan the stained gene chips, with the resultant images converted by the Command Console software 3.1 (Affymetrix) at default settings into corresponding numerical values that indicated their relative signal intensities. Raw data were normalized by robust multiarray average (RMA) quantile normalization analysis algorithm with the GeneSpring GX 12.5 software (Agilent Technologies, Santa Clara, CA, US) to generate CEL intensity files. All data on gene expression can be viewed at NCBI via GEO (GEO: GSE111044).

Quality control was performed by the following diagnostic plots: principal component analysis (PCA), boxplots, Pearson's correlation, and MvA plots, (Supplementary information Figure S1, S2). Moderated t-test analysis with Benjamini-Hochberg multiple testing correction was used to obtain DEGs whose fold change (FC) between SCEC and matched adjacent noncancerous tissues was ≥2 (with a false discovery rate (FDR) cut-off < 0.01). DEGs were visualized in volcano plots (Supplementary information Figure S3) and then imported to gene set enrichment analysis (GSEA) version 2.2.3 software to interpret the gene expression data. The focus was on oncogenic signatures gene sets (C6), rather than individual genes, that share common biological functions. Functional annotation and gene interaction networks of the enriched genes were analyzed by DAVID 6.8 and STRING 10.0, respectively.

2.4. Integrative Analysis of the aCGH and Expression Data. To locate genes whose expression was influenced by genomic CNVs, DEGs with FDR < 0.01 and FC ≥ 2 that were located in CNV regions of at least one SCEC sample were tracked using the RefSeq Transcript ID. These overlapping genes were subjected to functional annotation using DAVID 6.8. Deletions and amplifications were regarded as separate entities during the analysis.

Pearson's correlation coefficients were also calculated to determine potential correlations between gene expression and DNA copy number. Only genes located in chromosomal regions that possessed recurrent aberrations were analyzed. By determining DEGs that were associated with an abnormal DNA copy number, we sought to isolate stability genes, tumor suppressor genes, and potential oncogenes that carried out mechanistic functions in cancers. Gene median expression levels between samples with and without copy number deletions/amplifications were contrasted to determine the impact that copy number differences had on the expression of genes. Gene expression fold changes (FCs) were calculated by dividing the median expression in sample(s) with CNVs by the median expression in sample(s) without CNVs [6, 12]. Genes that were identified were those that possessed a minimum 2-fold copy number increase and an associated gene expression aberration (CNV-FC). We expected to find these genes to be expressed differentially between SCEC and normal esophageal tissues. This hypothesis was proved by hierarchical clustering of the 3 sample pairs using the average linkage method, and the clusters were visualized using the Java TreeViewer 1.1.3 software. With the help of the SPSS 19.0 software, we were able to determine the Pearson's correlation coefficients between DNA CNVs and changes in expression level for each selected gene in order to clarify the association between copy number and gene expression. Genes that possessed CNV-FC ≥ 2 and $r \geq 0.6$ ($p < 0.05$) were determined to be genes potentially associated with cancer.

2.5. Quantitative Reverse Transcription Polymerase Chain Reaction (qRT-PCR). qRT-PCR was performed to verify

Table 1: Oncogenic signatures gene sets significantly altered in SCEC.

Name	Size	NES	NOM p val	FDR q val
PTEN_DN.V2_UP	10	2.06	0.00252	0.0270
RB_P107_DN.V1_DN	13	2.04	0.00278	0.0264
RB_P130_DN.V1_DN	11	2.01	0.00270	0.0272
KRAS.300_UP.V1_DN	14	1.98	0.00882	0.0285
WNT_UP.V1_DN	13	1.84	0.0158	0.0580
IL2_UP.V1_UP	21	1.81	0	0.0630
IL15_UP.V1_UP	19	1.56	0.0262	0.221
KRAS.600.LUNG.BREAST_UP.V1_DN	27	1.55	0.0350	0.212
NOTCH_DN.V1_UP	18	1.51	0.0327	0.191
MEK_UP.V1_UP	28	1.50	0.0464	0.234
ERB2_UP.V1_UP	25	1.49	0.0425	0.207

Differentially expressed genes (DEGs) were annotated by gene set enrichment analysis (GSEA). Threshold values: size ≥ 10 and NOM p val < 0.05. FDR = false discover rate; NOM p val = nominal p value; NES = normalized enrichment score.

DEGs determined in through microarray analysis. Briefly, TRIzol reagent (Invitrogen) was used to extract total tissue sample RNA followed by cDNA synthesis utilizing PrimeScript RT reagents (Takara Bio Inc.). Using SYBR Green dye (Takara Bio Inc.), gene expression levels were determined on a 7500 Fast Real-Time PCR cycler (Applied Biosystems). Specific gene primers were designed and constructed by BioTNT Co. (Shanghai, China). All primer sequences are available in Table S1 (Supplementary information). All reactions were carried out in triplicates. The $2^{-\Delta\Delta Ct}$ method was used to determine relative gene expressions, normalized to the expression of housekeeping gene β-actin.

3. Results

3.1. Gene Expression Profile of SCEC. Data analysis through GeneSpring software revealed a total of 1485 DEGs in SCEC relative to the adjacent noncancerous tissues, with 879 upregulated and 606 downregulated genes. Among the 1485 DEGs, neuroendocrine-associated genes SYP (Syn; FC = 1.5, FDR = 0.04), CHGA (CgA; FC = 3.02, FDR = 0.04), NCAM1 (CD56; FC = 18.10, FDR = 0.006), ASCL1 (FC = 619.23, FDR = 0.0005), and GRP (FC = 5.33, FDR = 0.03) and proliferation-associated genes MKI67 (Ki-67; FC = 9.35, FDR = 0.007) and PCNA (FC = 4.20, FDR = 0.006) were overexpressed. GSEA C6 annotation identified that PTEN-, RB-, and WNT-related gene sets were upregulated while Notch-related gene sets were downregulated (Table 1). Table 2 lists the biological processes or pathways of the genes as annotated by DAVID based on their significance (count ≥ 10 and Benjamini $p < 0.01$), including DNA replication, cell cycle, mitosis, telomere maintenance, DNA repair, p53, and RB. Furthermore, SCEC tissues were found to possess interactive gene networks with FOXM1, TMPO, KIF11, NEK2, and CENPF as common skeleton centered on NUF2 (Supplementary information Figure S4). The genes involved in the SCEC-regulated network were involved in cell cycle, mitosis, cell cycle checkpoints, spindle organization, microtubule binding, cytoskeletal protein binding, and other biological processes (Supplementary information Table S2, S3).

3.2. Copy Number Variations in SCEC. CNVs were found to be expressed across the entire genome based on analyses of the mean frequencies of copy number gains and losses. Supplementary information Figure S5 depicts CNVs found across all chromosomes. The gained regions that were detected in all samples were located in 14q11.2, whereas the lost regions detected in all samples were located at 4q22.3-23.3. Regions of gain observed in 2 samples were located at 3q25.31-q29, 5p15.31-15.2, 8q21.11-24.3, 9p23-13.1, and 14q11.2-32.33, and regions of loss observed in 2 samples were located at 3p26.3-25.3, 4p16.3-11, 4q11-22.3, 4q23-25, 8p23.3, and 16p13.3 in decreasing order of frequency. Minimal common regions of these altered copy numbers, including the chromosomal position, potential target genes, frequency, and size of the base pair alterations, are shown in Table 3. Only genes that possessed a minimum twofold copy number along with associated variations in levels of gene expression and also a Pearson's correlation coefficient of less than 0.6 ($p < 0.05$) were selected.

3.3. Copy Number-Associated Gene Expression Changes. We identified 306 genes (194 upregulated and 112 downregulated) that consistently showed a change in copy number as well as expression levels. These genes were significantly enriched in the cell cycle, mitosis, DNA repair, p53 pathway, and RB pathways, according to the functional annotation (Supplementary information Table S4). Notably, most of the network genes in the gene expression profiling, such as NUF2, CCNE2, NFIB, ETV5, KLF5, ATAD2, NDC80, and ZWINT, were included in these 306 genes.

Thirty-nine individual genes had both a minimum 2-fold copy number-associated change in expression (median: 5.35, 95% CI: 4.53–16.98) and Pearson's correlation coefficient of less than 0.6 ($p < 0.05$; see Supplementary information Table S5 for details), and PTP4A3 showed the highest correlation (CNV-FC = 21362.13; Pearson's correlation

Table 2: DAVID annotation of DEGs in SCEC group.

Database	Name	Count	Benjamini p value
KEGG	*DNA replication*	19	$8.88E-10$
	Cell cycle	33	$8.61E-09$
	P53 signaling pathway	19	$4.80E-05$
	Progesterone-mediated oocyte maturation	18	0.00457
	Base excision repair	11	0.00419
	Oocyte meiosis	20	0.00790
REACTOME	*Cell cycle, mitotic*	100	$3.47E-36$
	DNA replication	29	$7.19E-08$
	DNA repair	22	0.00173
	Cell cycle checkpoints	23	0.00184
	Telomere maintenance	14	0.00713
PANTHER	*P53 pathway*	22	0.0456
GO BP (TOP10)	*M phase*	99	$3.91E-28$
	M phase of mitotic cell cycle	78	$1.97E-26$
	Mitosis	77	$2.12E-26$
	DNA replication	61	$2.41E-18$
	DNA metabolic process	98	$2.54E-13$
	Mitotic sister chromatid segregation	18	$1.73E-07$
	Spindle organization	20	$1.55E-07$
	Cell cycle checkpoint	27	$2.09E-06$
	Regulation of cell cycle process	28	$6.97E-05$
	DNA repair	50	$7.34E-05$
GO MF	*Pyrophosphatase activity*	91	0.00138
	Adenyl ribonucleotide binding	152	0.00573
	Guanyl ribonucleotide binding	44	0.0486

Threshold values: count ≥ 10 and Benjamini p value < 0.01. The biological processes or pathways in common between SCEC and SCLC are in italics. BP = biological process; GO = gene ontology; MF = molecular function.

coefficient = 0.9983; $p = 0.037$). An unsupervised two-way (genes and samples) hierarchical clustering of the 3 sample pairs based on these genes revealed two distinct clusters that separated the SCEC from adjacent noncancerous tissues (Figure 1). Several novel genes that may serve as SCEC biomarkers were revealed during an integrated analysis of gene copy number and expression; however, their clinical utility needs to be verified through further studies.

3.4. qRT-PCR Validation of Microarray Results. To substantiate the microarray results, qRT-PCR was performed on the following 10 out of the 39 genes: neuroendocrine-associated genes (INSM1, ASCL1, NRCAM, and SNAP25), one gene centered in the gene regulatory network (NUF2), and 5 possible cancer-associated genes (PTP4A3, RFC4, REST, APEH, and FBLN2). Seven of the 10 genes, that is, INSM1, ASCL1, NRCAM, SNAP25, NUF2, PTP4A3, and RFC4, were upregulated while REST, APEH, and FBLN2 were downregulated. The qRT-PCR results mirrored those obtained via high-throughput microarray analysis, thus validating the latter as well as highlighting some potential target genes (Figure 2).

4. Discussion

There are currently no effective therapeutic strategies for treating primary SCEC, a rare malignancy. Unfortunately, no major progress has been made in the last decades to elucidate the biology of SCEC. This study is the first to study the molecular and genetic basis of SCEC on a genome-wide level. Compared to previous studies, we have discovered more genes through global microarray analysis that may have a potential role in the mechanism of SCEC. The ability of a malignant tumor to proliferate is a feature of great prognostic value in the clinical setting [13]. Malignant SCEC cells have the propensity to multiply quickly, with patients rapidly developing hematogenous, bone, and lymph node metastasis early in the course of the disease. Consistent with this, and in line with previously published reports [14], we saw a significant upregulation in neuroendocrine-associated and proliferation-associated genes in SCEC tissues relative to corresponding normal tissues.

Although promalignant features like high levels of ki-67, proliferating cell nuclear antigen (PCNA) and telomerase activity, Bcl-2 positivity, rich neovascularization, and p53 overexpression have been reported in SCEC [14–16], detailed genetic studies are not available. PTEN was the most significantly altered (downregulated) gene in our genome-wide analysis of SCEC tissues. It is an effector of the PI3K/PTEN/AKT pathway; a critical pathway that regulates cell cycle progression, cell migration, metabolism, and survival. Furthermore, aberrant PTEN expression brought about either via promotor methylation silencing, deletions, or mutations is often commonly observed in several primary and metastatic human cancers. There appears to be a higher occurrence of mutations in the PTEN gene (36.84%) in patients of Chinese ethnicity with SCEC in contrast to EGFR, KARS, or PIK3CA mutations [4]. In addition, PTEN is often lost or mutated in SCLC [17, 18]. Taken together, PTEN presents itself as a potential therapeutic target for SCEC.

We also performed a genome-wide analysis of DNA CNVs in SCEC tissues to determine genes that possessed dysregulated expression levels as a result of altered copy numbers. 7 chromosomal regions were observed to have recurrent copy number losses, while 6 chromosomal regions demonstrated recurrent copy number gains. This highlights that these CNVs, in addition to the specific genes, may have a significant biological role in SCEC pathogenesis. We identified a total of 306 consistent DEGs that were significantly enriched in cell cycle, mitosis, DNA repair, p53, and RB pathways as per functional annotation.

To further highlight the association between the expression of genes located in chromosomes with recurrent aberration expression and copy number, we calculated their Pearson's correlation coefficient. Thirty-nine genes were found to possess an r value of ≥0.6, indicating that their expression fold changes correlated in a statistically significant manner to their copy number. The highest correlation was shown by PTP4A3 (CNV-FC = 21362.13; $r = 0.9983$;

Table 3: Minimal common regions of recurrent copy number amplification and deletion ($n \geq 2$).

Chromosomal aberration	Positon (Mb)	Size (Mb)	$n = 3$ (%)	Samples	Possible cancer-associated genes
Gains					
14q11.2	20.22–23.91	3.69	3 (100%)	1, 2, 3	—
3q25.31-q29	155.59–197.83	42.25	2 (67%)	1, 3	*TCTEX1D2*, *YEATS2*, *PIGX*, *LRCH3*, *RFC4*, *LSG1*, *CAMK2N2*
5p15.31-15.2	8.87–10.99	2.12	2 (67%)	1, 2	*PAIP1*
8q21.11-24.3	74.51–146.28	71.76	2 (67%)	1, 3	*ZNF704*, *PTP4A3*, *ZNF7*
9p23-13.1	9.38–39.07	29.7	2 (67%)	1, 2	*EXOSC3*
14q11.2-32.33	19.38–20.22	0.84	2 (67%)	1, 2	—
	23.91–107.29	83.37	2 (67%)	1, 3	—
Losses					
4q22.3-23	98.14–99.10	0.96	3 (100%)	1, 2, 3	—
3p26.3-25.3	0.07–90.25	90.07	2 (67%)	1, 2	*IP6K2*, *APEH*, *TMEM42*, *WNT5A*, *UQCRC1*, *C3orf38*, *RPL29*, *PRKAR2A*, *MAP4*, *AZI2*, *ALAS1*, *GOLGA4*, *FBLN2*, *SHQ1*, *ATG7*
4p16.3-11	0.72–49.06	48.99	2 (67%)	2, 3	*GBA3*, *SH3TC1*
4q11-22.3	52.69–98.14	45.45	2 (67%)	2, 3	*STAP1*, *GNRHR*, *REST*
4q23-25	99.10–107.92	8.22	2 (67%)	2, 3	
8p23.3	0.18–0.50	0.33	2 (67%)	2, 3	—
16p13.3	5.50–5.61	0.12	2 (67%)	1, 3	—
	6.75–6.82	0.06	2 (67%)	1, 3	—

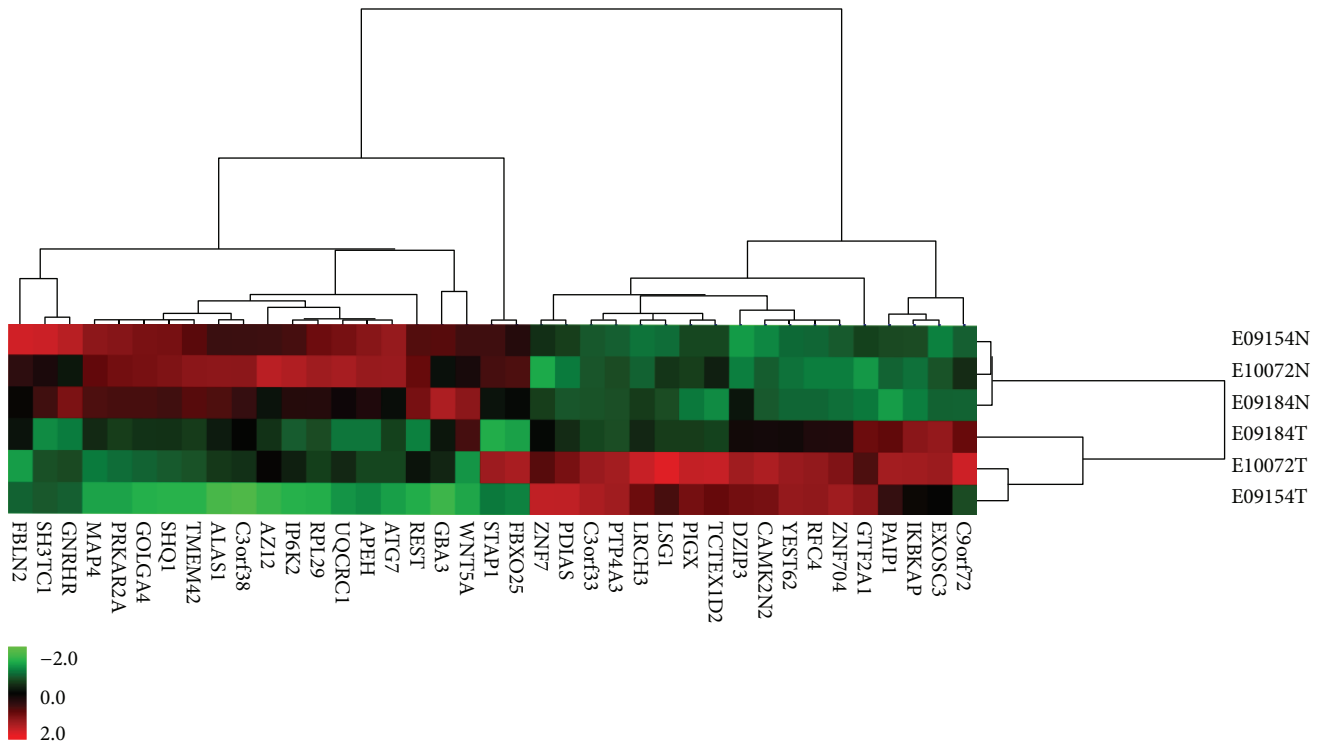

Figure 1: A 39-gene unsupervised hierarchical clustering of 3 pairs of SCEC samples uncovered two distinct clusters separating SCEC samples from adjacent noncancerous samples. Underexpressions are denoted in green while overexpressions are denoted in red.

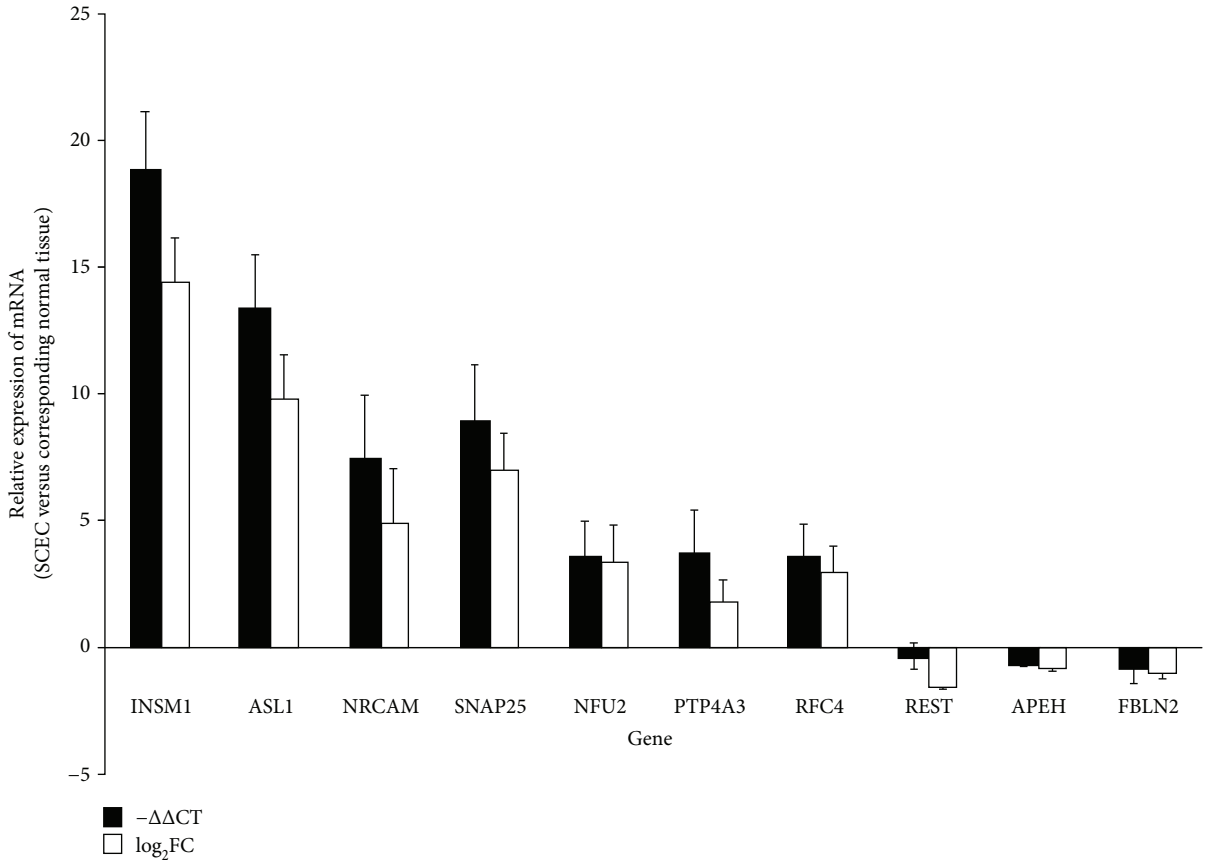

Figure 2: The mRNA level of *INSM1*, *ASCL1*, *NRCAM*, *SNAP25*, *NUF2*, *PTP4A3*, *RFC4*, *REST*, *APEH*, and *FBLN2* in SCEC. Expression levels in SCEC were compared with the corresponding normal tissues. The *x*-axis displays gene symbols, and the *y*-axis depicts gene expression log ratios derived from qRT-PCR or microarray. Bars: standard error (SE).

$p = 0.037$). PTP4A3, also known as phosphatase of regenerating liver-3 (PRL-3), is a protein tyrosine phosphatase closely related to metastasis, with its expression level found to correlate significantly with the survival and progression of a myriad of cancerous tumors. A recent study has documented that PRL-3 may adversely affect tumor development by mediating deleterious effects on telomere homeostasis [19]. Based on previous findings and the exceptionally aggressive nature of SCEC, we hypothesize that PTP4A3, with its key roles in SCEC genesis, development, and metastasis, may serve as a target for the development of therapeutic agents.

Although we only examined a small number of the primary samples, our study is the first to examine gene expression profiles and CNVs in SCEC patients on a genome-wide scale. Further studies are needed on larger sample cohorts to validate our findings and to single out the most useful genes. Furthermore, the clinical and therapeutic significance of PTP4A3 and other potential targets has to be validated. Taken together, our study is an important step in elucidating the mechanistic basis of SCEC genesis and metastasis and discovering novel therapeutic targets.

5. Conclusion

This study was the first to investigate the genomic signature of SCEC from genome-wide expression and copy number analysis. Our preliminary data indicates that stem cell-related genes and pathways might function to mediate the initiation, development, and metastasis of SCEC, although further validation is warranted.

Data Availability

The microarray data used to support the findings of this study have been deposited in the Gene Expression Omnibus (GEO). The GEO accession numbers are appended as follows: GSE111299: genome-wide analysis of gene expression and DNA copy number variations in small cell esophageal carcinoma, GSE111044: expression data from SCEC and corresponding normal samples, and GSE111298: aCGH data from SCEC and corresponding normal samples. Websites included are https://www.ncbi.nlm.nih.gov/geo/query/acc.cgi?acc=GSE111044 and https://www.ncbi.nlm.nih.gov/geo/query/acc.cgi?acc=GSE111298.

Disclosure

The study was presented in part at the 57th Annual Meeting of American Society for Radiation Oncology, San Antonio (October 18–21, 2015).

Conflicts of Interest

The other authors have no conflicts of interest to disclose.

Authors' Contributions

Di Liu and Xinyan Xu contributed equally to this study and share first authorship.

Acknowledgments

This study was supported by the National Project for Key Clinical Specialty Development (Grant no. 439) from the Chinese Ministry of Public Health and Research (Grant no. 14411965800) from the Science and Technology Commission of Shanghai Municipality.

Supplementary Materials

Figure S1: PCA, box plot, and Pearson's correlation matrix of SCEC group. Figure S2: MvA plot of each SCEC samples and adjacent normal tissues. Figure S3: volcano plots of SCEC groups. Figure S4: gene regulatory network plotted by the top 120 DEGs (ranked by FDR) of SCEC group using STRING 10.0.5. DNA copy number change profiles of 3 pairs of SCEC samples. Table S1: primers utilized in the qRT-PCR validation of gene expression microarray data. Table S2: list of regulatory network genes in SCEC group. Table S3: DAVID annotation of regulatory network genes in SCEC group. Table S4: DAVID annotation of genes changed consistently between mRNA expression and copy number in SCEC. Table S5: list of 39 possible cancer-associated genes in SCEC. *(Supplementary Materials)*

References

[1] W. W. Chen, F. Wang, D. S. Zhang et al., "Primary small cell carcinoma of the esophagus: clinicopathological study of 44 cases," *BMC Cancer*, vol. 14, no. 1, p. 222, 2014.

[2] F. Casas, F. Ferrer, B. Farrus, J. Casals, and A. Biete, "Primary small cell carcinoma of the esophagus: a review of the literature with emphasis on therapy and prognosis," *Cancer*, vol. 80, no. 8, pp. 1366–1372, 1997.

[3] M. Kukar, A. Groman, U. Malhotra et al., "Small cell carcinoma of the esophagus: a SEER database analysis," *Annals of Surgical Oncology*, vol. 20, no. 13, pp. 4239–4244, 2013.

[4] Z. Zhang, H. Xiao, F. Xie et al., "High-incidence of PTEN mutations in Chinese patients with primary small cell carcinoma of the esophagus," *BMC Cancer*, vol. 14, no. 1, p. 19, 2014.

[5] B. Vogelstein and K. W. Kinzler, "Cancer genes and the pathways they control," *Nature Medicine*, vol. 10, no. 8, pp. 789–799, 2004.

[6] S. Junnila, A. Kokkola, M. L. Karjalainen-Lindsberg, P. Puolakkainen, and O. Monni, "Genome-wide gene copy number and expression analysis of primary gastric tumors and gastric cancer cell lines," *BMC Cancer*, vol. 10, no. 1, p. 73, 2010.

[7] S. Myllykangas, S. Junnila, A. Kokkola et al., "Integrated gene copy number and expression microarray analysis of gastric cancer highlights potential target genes," *International Journal of Cancer*, vol. 123, no. 4, pp. 817–825, 2008.

[8] Y. Tsukamoto, T. Uchida, S. Karnan et al., "Genome-wide analysis of DNA copy number alterations and gene expression in gastric cancer," *The Journal of Pathology*, vol. 216, no. 4, pp. 471–482, 2008.

[9] S. Yang, H. C. Jeung, H. J. Jeong et al., "Identification of genes with correlated patterns of variations in DNA copy number and gene expression level in gastric cancer," *Genomics*, vol. 89, no. 4, pp. 451–459, 2007.

[10] A. Schroeder, O. Mueller, S. Stocker et al., "The RIN: an RNA integrity number for assigning integrity values to RNA measurements," *BMC Molecular Biology*, vol. 7, no. 1, p. 3, 2006.

[11] R. Edgar, M. Domrachev, and A. E. Lash, "Gene Expression Omnibus: NCBI gene expression and hybridization array data repository," *Nucleic Acids Research*, vol. 30, no. 1, pp. 207–210, 2002.

[12] L. Cheng, P. Wang, S. Yang et al., "Identification of genes with a correlation between copy number and expression in gastric cancer," *BMC Medical Genomics*, vol. 5, no. 1, p. 14, 2012.

[13] H. Kimura, Y. Yonemura, and A. L. Epstein, "Flow cytometric quantitation of the proliferation-associated nuclear antigen p105 and DNA content in advanced gastric cancers," *Cancer*, vol. 68, no. 10, pp. 2175–2180, 1991.

[14] H. Kimura, K. Konishi, T. Inoue et al., "Primary small cell carcinoma of the esophagus: flow cytometric analysis and immunohistochemical staining for the p53 protein and proliferating cell nuclear antigen," *Journal of Surgical Oncology*, vol. 68, no. 4, pp. 246–249, 1998.

[15] N. Koide, H. Saito, A. Suzuki et al., "Clinicopathologic features and histochemical analyses of proliferative activity and angiogenesis in small cell carcinoma of the esophagus," *Journal of Gastroenterology*, vol. 42, no. 12, pp. 932–938, 2007.

[16] K. Takubo, K. I. Nakamura, M. Sawabe et al., "Primary undifferentiated small cell carcinoma of the esophagus," *Human Pathology*, vol. 30, no. 2, pp. 216–221, 1999.

[17] M. C. Pietanza and M. Ladanyi, "Bringing the genomic landscape of small-cell lung cancer into focus," *Nature Genetics*, vol. 44, no. 10, pp. 1074-1075, 2012.

[18] S. P. D'Angelo and M. C. Pietanza, "The molecular pathogenesis of small cell lung cancer," *Cancer Biology & Therapy*, vol. 10, no. 1, pp. 1–10, 2014.

[19] S. Lian, L. Meng, Y. Yang et al., "PRL-3 promotes telomere deprotection and chromosomal instability," *Nucleic Acids Research*, vol. 45, no. 11, pp. 6546–6571, 2017.

Hindawi
Stem Cells International
Volume 2018, Article ID 9501747, 11 pages
https://doi.org/10.1155/2018/9501747

Research Article

Human Bone Marrow Mesenchymal Stem Cells Promote Gastric Cancer Growth via Regulating *c-Myc*

Bin Chen,[1] Jing Yu,[1,2] Qianqian Wang,[1] Yuanyuan Zhao,[1] Li Sun,[1] Changgen Xu,[3] Xiangdong Zhao,[3] Bo Shen,[4] Mei Wang,[1] Wenrong Xu,[1] and Wei Zhu[1]

[1]*School of Medicine, Jiangsu University, Zhenjiang, Jiangsu, China*
[2]*The Xuyi People's Hospital, Xuyi, Jiangsu, China*
[3]*Zhenjiang Provincial Blood Center, Zhenjiang, Jiangsu, China*
[4]*Department of Oncology, Jiangsu Cancer Hospital Affiliated to Nanjing Medical University, Nanjing, Jiangsu, China*

Correspondence should be addressed to Wei Zhu; zhuwei@ujs.edu.cn

Bin Chen and Jing Yu contributed equally to this work.

Received 27 January 2018; Revised 9 April 2018; Accepted 2 May 2018; Published 18 July 2018

Academic Editor: Hua Tan

Copyright © 2018 Bin Chen et al. This is an open access article distributed under the Creative Commons Attribution License, which permits unrestricted use, distribution, and reproduction in any medium, provided the original work is properly cited.

The clinical application of human bone marrow mesenchymal stem cells (hBM-MSCs) has generated a great deal of interest because of their potential use in regenerative medicine and tissue engineering. However, safety concerns over hBM-MSCs limit their clinical application. In this study, we observed that hBM-MSC-conditioned medium (hBM-MSC-CM) promotes gastric cancer development via upregulation of c-Myc. Our results showed that c-Myc was upregulated in MGC-803 and BGC-823 cells after hBM-MSC-CM treatment. Moreover, we found that the c-Myc inhibitor JQ1 and c-Myc siRNA decreased the expression of c-Myc in hBM-MSC-CM-treated tumor cells *in vitro*. Additionally, hBM-MSC-CM enhanced the migration and glucose uptake of gastric cancer cells. *In vivo* studies showed that JQ1 inhibited hBM-MSC-CM-induced gastric cancer growth. These results indicated that hBM-MSC-CM induced gastric cancer growth via upregulation of c-Myc, which may be a potential risk factor and/or a therapeutic target for clinical applications.

1. Introduction

Due to their multidirectional differentiation capacity, mesenchymal stem cells (MSCs) have been widely used in tissue engineering and cell replacement therapy [1]. However, studies have increasingly demonstrated that human bone marrow MSCs (hBM-MSCs) can promote tumor growth and metastasis [2, 3], making safety of hBM-MSCs in clinical applications controversial.

Because of their promise for clinical applications, a variety of models have been used to prove the safety and effectiveness of hBM-MSCs [4, 5]. Some previous clinical studies have concluded that hBM-MSCs do not pose an obvious risk of tumorigenesis when used to treat cartilage injuries or other diseases [6, 7]. However, other studies have found that hBM-MSCs promote tumor proliferation, migration, and stemness *in vitro* and that hBM-MSCs promote tumor development *in vivo* [3, 8, 9]. Therefore, there is an urgent need to identify the factors from hBM-MSCs that promote tumor growth.

In this study, we found that hBM-MSC-CM caused gastric cancer cells to upregulate c-Myc expression, which is a well-known oncogene that is involved in tumor initiation and development. Abnormal c-Myc activation is responsible for a range of human cancers, including neuroblastoma [10], lung carcinoma [11], and gastric carcinoma [12]. By promoting c-Myc expression, hBM-MSC-CM increased the metabolism, migration, and proliferation of gastric cancer cells. Furthermore, we showed that the c-Myc inhibitor JQ1 inhibits the tumor-promoting effects of hBM-MSC-CM. Thus, we show that hBM-MSC-CM can upregulate c-Myc expression in gastric cancer cells, which may be a key factor in carcinogenesis and, therefore, a potential target for cancer prevention.

2. Materials and Methods

2.1. Xenograft Tumor Model. This study and its consent procedure were approved by the local ethics committee of Jiangsu University (Jiangsu, China). BALB/c-nu/nu male mice ($n = 30$; aged 4-5 weeks) were purchased from SLAC Laboratory Animal (Shanghai, China) and maintained in pathogen-free conditions with sterilized chow and autoclaved water. The animals were randomly divided into five groups ($n = 6$ mice per group). MGC-803 cells were treated with either Dulbecco's modified Eagle's medium (DMEM; Gibco/Life Technologies, Carlsbad, CA, USA), dimethyl sulfoxide (DMSO; Sigma-Aldrich, St. Louis, MO, USA), hBM-MSC-conditioned media (hBM-MSC-CM), JQ1 (0.8 μM), or hBM-MSC-CM + JQ1 for 48 h. In the hBM-MSC-CM + JQ1 group, MGC-803 cells were pretreated with JQ1 for 4–6 h, washed three times with phosphate-buffered saline (PBS), and then treated with hBM-MSC-CM + JQ1. Then, subcutaneous xenografts were established by injection of 2×10^6 MGC-803 cells in 200 μL of PBS per mouse. Once tumors formed, tumor sizes were measured using Vernier calipers and tumor volumes were calculated using the following formula: tumor volume = length × width^2/2. The experiment was stopped on day 30, when all mice were euthanized.

2.2. Cell Culture. Healthy donor-derived bone marrow cells were collected at the Affiliated Hospital of Jiangsu University, and all protocols were approved by the local ethics committee of the Affiliated Hospital of Jiangsu University, China. Additionally, informed consent was received from all donors. The bone marrow cells were diluted in an equal volume of PBS, isolated with 1.077 g/mL Ficoll, and centrifuged at 800 ×g for 20 min. The cells were then rinsed with PBS and cultured in DMEM containing 10% fetal bovine serum (FBS; Gibco) at 37°C in a humidified incubator infused with 5% CO_2; adherent cells were collected after 5 days. The human gastric cancer cell lines MGC-803 and BGC-823 and normal line GES-1 were purchased from the Cell Bank of Type Culture Collection of Chinese Academy of Sciences (Beijing, China) and were maintained in DMEM supplemented with 10% FBS at 37°C in 5% CO_2.

2.3. Preparing hBM-MSC-CM and Coculture with Gastric Cancer Cells. When hBM-MSCs had grown to 70% confluency, they were washed with PBS and incubated with fresh medium for 48 h. Then, the supernatant was collected, filtered through a 0.22 μm filter, and diluted at 1 : 1 with DMEM supplemented with 10% FBS (hBM-MSC-CM). MGC-803 and BGC-823 cells were washed with PBS and then treated with DMEM, DMSO, hBM-MSC-CM, JQ1 (0.8 μM), or hBM-MSC-CM + JQ1 at 37°C in 5% CO_2 for 48 h prior to being collected for use in subsequent experiments.

2.4. Transwell Migration Assay. Transwell migration assays were performed to evaluate the effect of JQ1 or c-Myc knockdown on the hBM-MSC-CM-induced migration of gastric cancer cells. In the experiment using JQ1, 1×10^5 MGC-803 or BGC-823 cells were plated in six-well plates (Corning Inc., Corning, NY, USA) and then treated with DMEM, DMSO, hBM-MSC-CM, JQ1 (0.8 μM), and hBM-MSC-CM + JQ1. In the experiment using c-Myc knockdown, the cells after c-Myc knockdown were cocultured with hBM-MSC-CM. After 48 h, the cells were collected by centrifugation (800 rpm/min) and 8×10^4 cells were seeded in the upper wells of a Transwell chamber in 200 μL of serum-free DMEM. The lower compartment of the chamber was filled with 500 μL DMEM supplemented with 10% FBS. The cells were incubated for 8 h, and after incubation, we used a cotton swab to remove the cells that did not migrate. Migrated cells were fixed with 4% formaldehyde for 30 min, stained with crystal violet, and then photographed. For quantitation, three random fields from each well were counted under a microscope (Ti-S; Nikon, Tokyo, Japan), and each experiment was independently repeated in triplicate.

2.5. Glucose Uptake Assay. Glucose uptake assays were performed to evaluate the effect of hBM-MSC-CM on the glucose utilization of gastric cancer cells. Briefly, 1×10^5 MGC-803 or BGC-823 cells were plated in six-well plates (Corning Inc.) and then treated with DMEM, DMSO, hBM-MSC-CM, JQ1 (0.8 μM), and hBM-MSC-CM + JQ1. After 48 h, the cells were collected by centrifugation (800 rpm/min) and 1×10^6 cells/mL were seeded in 48-well plates and incubated for 8 h in DMEM. Then, a clinical chemistry analyzer (Xunda, XD811, Shanghai, China) and the hexokinase method were used to detect supernatant glucose concentrations.

2.6. Cell Viability Assay. We performed 3-[4,5-dimethylthiazol-2yl] diphenyltetrazolium bromide (MTT) assays to assess the half maximal inhibitory concentration (IC50) of JQ1. Cells were seeded into 96-well plates (Corning Inc.) at a density of 2×10^3 per well and incubated overnight at 37°C in 5% CO_2. Then, the plates were incubated with DMSO or different JQ1 concentrations (0.4 and 0.8 μM) and cultured for 24, 48, or 72 h. MTT (5 mg/mL) was added to the cells for 4 h at 37°C. After 4 h, we added DMSO to terminate the reaction; results were determined by measuring optical density at 490 nm with a multiwell plate reader (FLx800, BioTek, Winooski, VT, USA). Each experiment was repeated three times.

2.7. Western Blot Analysis. Total proteins were extracted from cells using RIPA lysis buffer (Invitrogen, Carlsbad, CA, USA). After determining protein concentration, 20 μg of total protein from each sample was separated with 12% sodium dodecyl sulfate polyacrylamide gel electrophoresis and then transferred to polyvinylidene fluoride membranes (Millipore, Billerica, MA, USA). The membranes were blocked with 5% nonfat milk and incubated with anti-human c-Myc (dilution, 1 : 300; 10057-1-AP, Proteintech, Chicago, IL, USA), Bcl-2 (dilution, 1 : 200; 2870, Cell Signaling Technology, USA), Bax (dilution, 1 : 200; BS2538, Bioworld, USA), cyclin-D1 (dilution, 1 : 500; BS1741, Bioworld, USA), and Glut1 (dilution, 1 : 1000; FO6231163, Wanleibio, Shenyang, China) antibodies overnight at 4°C and then incubated with goat anti-mouse (dilution,

1 : 2000; CW0102, CWBIO, Beijing, China) and goat anti-rabbit (dilution, 1 : 2000; CW0103, CWBIO, Beijing, China) secondary antibodies for 1 hour at 37°C. The blots were visualized using the enhanced chemiluminescent detection system (Amersham, Amersham, UK) and analyzed using Image-Pro Plus version 5.1 (Media Cybernetics Inc., Rockville, MD, USA).

2.8. Cell Cycle Analysis. The effects of hBM-MSC-CM and JQ1 on cell cycle distributions were measured using a flow cytometer (FACSCalibur, BD Biosciences, Franklin Lakes, NJ, USA). Briefly, 1×10^5 cells per well were seeded into six-well plates, incubated overnight, and then treated with DMEM, DMSO, hBM-MSC-CM, JQ1 (0.8 μM), and hBM-MSC-CM + JQ1. After 48 h, 1×10^6 cells per well were collected by centrifugation and stained with propidium iodide in PBS for 30 min at 4°C in the dark before being analyzed with flow cytometry.

2.9. Colony Formation Assay. MGC-803 or BGC-823 cells were treated with DMEM, DMSO, hBM-MSC-CM, JQ1, and hBM-MSC-CM + JQ1 for 48 h, and then cells were seeded at 500 cells per well in 6 cm well plates in triplicate. After 7 days of growth, the cells were washed with PBS, fixed with 4% paraformaldehyde, and stained with crystal violet. We counted the number of colonies per well under a dissecting microscope.

2.10. c-Myc Knockdown. c-Myc siRNA (50 nM) (5′-GGACTA TCCTGCTGCCAAG-3′) and negative control (NC) (50 nM) were purchased from Guangzhou RiboBio. siRNA were transfected into MGC-803 with Lipofectamine® 2000 reagent (Invitrogen; Thermo Fisher Scientific Inc.) according to the instructions.

2.11. Statistical Analysis. All data analyses were performed using GraphPad Prism 6 (Graph Software, La Jolla, CA, USA). Differences between groups were analyzed using one-way analysis of variance. The Kruskal–Wallis *H* test was used to analyze differences between *in vivo* tumor growths. A P value < 0.05 was considered statistically significant.

3. Results

3.1. HBM-MSC-CM Increased c-Myc Expression in Gastric Cancer Cells. The c-Myc oncogene has been reported to play important roles in gastric cancer; thus, we examined c-Myc levels in the gastric cancer cell lines MGC-803 and BGC-823 and normal line GES-1 with Western blot. GES-1 cells showed the lowest c-Myc expression, and the BGC-823 cells showed the highest c-Myc expression (Figure 1(a)). Next, we investigated whether treating the gastric cancer cells with hBM-MSC-CM for 48 h affected c-Myc protein levels. Compared with the untreated groups, c-Myc levels were increased in both MGC-803 and BGC-823 cells after hBM-MSC-CM treatment (Figure 1(b)). The upregulation of c-Myc expression in MGC-803 cells could maintain 12 hours after withdrawal of hBM-MSC-CM (Figure 1(c)). JQ1 has been shown to have antiproliferative effects in many cancers, primarily through inhibition of c-Myc [13]. MTT assays showed that 0.8 μM JQ1 for 72 h has significantly antiproliferative effects on MGC-803 (Figure 1(d)). Then, we used JQ1 at 0.8 μM concentration in the following experiment. Western blot analysis indicated that hBM-MSC-CM treatment can significantly increase the expression level of c-Myc protein, and the effect of hBM-MSC-CM upregulation of c-Myc in MGC-803 and BGC-823 cells can also be suppressed by JQ1 (Figures 1(e) and 1(f)).

3.2. JQ1 Inhibited the Gastric Cancer Cell Proliferation In Vitro. The effect of hBM-MSC-CM and hBM-MSC-CM + JQ1 on the proliferation of gastric cancer cells was analyzed with colony formation and MTT assays. The colony formation assays showed that the hBM-MSC-CM + JQ1 group formed fewer colonies than the hBM-MSC-CM group ($P < 0.001$, Figures 2(a)–2(d)). Consistent with the colony formation assays, MTT assays showed that JQ1 inhibited the proliferation rate of MGC-803 and BGC-823 cells ($P < 0.001$, Figures 2(e) and 2(f)).

3.3. Effect of hBM-MSC-CM on Cell Cycle Progression and Apoptosis. Cell cycle analysis revealed that JQ1 treatment increased the percentage of G1-phase cells from 51.42% to 61.49%, while the fraction of S-phase cells decreased from 30.31% to 22.3%, which were not statistically significant changes (Figure 3(a)). Additionally, hBM-MSC-CM had no effect on the cyclin-D1 expression or the apoptosis rates of MGC-803 cells (Figures 3(b) and 3(c)); however, JQ1 inhibited cyclin-D1 expression.

3.4. HBM-MSC-CM Promoted Migration and Glucose Uptake in MGC-803 and BGC-823 Cells. To determine whether *in vitro* hBM-MSC-CM treatment promoted migration and glucose uptake in MGC-803 and BGC-823 cells (common features of cells with c-Myc upregulation), we performed Transwell migration, Western blot, and glucose uptake assays. Transwell migration assays showed that hBM-MSC-CM increased the migratory ability of MGC-803 and BGC-823 cells and that JQ1 significantly inhibited these effects (both $P < 0.001$; Figures 4(a)–4(d)). In order to further verify the hBM-MSC-CM promoting gastric cancer development via upregulation of c-Myc directly, we chose to use c-Myc siRNA which can inhibit c-Myc expression directly. c-Myc siRNA can inhibit the expression of c-Myc in MGC-803 cells (Figure 4(e)). Reducing the expression of c-Myc in MGC-803 cells can inhibit the effect of hBM-MSC-CM on tumor migration (Figures 4(f) and 4(g)). Western blot and glucose uptake assays also showed that JQ1 inhibited hBM-MSC-CM-induced increases in Glut1 expression in MGC-803 and glucose uptake in MGC-803 and BGC-823 cells (Figures 4(h)–4(j)).

3.5. HBM-MSC-CM Increased Gastric Cancer Growth In Vivo. To determine whether hBM-MSC-CM promoted *in vivo* tumor growth, we injected MGC-803 cells treated with DMEM, DMSO, JQ1, hBM-MSC-CM, and hBM-MSC-CM + JQ1 for 48 h into BALB/c-nu/nu mice. Consistent with our previous studies, hBM-MSC-CM promoted tumor growth *in vivo*. Additionally, tumor volumes and weights of the JQ1 and hBM-MSC-CM + JQ1 groups were

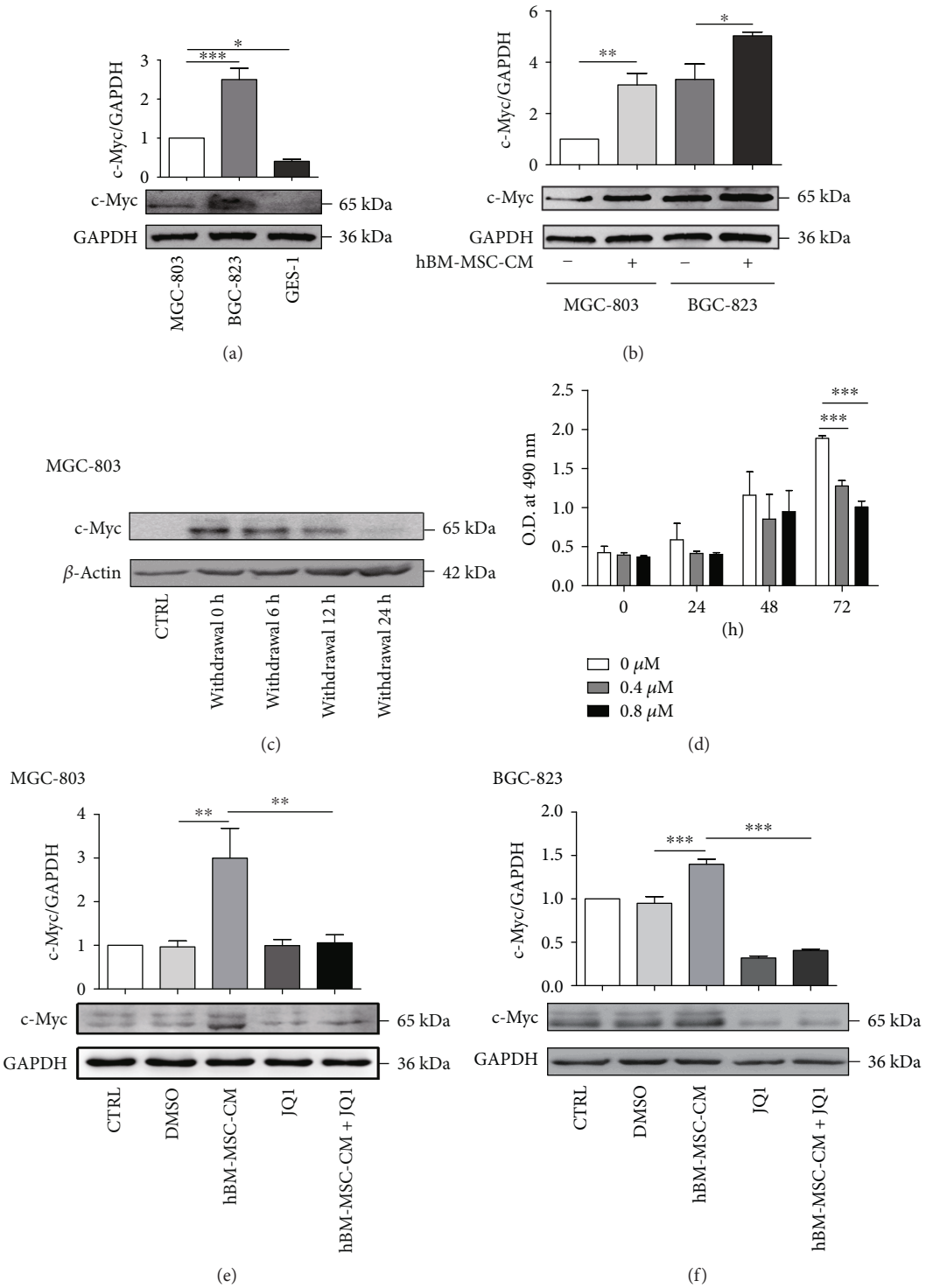

Figure 1: hBM-MSC-CM increased c-Myc expression in gastric cancer cells. (a) c-Myc protein levels in MGC-803, BGC-823, and GES-1 were detected by Western blot analysis. $^{*}P < 0.05$, $^{***}P < 0.001$. (b) c-Myc levels after 48 h hBM-MSC-CM treatment. $^{*}P < 0.05$, $^{**}P < 0.01$ (c) c-Myc protein levels maintained after withdrawal of hBM-MSC-CM treatment were detected by Western blot analysis. (d) MGC-803 cells were treated with 0.4 and 0.8 μM JQ1 for 24, 48, and 72 h. $^{***}P < 0.001$. (e, f) Compared with hBM-MSC-CM, hBM-MSC-CM + JQ1 decreased c-Myc expression in MGC-803 or BGC-823 cells. $^{**}P < 0.01$, $^{***}P < 0.001$.

smaller than those of the hBM-MSC-CM and control groups ($P < 0.001$; Figures 5(a)–5(c)). Western blotting of xenograft tumor tissue showed that hBM-MSC-CM could not maintain the upregulation of c-Myc *in vivo* (Figure 5(d)).

4. Discussion

Previous studies have suggested that MSCs are closely associated with tumor progression and growth [3]; thus, there are

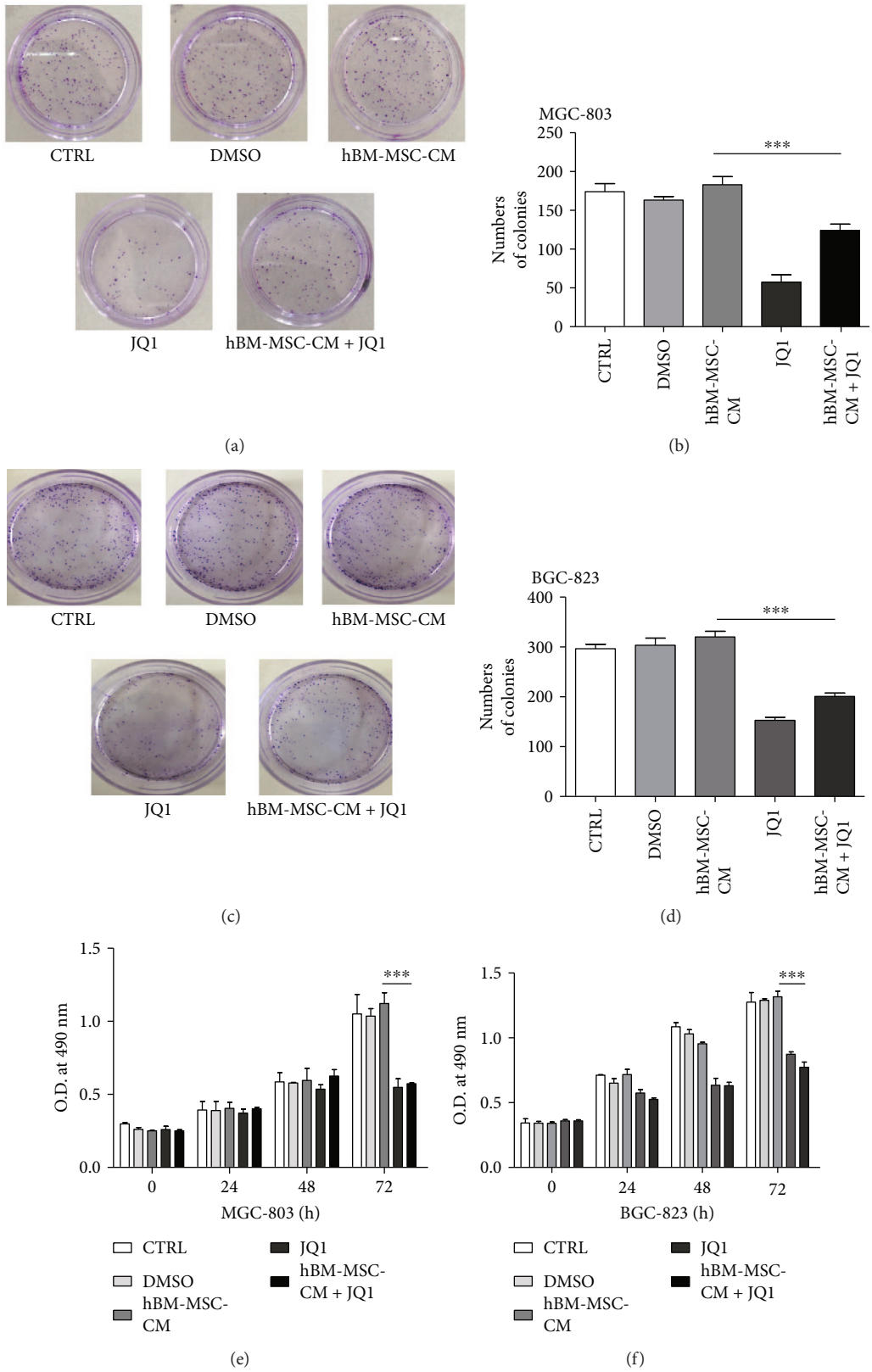

FIGURE 2: JQ1 inhibited the gastric cancer cell proliferation *in vitro*. (a, c) JQ1 reduced MGC-803 or BGC-823 colony formation rates with and without hBM-MSC-CM. (b, d) The colony formation rate of the hBM-MSC-CM + JQ1 group was lower than that of the hBM-MSC-CM group. $^{***}P < 0.001$ by a one-way analysis of variance. (e, f) MTT assays showed that JQ1 decreased the proliferation rate of MGC-803 or BGC-823 cells compared with the hBM-MSC-CM group. $^{***}P < 0.001$ by a one-way analysis of variance.

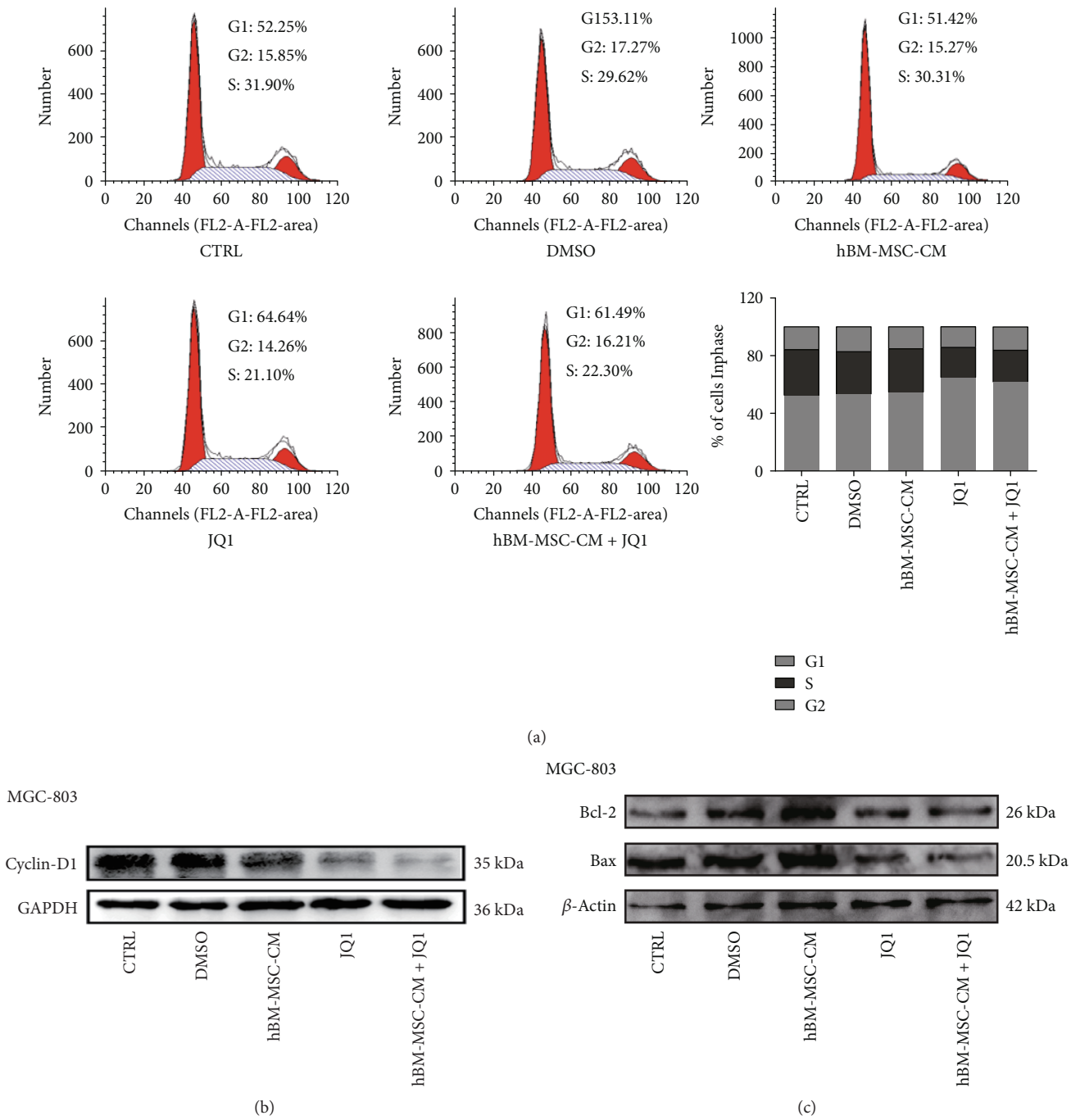

Figure 3: Effect of hBM-MSC-CM on cell cycle progression and apoptosis in gastric cancer cells. (a) hBM-MSC-CM + JQ1 induced a G1 arrest compared with the hBM-MSC-CM group; the changes in cell cycle distribution were not significant after three experiments. (b) Western blot analysis of cyclin-D1 expression in hBM-MSC-CM + JQ1-treated MGC-803 cells. (c) Western blot analysis of Bcl-2 and Bax expression in hBM-MSC-CM + JQ1-treated MGC-803 cells.

legitimate safety concerns that limit their clinical application. Our previous study revealed that MSCs promote tumor growth *in vivo*, which suggested that these cells secrete mitogenic paracrine factors [8, 9]. Jung et al. demonstrated that the MSCs recruited by tumors facilitate metastasis [14], and Li et al. revealed that gastric cancer-derived MSCs enhanced the proliferation and migration of gastric cancer cell lines [15]. Djouad et al. reported that *in vivo* tumor growth was increased when melanoma cells were coinjected with MSCs [16]. Interestingly, Karnoub et al. found that in situ breast cancer was unchanged in the absence of MSCs; however, the migratory ability of tumor cells was significantly increased when exogenous MSCs were added [17]. In this study, we chose MGC-803 and BGC-823 cells as representative cell lines to further study the mechanism through which hBM-MSC-CM promotes tumor growth.

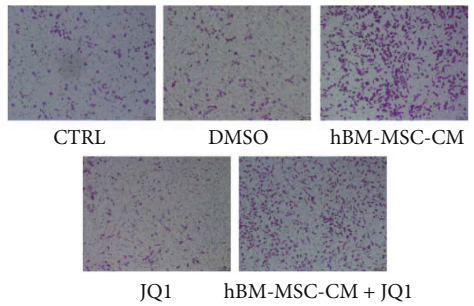

(a)

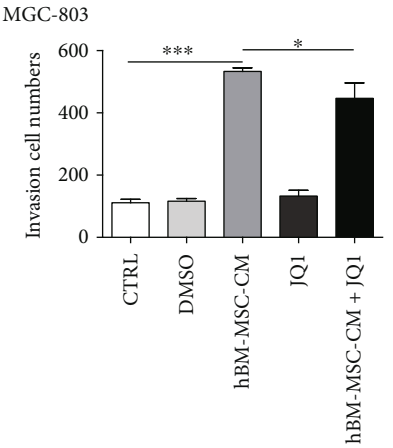

(b)

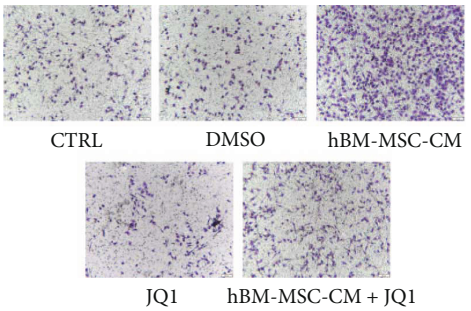

(c)

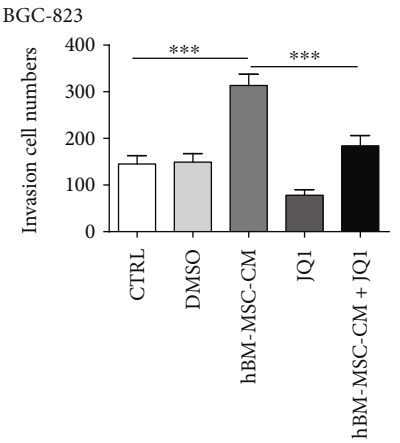

(d)

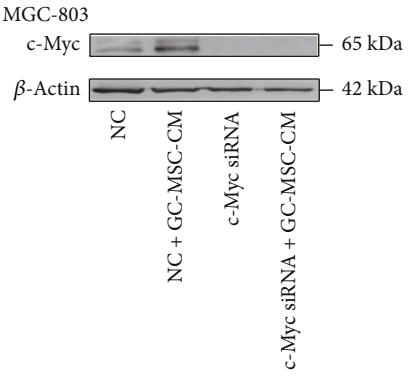

(e)

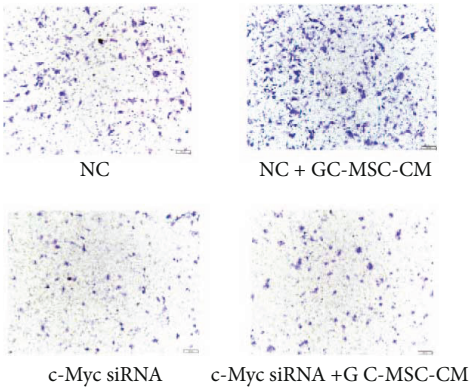

(f)

Figure 4: Continued.

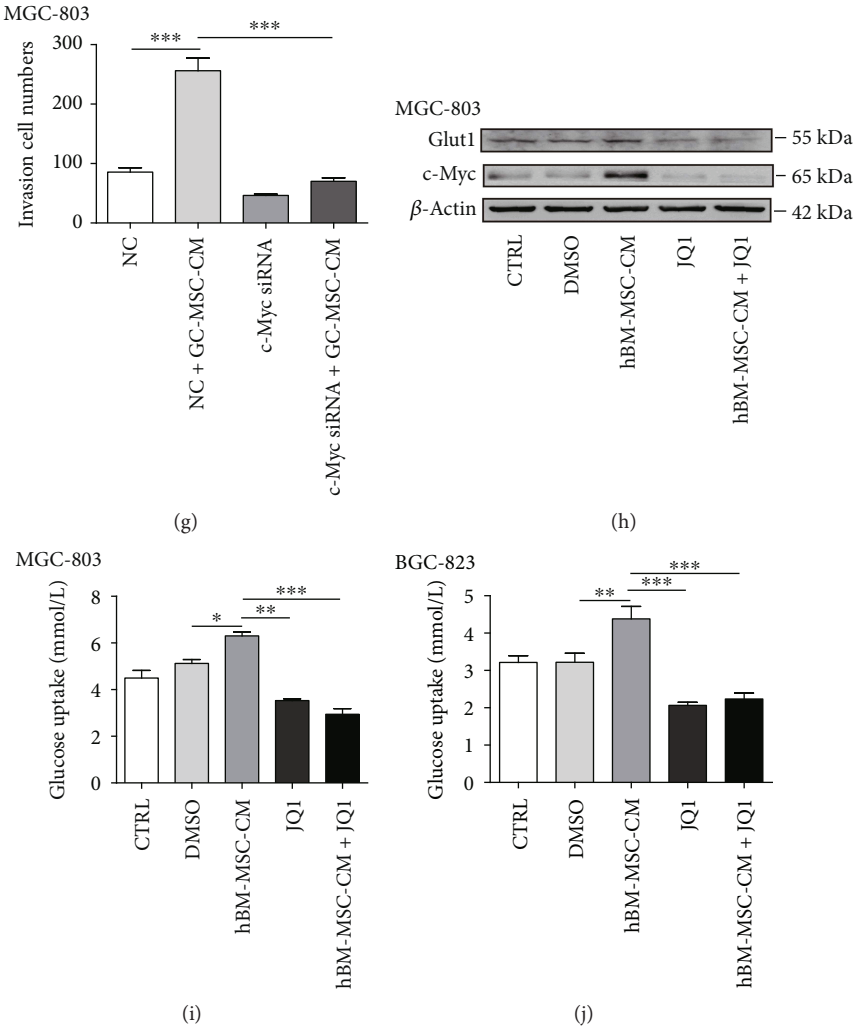

Figure 4: hBM-MSC-CM promoted migration and glucose uptake of MGC-803 and BGC-823 cells. (a, c) Transwell migration assays showed that hBM-MSC-CM increased the migratory ability of gastric cancer cells and that this activity was inhibited by JQ1 (scale bar: 100 μm). (b, d) The numbers of migrated cells were analyzed by a one-way analysis of variance ($^{*}P < 0.05$, $^{***}P < 0.001$). (e) c-Myc siRNA can inhibit the expression of c-Myc induced by hBM-MSC-CM in MGC-803 cells. (f, g) The effect of hBM-MSC-CM on MGC-803 cell migration can be suppressed by c-Myc siRNA ($^{***}P < 0.001$). (h) hBM-MSC-CM-induced Glut1 upregulation in MGC-803 cells was detected with Western blot. (i, j) The glucose uptake of MGC-803 and BGC-823 cells after the indicated treatments was detected using a clinical chemistry analyzer ($^{*}P < 0.05$, $^{**}P < 0.01$, $^{***}P < 0.001$).

We explored the potential risks of using hBM-MSCs in clinical applications. Although the tumor-promoting activity of patient-derived hBM-MSCs may be more dramatic, patient-derived hBM-MSCs could not be used in clinical applications; thus, we used healthy donor-derived hBM-MSCs. Our preliminary studies showed that the mitogenic activity of hBM-MSCs on tumor cells was primarily through paracrine signaling [8]. So, we subsequently focused on the potential factors from hBM-MSCs that promoted cancer progression, as these comprised the molecular signature of potential targets that could allow their clinical application.

c-Myc is a protooncogene that is mutated in approximately 20% of human cancers and has particularly important functions in gastric carcinogenesis [18]. In the present study, we found that c-Myc expression was increased in hBM-MSC-CM-treated gastric cancer cells, suggesting that hBM-MSC-CM may promote tumor growth by upregulating c-Myc. Moreover, c-Myc has been shown to maintain normal adult stem cells and tumor stem cells [19]. It is worth noting that the effects of hBM-MSC-CM on tumor cell proliferation and cell cycle progression were not obvious *in vitro*. The experimental results showed that the upregulation of c-Myc expression in tumor cells could maintain 12 hours after withdrawal of hBM-MSC-CM. However, the inhibitory effect of JQ1 on tumor cells was clear in this setting. Our previous studies have shown that hBM-MSCs promote tumor angiogenesis through paracrine signaling, and Rahl et al. found that upregulating c-Myc also promotes tumor angiogenesis [20]. After pretreatment of tumor cells, the upregulation of c-Myc induced by hBM-MSC-CM cannot be maintained for a long time. Though the upregulation of c-Myc in tumor tissue was

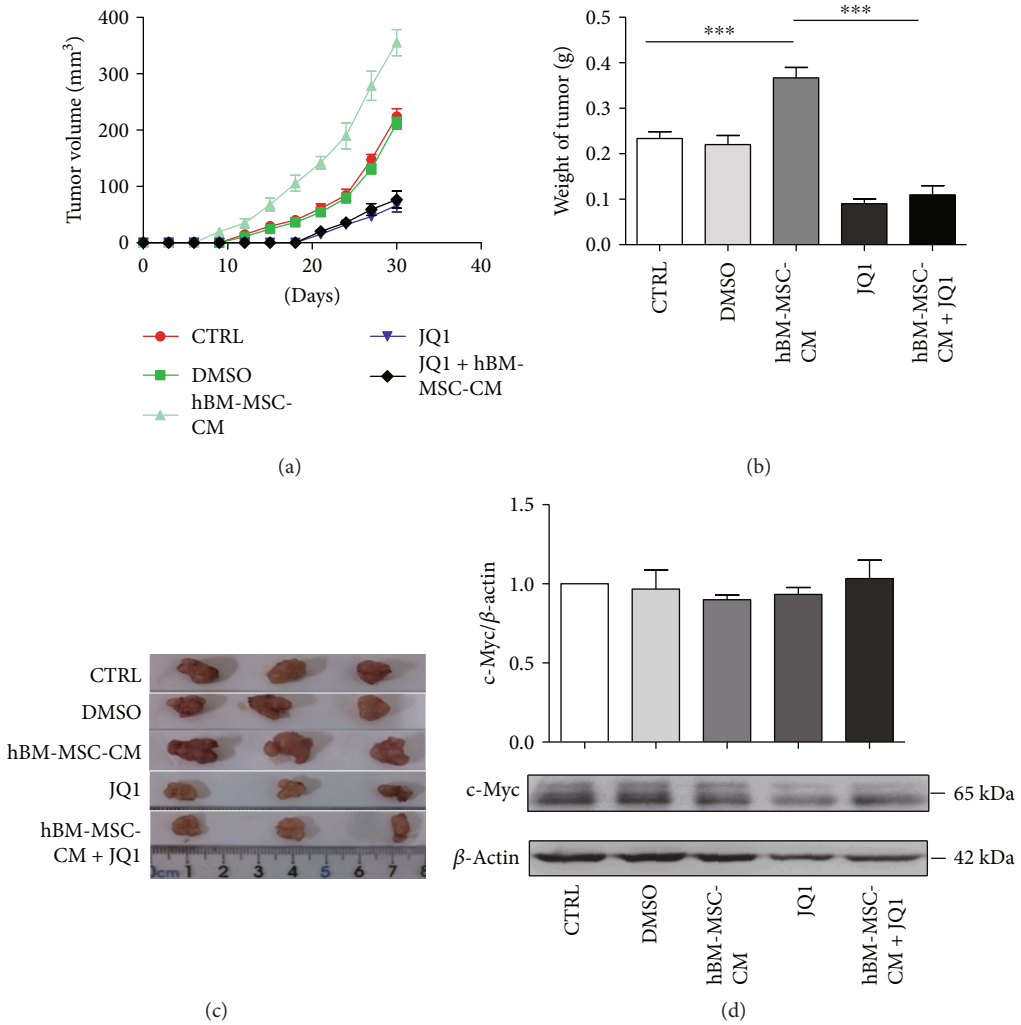

FIGURE 5: hBM-MSC-CM increased *in vivo* gastric tumor growth by upregulating c-Myc expression. (a) Tumor volumes of MGC-803 xenografts in immunocompromised mice. Tumor volumes of the JQ1 and hBM-MSC-CM + JQ1 groups were reduced compared with those of the hBM-MSC-CM and control groups; $^{***}P < 0.001$ by Kruskal–Wallis H test. (b, c) Comparison of tumor weights in each group at day 30; $^{***}P < 0.001$ by Kruskal–Wallis H test. (d) Expression of c-Myc in MGC-803 xenograft tissues of the different treatment groups was also detected with Western blot.

not maintained, the upregulation of c-Myc in tumor cells has the effect of initiating tumor development in mice. HBM-MSC-CM upregulated the expression of c-Myc in tumor cells, which may lead to reprogramming of tumor cells and affect tumor growth by promoting angiogenesis or the increase of glycolysis *in vivo*. This effect does not depend on the long-term expression of c-Myc. We now hypothesize that hBM-MSC-CM promotes tumor angiogenesis via upregulation of c-Myc, and thus, there are both cell-intrinsic and cell-extrinsic *in vivo* effects of hBM-MSC-CM that increase tumor growth. We will continue to explore these processes in future studies. In conclusion, our data show that hBM-MSC-CM in the tumor microenvironment increases c-Myc expression in tumor cells, which directly promotes tumor cell proliferation and increases vascularization.

JQ1 is a small selective bromodomain and extraterminal (BET) motif inhibitor that can inhibit c-Myc expression and tumor growth [21, 22]. Other studies have reported that a critical mechanism of JQ1 in suppressing tumor growth is its ability to block c-Myc expression [23–26]. We found that JQ1 inhibits the expression of c-Myc. Moreover, hBM-MSC-CM promoted glucose uptake and cell migration via upregulating c-Myc in gastric cancer, both of which were suppressed by JQ1. Finally, *in vivo* studies showed that JQ1 inhibited the increased growth of gastric cancer xenografts that was induced by hBM-MSC-CM. Clinical trials have proven that hBM-MSCs do not undergo tumorigenesis [4, 6]. But tumor occurrence is the result of variety of tumor-promoting factors. However, BM-MSCs are immunosuppressive, and factors that affect the immune system should be a concern with regard to tumorigenesis [27, 28]. In the present study, we found that hBM-MSC-CM can promote tumor cell proliferation, migration, and glucose uptake via upregulating c-Myc. Although there are no reports of

hBM-MSCs causing tumor formation, their potential to promote tumorigenesis is worthy of concern for potential applications in tissue engineering.

5. Conclusions

hBM-MSC-CM promotes gastric cancer cell proliferation by upregulating c-Myc. c-Myc inhibitors may be effective at preventing the protumor effects of hBM-MSC-CM and, therefore, could solve the clinical safety issues of hBM-MSCs.

Abbreviations

MSCs:	Mesenchymal stem cells
hBM-MSCs:	Human bone marrow MSCs
hBM-MSC-CM:	hBM-MSC-conditioned medium
BRDs:	Bromodomain-containing proteins
PBS:	Phosphate-buffered saline
FBS:	Fetal bovine serum
DMEM:	Dulbecco's modified Eagle's medium
BET:	Bromodomain and extraterminal motif.

Data Availability

The data used to support the findings of this study are included within the article.

Ethical Approval

This study and the consent procedure were approved by the local ethics committee of Jiangsu University, China. The procedure for deriving bone marrow cells from healthy donors was approved by the local ethics committee of the Affiliated Hospital of Jiangsu University, China. Informed consent was given by all donors.

Conflicts of Interest

The authors declare that they have no conflicts of interests.

Authors' Contributions

Bin Chen and Jing Yu participated in the experimental design and manuscript writing and performed the experiments. Yuanyuan Zhao, Li Sun, and Qianqian Wang were involved in establishing the animal models and manuscript. Bo Shen and Changgen Xu contributed to the study design and provided fresh bone marrow samples. Xiangdong Zhao participated in data analysis and cell culture. Wenrong Xu and Mei Wang contributed to the study design and manuscript guidance. Wei Zhu participated in the experimental design, manuscript writing, manuscript revision, and data analysis.

Acknowledgments

This work was supported by the National Natural Science Foundation of China (Grant no. 81472334), Jiangsu Province's Project of Key Research and Development Plan (Social Development) (Grant no. BE2017694), the Nanjing Science and Technology Commission (Grant no. 201605005), and the Jiangsu Provincial Health and Family Planning Commission (Grant no. LGY 2016026).

References

[1] N. Naftali-Shani, L. P. Levin-Kotler, D. Palevski et al., "Left ventricular dysfunction switches mesenchymal stromal cells toward an inflammatory phenotype and impairs their reparative properties via toll-like receptor-4," *Circulation*, vol. 135, no. 23, pp. 2271–2287, 2017.

[2] J. Zhan, Y. Li, J. Yu et al., "Culture medium of bone marrow-derived human mesenchymal stem cells effects lymphatic endothelial cells and tumor lymph vessel formation," *Oncology Letters*, vol. 9, no. 3, pp. 1221–1226, 2015.

[3] W. Zhu, W. Xu, R. Jiang et al., "Mesenchymal stem cells derived from bone marrow favor tumor cell growth in vivo," *Experimental and Molecular Pathology*, vol. 80, no. 3, pp. 267–274, 2006.

[4] P. H. Lee, J. W. Kim, O. Y. Bang, Y. H. Ahn, I. S. Joo, and K. Huh, "Autologous mesenchymal stem cell therapy delays the progression of neurological deficits in patients with multiple system atrophy," *Clinical Pharmacology and Therapeutics*, vol. 83, no. 5, pp. 723–730, 2008.

[5] L. Perico, M. Morigi, C. Rota et al., "Human mesenchymal stromal cells transplanted into mice stimulate renal tubular cells and enhance mitochondrial function," *Nature Communications*, vol. 8, no. 1, p. 983, 2017.

[6] S. Wakitani, T. Okabe, S. Horibe et al., "Safety of autologous bone marrow-derived mesenchymal stem cell transplantation for cartilage repair in 41 patients with 45 joints followed for up to 11 years and 5 months," *Journal of Tissue Engineering and Regenerative Medicine*, vol. 5, no. 2, pp. 146–150, 2011.

[7] L. Wang, L. Wang, X. Cong et al., "Human umbilical cord mesenchymal stem cell therapy for patients with active rheumatoid arthritis: safety and efficacy," *Stem Cells and Development*, vol. 22, no. 24, pp. 3192–3202, 2013.

[8] W. Zhu, L. Huang, Y. Li et al., "Mesenchymal stem cell-secreted soluble signaling molecules potentiate tumor growth," *Cell Cycle*, vol. 10, no. 18, pp. 3198–3207, 2011.

[9] W. Zhu, L. Huang, Y. Li et al., "Exosomes derived from human bone marrow mesenchymal stem cells promote tumor growth *in vivo*," *Cancer Letters*, vol. 315, no. 1, pp. 28–37, 2012.

[10] A. Henssen, K. Althoff, A. Odersky et al., "Targeting MYCN-driven transcription by BET-bromodomain inhibition," *Clinical Cancer Research*, vol. 22, no. 10, pp. 2470–2481, 2016.

[11] J. Li, B. Fang, F. Kinose et al., "Target identification in small cell lung cancer via integrated phenotypic screening and activity-based protein profiling," *Molecular Cancer Therapeutics*, vol. 15, no. 2, pp. 334–342, 2016.

[12] S. Zhu, P. Sun, Y. Zhang, L. Yan, and B. Luo, "Expression of c-myc and PCNA in Epstein-Barr virus-associated gastric carcinoma," *Experimental and Therapeutic Medicine*, vol. 5, no. 4, pp. 1030–1034, 2013.

[13] J. Wang, Z. Liu, Z. Wang et al., "Targeting c-Myc: JQ1 as a promising option for c-Myc-amplified esophageal squamous cell carcinoma," *Cancer Letters*, vol. 419, pp. 64–74, 2018.

[14] Y. Jung, J. K. Kim, Y. Shiozawa et al., "Recruitment of mesenchymal stem cells into prostate tumours promotes metastasis," *Nature Communications*, vol. 4, no. 1, p. 1795, 2013.

[15] W. Li, Y. Zhou, J. Yang et al., "Gastric cancer-derived mesenchymal stem cells prompt gastric cancer progression through

secretion of interleukin-8," *Journal of Experimental & Clinical Cancer Research*, vol. 34, no. 1, p. 52, 2015.

[16] F. Djouad, C. Bony, F. Apparailly, P. Louis-Plence, C. Jorgensen, and D. Noël, "Earlier onset of syngeneic tumors in the presence of mesenchymal stem cells," *Transplantation*, vol. 82, no. 8, pp. 1060–1066, 2006.

[17] A. E. Karnoub, A. B. Dash, A. P. Vo et al., "Mesenchymal stem cells within tumour stroma promote breast cancer metastasis," *Nature*, vol. 449, no. 7162, pp. 557–563, 2007.

[18] C. V. Dang, "C-Myc target genes involved in cell growth, apoptosis, and metabolism," *Molecular and Cellular Biology*, vol. 19, no. 1, pp. 1–11, 1999.

[19] X. Fang, W. Zhou, Q. Wu et al., "Deubiquitinase USP13 maintains glioblastoma stem cells by antagonizing FBXL14-mediated Myc ubiquitination," *The Journal of Experimental Medicine*, vol. 214, no. 1, pp. 245–267, 2017.

[20] P. B. Rahl, C. Y. Lin, A. C. Seila et al., "C-Myc regulates transcriptional pause release," *Cell*, vol. 141, no. 3, pp. 432–445, 2010.

[21] P. L. Garcia, A. L. Miller, K. M. Kreitzburg et al., "The BET bromodomain inhibitor JQ1 suppresses growth of pancreatic ductal adenocarcinoma in patient-derived xenograft models," *Oncogene*, vol. 35, no. 7, pp. 833–845, 2016.

[22] S. E. Lochrin, D. K. Price, and W. D. Figg, "BET bromodomain inhibitors—a novel epigenetic approach in castration-resistant prostate cancer," *Cancer Biology & Therapy*, vol. 15, no. 12, pp. 1583–1585, 2014.

[23] P. Filippakopoulos, J. Qi, S. Picaud et al., "Selective inhibition of BET bromodomains," *Nature*, vol. 468, no. 7327, pp. 1067–1073, 2010.

[24] J. E. Roderick, J. Tesell, L. D. Shultz et al., "C-Myc inhibition prevents leukemia initiation in mice and impairs the growth of relapsed and induction failure pediatric T-ALL cells," *Blood*, vol. 123, no. 7, pp. 1040–1050, 2014.

[25] Q. Shao, A. Kannan, Z. Lin, B. C. Stack, J. Y. Suen, and L. Gao, "BET protein inhibitor JQ1 attenuates Myc-amplified MCC tumor growth *in vivo*," *Cancer Research*, vol. 74, no. 23, pp. 7090–7102, 2014.

[26] A. Wyce, G. Ganji, K. N. Smitheman et al., "BET inhibition silences expression of MYCN and BCL2 and induces cytotoxicity in neuroblastoma tumor models," *PLoS One*, vol. 8, no. 8, article e72967, 2013.

[27] G. R. Willis, A. Fernandez-Gonzalez, J. Anastas et al., "Mesenchymal stromal cell exosomes ameliorate experimental bronchopulmonary dysplasia and restore lung function through macrophage immunomodulation," *American Journal of Respiratory and Critical Care Medicine*, vol. 197, no. 1, pp. 104–116, 2018.

[28] L. Zanotti, R. Angioni, B. Calì et al., "Mouse mesenchymal stem cells inhibit high endothelial cell activation and lymphocyte homing to lymph nodes by releasing TIMP-1," *Leukemia*, vol. 30, no. 5, pp. 1143–1154, 2016.